FINITE DEFORMATION, ELASTIC-PLASTIC, FINITE ELEMENT ANALYSIS OF PLANAR CRACKS

A THESIS

Presented to

The Faculty of the Division of Graduate Studies

By

Wen-Hwa Chen

In Partial Fulfillment

of the Requirements for the Degree

Doctor of Philosophy in the School

of Engineering Science and Mechanics

Georgia Institute of Technology

May, 1977

FINITE DEFORMATION, ELASTIC-PLASTIC,

FINITE ELEMENT ANALYSIS OF PLANAR CRACKS

Approved:

S. N. Atluri, Chairman

M. C. Bernard

J. T. Berry

D. V. Ho

T. S. Wang

Date approved by Chairman 7/25/77.

ACKNOWLEDGMENTS

The author wishes to sincerely thank his advisor, Dr. S. N. Atluri, for the encouragement, guidance, and inspiration conveyed to him during the preparation of this thesis. Deepest gratitude is also expressed to Dr. D. V. Ho and Dr. J. T. S. Wang, members of the reading committee, for their considerate encouragement and helpful suggestions. The author's thanks go also to Dr. M. C. Bernard and Dr. J. T. Berry for their interest in the research. Dr. M. Nakagaki's discussions and suggestions at various stages of the research were of invaluable assistance.

The author is very thankful to Dr. M. E. Raville, Director of the School of Engineering Science and Mechanics, for his encouragement during this study. In addition, the author gratefully wishes to acknowledge the financial support of the President's Fellowship which he received in 1973 and the support for this work provided by The Air Force Office Scientific Research under the Grant 74-2667 to Georgia Institute of Technology with Dr. S. N. Atluri as principal investigator.

The author would like to dedicate this thesis to his wife, Hsiao-Chen, whose love, encouragement, patience and sacrifice have made this work possible. The author's deepest appreciation also goes to his parents, Mr. and Mrs. Chi Chen, and all the members of the family for their support and understanding during the entire period of this study.

Finally, the author would like to thank Mrs. Jackie Van Hook for typing the final manuscript.

TABLE OF CONTENTS

TABLE OF CONTENTS (Continued)

LIST OF ILLUSTRATIONS

LIST OF ILLUSTRATIONS (Continued)

LIST OF ILLUSTRATIONS (Continued)

SUMMARY

Because linear elastic fracture analysis has been proved to be insufficient in predicting the failure of cracked bodies, in recent years, a number of fracture concepts have been studied which remain applicable even in the presence of large-scale plasticity. Two such concepts, the crack-tip opening displacement (COD) for materials with significant ductility and Rice's path independent contour integral J, are established and demonstrated numerically as acceptable ductile initiation fracture criteria in this dissertation. The relationship of J with the "COD" concept is also explored in detail using the various definitions for "COD" available in literature.

This work thereby presents a numerical procedure, as accurate as possible, to analyze plane problems of ductile fracture under large-scale yielding conditions, with arbitrary geometrical domains, under arbitrary loading conditions, and when the material properties can be characterized as elastic-plastic with arbitrary strain hardening. Based on a continuously updated Lagrangean incremental theory, a consistent finite deformation finite-element analysis procedure is employed to account for large geometry changes near the crack-tip (crack-tip blunting). To account for this geometrical nonlinearity as well as the arbitrary strain-hardening behavior, an incremental "tangent modulus" method of analysis is considered. The incremental plastic flow has been described by a Prager-Ziegler type kinematic hardening law, which

is capable of accounting for the Bauschinger effect in unloading conditions. The dominant singular behavior for strains and stresses corresponding to the well known Hutchinson-Rice-Rosengren solution for power-hardening materials is embedded in each of circular-sector shaped "embedded-singularity" elements near the crack-tip. Continuity of displacements and tractions between these near-tip elements with "singular" field assumptions and the neighboring elements with "regular" field assumptions is enforced through a hybrid displacement finite element model, which is based essentially on a modified principle of potential energy. Also, the uniaxial stress-strain relation of the material is considered to be of Ramberg-Osgood type.

Three fracture test specimens made of Ni-Cr-Mo-V rotor steel and A533B steel are solved: (1) three-point bend, (2) center-cracked, and (3) compact tension types. The computed results are compared with available experimental results for the same specimens. Excellent correlation between the directly computed results and available experimental results has been obtained for the functional relationship between the J-integral and the displacement δ. This J versus δ relationship provides a criterion, the so-called "J_{IC} fracture criterion", which can predict the initiation of crack growth only.

In order to provide a realistic analysis for fracture, this dissertation is also devoted to finite element approaches which attempt to describe crack extension. Thus, a rigorous finite-element modeling, involving the translation of entire "singular" near-tip elements and consideration of global energy balance, is developed. To study the

global energy release rate G* for crack propagation, the Kfouri et al.'s center-cracked problem together with the above compact tension specimen are first solved. Then, because the J resistance curve for the compact tension specimen using Ni-Cr-Mo-V rotor steel has already been experimentally obtained, crack growth phenomenon in a compact tension specimen made of Ni-Cr-Mo-V rotor steel is studied. Due to the lack of an acceptable fracture criterion associated with stable crack growth, providing a complete scheme of stable crack growth based on the present analysis is impossible and thus remains for further work.

LIST OF SYMBOLS*

σ_{ij}	Stress Tensor
ϵ_{ij}	Strain Tensor
U_i	Total Displacements from C_o to C_N
r	Polar Coordinate
θ	Polar Coordinate, Local Angular Coordinate (Figure 11)
n	Power for the Power-Law Hardening Material
K_σ, K_ϵ	Stress and Strain Intensity Factors Obtained by Power Law Hardening Rule
E	Young's Modulus
σ_y	Yield Stress
G	Strain Energy Release Rate
G_{IC}	Critical Strain Energy Release Rate for Mode I
K_{IC}	Plane Strain Fracture Toughness
ν	Poisson Ratio
J	Rice's J-Integral
J_2	Second Invariant of Deviatoric Stress Tensor
Γ, γ	Surface Energy
T_i	Tractions
x_1, x_2	Cartesian Coordinates
V	Total Potential Energy
t_i	Piola-Lagrange Tractions

*The symbols which are not found here are explained wherever they first appear.

t_{ij}	Piola-Lagrange Stress Tensor
τ_{ij}	Euler Stress Tensor
S_{ij}	Kirchhoff-Trefftz Stress Tensor
J_{IC}	Critical Value of J
COD	Crack-Tip Opening Displacement
CGD, V_M	Clip-Gage Displacement
$E_{ijk\ell}$	Elasticity Compliance Tensor
$E^t_{ijk\ell}$	Updated Elasticity-Plasticity Tensor
f	Yield Function
α_{ij}	Translation of the Center of the Yield Surface
ΔS_{ij}	Incremental Truesdell Stress Tensor
Δg_{ij}	Incremental Green Strain Tensor
δ	Displacement, Variational Quantity
n_i	Components of Outer Normal Vector at a Boundary
$\Delta U_{i\rho}$	Incremental Element Boundary Displacements
$T_{i\rho}$	Lagrange Multiplier Boundary Tractions
β_i	Parameters in Incremental Interior Displacements
α_i	Parameters in Boundary Tractions
N_i	Shape Functions
ξ, η	Isoparametric Coordinates
φ	Polar Coordinate (Figure 11)
a	Crack Length
P	External Load, Plastic Work Rate
G^{Δ}	Crack Separation Energy Rate
G*	Global Energy Release Rate
J'	Palmer and Rice's Integral

CHAPTER I

INTRODUCTION

A fracture criterion which accurately predicts the initiation of crack growth or failure of cracked bodies is essential for both the evaluation of structural integrity and the selection of materials. Linear elastic fracture mechanics provides a one parameter fracture criterion, the so-called Griffith fracture criterion (G_{IC}), only for a limited class of problems; those of cracked bodies with small scale yielding where the crack-tip plastic region is small compared to the crack length.

However, ductile engineering materials such as metals which are of great importance in many structural applications usually are able to undergo large-scale yielding. This large-scale yield property limits the use and versatility of linear elastic analysis. Thus, motivated by this insufficiency, the present research is undertaken to establish a fracture criterion which can be applicable in cases of both small and large scale plasticity.

First of all, it is necessary to clearly establish in detail the stress and deformation fields near the crack-tip in elastic-plastic materials. The structure of the dominant singularity in stresses and strains near a crack-tip in plane problems for linear elastic materials was studied by Williams [1].* He found that the local stress variations

*Numbers in brackets designate references at the end of this dissertation.

are proportional to inverse-square-root of the distance from the crack-tip in the vicinity of the base of the crack. Also, the strain field, which has the same variation near the crack-tip, as well as the displacement field are obtained.

Most of the recent works use various nonlinear constitutive relations instead of linear stress-strain law under the kinematic assumption of infinitesimal deformations. The work of Rice and Rosengren [2] predicted, the application of a path independent integral, that the product of the stress and strain has an exact $\frac{1}{r}$ singularity as the crack-tip is approached, i.e.

$$\sigma_{ij}\epsilon_{ij} \sim \frac{R(\theta)}{r} \qquad \text{as } r \to 0$$

where r and θ are polar coordinates (Figure 1). $R(\theta)$ is a function of θ only. Furthermore, Hutchinson [3,4] and Rice and Rosengren [2] used a pure power law hardening material to obtain the following stress, strain and displacement field distributions near the crack-tip:

$$\begin{aligned} \sigma_{ij} &= k_\sigma r^{-\frac{1}{n+1}} \sigma_{ij}(\theta) \\ \epsilon_{ij} &= k_\epsilon r^{-\frac{n}{n+1}} \epsilon_{ij}(\theta) \\ u_i &= k_\epsilon r^{\frac{1}{n+1}} u_i(\theta) \end{aligned} \tag{1.1}$$

where n is the power hardening coefficient in the assumed uniaxial

stress-strain law, which is of the form $\epsilon \sim \sigma^n$. $K\sigma$ and $K\epsilon$ will be referred to as the amplitude of the singularity. The θ-dependence of the above asymptotic fields is determined in [3] from the numerical solution of a nonlinear fourth order ordinary differential equation. For $n = 1$, equations (1.1) degenerate to the linear-elastic case and are in agreement with the inverse-square-root singularities obtained by Williams [1].

The analytical solutions to two dimensional crack problems, even for elastic cases, are limited to relatively simple boundary conditions and geometrical configurations. In view of the complexity of the boundary conditions, numerical procedures are employed to obtain approximate results. Among the several approximate numerical methods summarized by Rice [5], the finite element method provides the greatest versatility: It allows for the analysis of complicated geometries, enables treatment of complex problems of combined mechanical and thermal loadings, and, importantly, permits the use of "elastic-plastic" elements to account for the effects of plasticity, etc.

A thorough treatment of the principles and applications of finite element techniques is given by Zienkiewicz [6] and Martin et al. [7]. The continuum, with its infinite degrees of freedom, is replaced by a finite number of structural elements of finite size interconnected only at their nodal points. (See Figure 21 and Figure 29, etc.) Forces between the elements can be transmitted only via these nodal points. The value of field variables at the nodes constitute the unknowns in the problems.

Early attempts to solve crack problems by finite element techniques used only conventional elements [8-10]. Since those elements did not incorporate the characteristic crack-tip stress singularity, very detailed element breakdown was required in the vicinity of the crack-tip. Such analyses with very fine finite element meshes were costly and inefficient.

Several early investigators [11,12] created a special element near the crack tip which contained, for elastic analysis, the correct William's singularity. However, this element did not satisfy inter-element displacement continuity conditions, and thus convergence properties of such a solution could not be guaranteed [13]. It would be preferable to construct a model in finite element analysis such that the crack-tip singularities are embedded in several elements surrounding the crack-tip and the interelement displacement continuity conditions are still satisfied. The hybrid displacement model used by Atluri et al. [14,15,16] appears to provide these qualities.

In the hybrid displacement finite element model, [14,15,16], an arbitrary displacement field which includes the correct near-tip $\sqrt{r}$ type asymptotic solution for elastic analysis is assumed within an element near the crack-tip. One then assumes a boundary displacement (compatible with the neighboring elements) which may be interpolated in terms of element nodal displacements and a set of Lagrange multiplier boundary tractions which are used to enforce interelement displacement continuity. Results have shown that elastic crack solutions obtained using the hybrid displacement elements require a much smaller number of degrees of freedom than conventional elements.

In contrast to linear elastic fracture mechanics, the application of finite element methods in the inelastic range have been much less developed. To account for the nonlinear material behaviors, the works in References [2,3,4] utilize an asymptotic treatment in accordance with a deformation theory of plasticity. The use of the deformation theory of plasticity, which is undistinguishable from the nonlinear theory of elasticity (except for materials which obey a yield condition), is invalid when applied to situations where significant unloading is observed. Such unloading situations will be, for example, encountered in the study of the process of crack growth. In such cases, the use of the incremental flow theory of plasticity, the so-called J_2-flow theory, is imperative in the yield zone.

Also, in order to obtain accurate predictions of the near-tip stress and deformation states, the effect of crack-tip blunting, which frequently exists in ductile fracture, must be investigated. Thus, in this work, a finite deformation analysis is employed instead of small deformation analysis as in References [2,3,4] to account for the finite changes in geometry near the crack-tip. This calls for an incremental finite element analysis to deal with not only material nonlinearity, but also geometrical nonlinearity. Hence, a "tangent modulus" numerical method [17,18] of incremental finite element analysis is thought to be most appropriate in such a case.

The incremental plastic flow is described by a Prager-Ziegler type kinematic hardening rule [19,20] to take into account the Bauschinger effect. The material is assumed to obey the

Huber-Mises-Hencky yield criterion, and the uniaxial stress-strain curve of the material is considered to be of Ramberg-Osgood type:

$$\epsilon = \frac{\sigma}{E} \qquad \sigma < \sigma_y \; ; \qquad \epsilon = \frac{\sigma}{E} + \left(\frac{\sigma}{B_o}\right)^n \qquad \sigma \geq \sigma_y$$

where E is Young's modulus, σ_y is the yield stress, n is the power hardening coefficient and B_o is the plastic modulus.

One of the major contributions of this research is the construction and verification of an acceptable one-parameter ductile fracture criterion in the presence of large-scale plastic yielding with finite deformation assumptions. Given the conditions at which fracture begins for a particular case, the same mode of failure for the same material in any other case can be predicted by calculating the values of the parameter for both cases and comparing to see if failure will occur. For elastic materials the stress intensity factor K is used. However, for elastic-plastic materials, the stress intensity factor K depends on the hardening coefficient n (in the limit of a nonhardening material, stresses are not singular) and is no longer applicable. Thus, another acceptable parameter is required for elastic-plastic materials.

In the recent years several concepts such as the J-integral, the crack-tip opening displacement (COD), the R-curve method, and nonlinear energy release rate have been developed which remain applicable even in the presence of large scale plasticity. Among those various ductile fracture concepts, the J integral introduced by Rice [21], and earlier by Eshelby [22], appears most attractive. The advantage of using the

J-integral is as follows:

(1) The J-integral is path-independent (exactly under deformation theory, and approximately under monotonic loading and J_2 flow theory) and can be calculated on a contour well away from the crack-tip where the stresses and strains can be more accurately determined.

(2) The evaluation of the J-integral is faster and easier than calculation of crack tip features, especially for finite element techniques.

(3) The J-integral can be evaluated experimentally, using inexpensive, small test specimens.

The path-independence of the J-integral is valid if the strain energy is a single-valued function of the strains, as is the case if a total strain theory is used, and as long as the effective stress is not decreased. Under the use of a J_2-flow theory of plasticity as mentioned above the path-independence of the J-integral, even under monotonic loading, cannot be established. However, under monotonic loading, the use of a total strain theory is justifiable when studying stress and strain fields near a stationary crack, because approximately proportional loading occurs. During the loading of a cracked body from the initial state to the critical state, the effective stress can be expected to increase everywhere in the region. Thus, under monotonic loading, approximate path independence of the J-integral may be expected even under J_2-flow theory of plasticity.

When small-scale yielding exists, J (within the framework of the deformation theory of plasticity) is related to the elastic intensity

factor by a simple formula identical to the energy release rate G [21]. For large-scale yielding such simple calculations are not possible since J depends in a complicated way on geometry, applied loading, and material constitutive law. However, using the present finite element analysis the J versus δ (load point displacement or load-line displacement) relation can be first established. Thus, assuming that the critical displacement δ_c at crack-growth initiation is known from experiments, the critical J value (J_{IC}) which specifies the critical state of the cracked body can then be determined.

Also, the computed data is analyzed with special attention to the relationship of J with the "COD" concept using the various definitions for "COD" available in literature [23,24,25,26].

It is noted that the criterion of critical J (J_{IC}) is only a criterion for initiation of crack growth without any statement of stability or instability of such a crack growth. However, the extents of stable crack growth in "plane stress fracture" situations, in thin sheets, can be substantial as observed by Broek [27], Link and Muntz [28], and Bergkvist and Anderson [29]. Therefore, a realistic analytical framework of fracture must include not only models for initiation of crack growth, but also models for subsequent stable crack growth, and especially for its terminal loss of stability. Unfortunately, due to the lack of an acceptable fracture criterion associated with stable crack growth, providing a complete scheme of stable growth based on the above procedure is impossible. However, the study of global energy release rate G* corresponding to the available experimental J resistance

curve [30] should be very helpful in the investigation of stable crack growth. Thus, a rigorous finite-element modeling of the study of global energy release rate G*, involving the translation of entire "singular" near-tip elements and consideration of global energy balance, is also included in this work.

In summary, this dissertation has the following objectives:

(a) Developing circular sector shaped embedded singularity elements near the crack-tip. The correct r dependence of the dominant singular solution corresponding to the material nonlinearity, is embedded in these near-tip (singular) elements, wheras the θ variation is approximated in each sector singular element and solved for in the sense of the finite-element method.

(b) Maintaining continuity of displacements and tractions between near-tip singular elements with singular stress/strain assumptions and the far field (regular) elements through a hybrid displacement and conventional finite element model.

(c) Using a J_2-flow theory of plasticity and arbitrary kinematic hardening which will accurately model the Bauschinger effect under fully reversed and cyclic loading.

(d) Using an incremental finite element analysis based on a continuously updated Lagrangean approach [31] to deal with the elastic-plastic, finite deformation, two dimensional mode I (Appendix A) crack problem; and establishing the J-δ relations computationally for materials with strain hardening under large scale yielding. The "tangent modulus" incremental numerical method [17,18] is used for this purpose.

(e) Developing a more accurate finite element method for incremental analysis of elastic-plastic problems. To have a smoother definition of the yield zone, higher-order elements are used and the stresses are evaluated at the Gaussian integration points within the element for each load step. Thus, a portion of element can yield, while the rest of the element can remain elastic. Thus, a very fine finite element mesh around the crack-tip is no longer needed.

(f) Developing a rigorous finite element model of crack propagation involving the translation of entire "singular" near-tip elements to study the global energy release rate G* thoroughly.

Using the procedure developed in the Chapters 3, 4, and 5, detailed analyses of the conditions for initiation of crack growth were performed for test specimens of three-point bend, center-cracked and compact tension types. The materials considered were N_i-C_r-M_o-V rotor steel and A533B steel respectively. The correlation of the variation of J with displacement (δ) was noted for all three specimens, using the computed results and the experimental results available in literature [32,33,34]. To study the global energy release rate G^* for crack propagation, the Kfouri et al.'s center-cracked problem [75] together with the above compact-tension specimen were first solved. Then, because the J resistance curve for the compact tension specimen using N_i-C_r-M_o-V rotor steel has already been experimentally obtained [30], crack growth phenomenon in a compact tension specimen made of this rotor steel was studied. Some possible extensions of the work and recommendations for further study in this area are given in Chapter 8.

Also, for clarity, some details of the solution procedure and a flow chart of the present finite element crack growth analysis are provided in the Appendices.

CHAPTER II

SOME COMMENTS ON FRACTURE CRITERIA

Conventional design criteria based on yield or ultimate strengths are inadequate for predicting the behavior of materials when there is the likelihood of cracks. Fracture mechanics can supply the methodology needed to compensate for the inadequacies of conventional design criteria. Several existing valid fracture criteria which can predict the behavior of cracked bodies are discussed in this chapter. The discussion is divided into three parts: (1) the Griffith criterion, (2) the critical J (J_{IC}) criterion, and (3) the crack-tip opening displacement (COD) criterion.

Griffith Criterion

Although fracture mechanics has been developed mainly in the last two decades, one of the basic equations was established in 1921 by Griffith [35]. His principal contribution was an analysis of crack stability based on energy equilibrium. Griffith stated that crack growth can occur only if the energy released upon crack extension is sufficient to provide all the energy that is required for crack growth. If this is not the case, then the stress has to be increased. The condition for crack growth is:

$$\frac{\partial U}{\partial a} = \frac{\partial S}{\partial a}$$

where U is the strain energy, S is the energy required for crack growth, and a is the crack length.

Usually $\partial U/\partial a$ is replaced by G which is the so-called "energy release rate" or "crack extension force". To a first approximation it can be assumed that $\partial S/\partial a$ is a constant. This means that G must be at least equal to a certain critical value G_{IC} ($= \partial S/\partial a$) before crack growth can occur. Also G_{IC} can be related to the "plane strain fracture toughness" (or the critical stress intensity factor) K_{IC} by a simple formula. i.e.

$$\frac{K_{IC}^2}{E} = G_{IC} \qquad \text{(Plane stress)}$$

and

$$\frac{(1-\nu^2)K_{IC}^2}{E} = G_{IC} \qquad \text{(Plane strain)}$$

where E is Young's modulus and ν is Poisson's ratio. The subscript "I" stands for mode I (Appendix A).

It should be noted that the above relations are valid only if the material is truely brittle and $\partial S/\partial a$ consists of surface energy only. However, for ductile materials, significant plastic deformation occurs at the crack-tip. Thus, $\partial S/\partial a$ includes not only the surface energy, but also a quantity called "plastic work". In other words, the G_{IC} fracture criterion is not applicable for ductile materials.

Critical $J(J_{IC})$ Criterion

The well-known path independent J integral of fracture mechanics,

introduced by Eshelby [21] and Rice [22] has played an important role in the analysis of crack extension. This line integral has the same value for all paths surrounding the crack tip in the two-dimensional strain field of an elastic (linear or nonlinear) or deformation-type elastic-plastic materials. The J-integral is defined (for small deformations) as:

$$J = \int_{\Gamma} \left(W \, dx_2 - T_i \frac{\partial U_i}{\partial x_1} \, ds \right) \tag{2.1}$$

Where x_1 and x_2 are Cartesian coordinates (x_2 being perpendicular to the crack surface), ds is a differential arc length along any contour Γ beginning along the bottom surface of the crack and ending along the top surface, W is the strain energy density, T_i are components of traction on the surface of the interior body cut by Γ, and U_i are displacement components (See Figure 3).

In the case of an elastic solid, the J-integral can be interpreted as the rate of energy release per unit crack extension [36]. This energy release interpretation of J cannot be applied to the process of crack extension in elastic-plastic solids even with a deformation theory of plasticity. Rather, under the use of the deformation theory of plasticity, the J-integral can be interpreted as "the potential energy difference between two identically loaded bodies having neighboring crack sizes" [32]. That is

$$J = - \frac{\partial V}{\partial a} \tag{2.2}$$

where V is the potential energy and a is the crack length.

To develop the fracture criterion which can be applicable to large-scale yielding problems, called J_{IC} criterion, Begley and Landes [32,33] suggested a procedure for calculating the J-integral from the experimental load versus representative displacement curves of standard fracture toughness test specimens. The load-displacement (P versus δ) curves can be easily converted into potential energy - crack length curves and then into the J-integral - displacement curves by using formula (2.2). Given the J versus displacement relationship for a given crack size and assuming the critical fracture displacement is known, the critical value J_{IC} can then be determined. However, this method required both procurement and analysis of a large quantity of experimental load-displacement data which is both time consuming and costly.

In Begley and Landes [32,33], the measurement point for J_{IC} was not precisely defined. Later, Landes and Begley [37] suggested a way of picking the J_{IC} measurement point by presenting the experimental J data in the form of a resistance curve by plotting J versus the measured crack extension Δa (Figure 4). By assuming that the initial crack stretch zone is approximately 1/2 of the crack opening displacement (COD), and that COD = $(J/\lambda\sigma_y)$ (σ_y is the yield stress, and λ is a constant which is assumed to be 1 in [37]), a J value versus stretch zone line ($J = 2\sigma_y \Delta a$) is constructed. The intersection point between this stretch zone line and the curve fitted to the J versus measured crack extension (Δa) point was suggested as a method of defining the J_{IC} measurement point (See Figure 4). As will be discussed in Chapter 7,

great discrepancies appear to exist among the various estimates given in literature for the constant λ ranging from $\pi/4$ to greater than 2. More detailed discussions regarding crack-opening displacement (COD) are given in the next section.

Rice et al. [38] in 1972 proposed a simple empirical method for measuring J from a single specimen test data for deeply notched bend type test specimens. For this technique a bend type specimen, bend bar, or compact tension with a deep crack is loaded to the displacement of interest and J is determined as a function of the displacement from the expression

$$J = \frac{2A}{Bb} \tag{2.3}$$

where A is the area under the load-displacement curve taken at the displacement of interest, B is the specimen thickness, and b is the length of the uncracked ligament.

More recently, corrections to this empirical formula to account for not only the bending effect, but also for the effect of axial force in the case of a compact tension specimen, were derived by Merkle and Corten [39]. The empirical formula of Merkle and Corten [39] can be stated as,

$$J = \frac{1}{2}\frac{P^2}{B}\frac{\partial\left(\frac{1}{K}\right)}{a} + \frac{2(1+\alpha)}{b(1+\alpha^2)}\int_0^{\Delta_P}\left(\frac{P}{B}\right)\,d\Delta_p + \frac{2\alpha}{b}\frac{(1-2\alpha-\alpha^2)}{(1+\alpha^2)^2}\int_0^{\frac{P}{B}}\Delta_p\,d\left(\frac{P}{B}\right) \tag{2.4}$$

where

$$\alpha = \left[\left(\frac{a}{c}\right)^2 + 2\left(\frac{a}{c}\right) + 2\right]^{1/2} - \left(\frac{a}{c} + 1\right)$$

and further, a = crack length, c = half the net ligament width, p = applied force, B = specimen thickness, k = elastic stiffness at the load point, Δ_p = plastic displacement of the applied load due to the crack, and b = 2C. The accuracy of formulae (2.3) and (2.4) will also be compared and discussed in Chapter 7.

Bucci, et al. [34] used an approximate procedure for estimating the relation between J and the displacement δ. This method extrapolates from the small scale yielding range into the fully plastic range using Irwin's plasticity adjustments of the elastic predictions together with results based on a perfect plasticity analysis. This highly approximate procedure is limited to materials of the elastic-perfectly plastic types of behavior.

Goldman and Hutchinson [40] developed another approximate procedure for obtaining J versus δ relation for materials characterized by a pure power hardening relation between stresses and strains in simple tension problems. Thus there is the need for solving the more difficult problem of computing J-δ relations for elastic-plastic materials with strain hardening under large scale yield conditions.

We note that the theoretical frame work of [32,33,34,37,40] is restricted to problems considering a deformation theory of plasticity. For the path independence of J in elastic-plastic problems the materials

must follow the deformation theory of plasticity. When a J_2-flow theory is used, a general proof of path-independence of the J integral cannot be formulated even in the absence of unloading since the strain energy is no longer a unique function of strains. However, as was mentioned in Chapter I, under monotonic loading, approximate path independence of the J-integral can be expected even under J_2-flow theory of plasticity.

Since the present research is based on finite deformation analysis, the J-integral applicable to infinitesimal deformations as introduced by (2.1) needs to be redefined. As shown by Knowles and Sternberg [41], the modified J-integral (for finite deformations) can be written as

$$J = \int_{\Gamma} \left[W \, dx_2 - t_i \frac{\partial U_i}{\partial x_1} \, dS \right] \qquad (2.5)$$

where t_i are Piola-Lagrange tractions, derived from the unsymmetric Piola-Lagrange stress tensor, t_{ij}. Thus, $t_i = n_j t_{ji}^{(N)}$, where n_j are the direction cosines of a unit normal to Γ in the initial configuration. U_i are the total displacements. x_1, x_2 are Cartesian coordinates.

The unsymmetric Piola-Lagrange stress tensor $t_{ij}^{(N)}$, measured per unit area in the initial undeformed state* C_o and, in the fixed Cartesian metric, is related to the symmetric Kirchhoff-Trefftz stress ($S_{ij(O)}^{(N)}$), measured per unit area in C_o state but in the deformed metric in C_N state, and symmetric Euler stress ($\tau_{ij}^{(N)}$), measured per unit area in C_N

*An elaborate discussion of the loading path is given in Chapter IV.

state and in the metric of the fixed Cartesian system, through the relations [31]

$$t^{(N)}_{mj} = \tau^{(N)}_{ij} \frac{\partial x_m}{\partial X^N_i} \det [J] = S^{(N)}_{mn(O)} \frac{\partial X^N_j}{\partial x_n}$$

where X^N_i are coordinates of a material point in C_N state, χ_i are material coordinates in C_o state and

$$\det[J] = \det \left| \frac{\partial X^N_\ell}{\partial x_m} \right|$$

Thus, as stated earlier, under a J_2-flow theory of plasticity, the approximate path-independent J integral (for finite deformations) can be defined by

$$J = \int_\Gamma \left[\left(\int_o^{e_{ij}} t_{ij} \, de_{ij} \right) dx_2 - t_i \frac{\partial U_i}{\partial x_1} \, dS \right] \tag{2.6}$$

where t_{ij} is the Piola-Lagrange stress at any point and $e_{ij} = u_{j,i}$ is the total deformation gradient at that point.

Now, in a given plane crack problem of arbitrary domain, arbitrary loading, and arbitrary strain hardening material properties, the present finite element numerical computation procedure can be used to compute the desired J-δ relation directly. When the critical J_{IC} governing the onset of crack growth is determined experimentally, it becomes a material parameter. Comparing the J value of interest with

the material parameter J_{IC}, the situation can thus be assessed as to whether or not the crack in the given case is on the verge of growing.

For small-scale yielding, Rice [21] has shown that J is equal to the energy release rate. This implies that, for small-scale yielding, J_{IC} is related to plane strain fracture toughness K_{IC} (mode I) as

$$J_{IC} = G_{IC} = \frac{K_{IC}^2}{E} \qquad \text{(plane stress)}$$

$$= \frac{(1-\nu^2)\, K_{IC}^2}{E} \qquad \text{(plane strain)} \tag{2.7}$$

Since the J-integral approach to elastic-plastic fracture is based on a model which allows large-scale yielding, the approach represents a considerable advance in the important engineering problem of characterizing plane strain fracture toughness of materials using inexpensive and small fracture test specimens.

Again, it is emphasized that the criterion $J = J_{IC}$ is a criterion of initiation of crack growth without any statement of stability or instability. However, in cases where there is significant stable crack growth, i.e., instability occurs when the value J_{IC} is reached, then it is also a fracture criterion.

Crack-tip Opening Displacement (COD) Criterion

The COD concept was first proposed by Wells [42,43] as a possible ductile fracture criterion to deal with crack problems in high toughness materials. If the COD ductile criterion is adopted, then there exists a critical $(COD)_C$ which is to be established as a material

constant and crack extension or fracture could be assumed to occur as soon as the COD exceeds this critical value $(COD)_C$. As shown in Reference [44], this criterion is equivalent to the G_{IC} (or K_{IC}) criterion in cases where linear elastic fracture mechanics is applicable. This generates some confidence in the general validity of this scheme.

However, one of the drawbacks of the COD criterion is the fact that there is a considerable amount of ambiguity regarding the definition of the COD. Strictly speaking, at the very crack tip the displacement is actually zero, and the COD is therefore a fictitious displacement. Ideas such as defining the position of the COD to be at the intercept of the elastic-plastic boundary with the crack profile; or *defining COD* to be the diameter of a circle inscribed in the crack-surface near the stationary crack-tip have been discussed by Srawley et al. [24]. From the theoretical treatments [21,44,45] the relations between COD and the energy release rate G (or the J-integral) for mode I case can be roughly expressed as:

$$COD = \frac{G_I}{\lambda \sigma_y} = \frac{J}{\lambda \sigma_y}$$

and from (2.7)

$$COD = \frac{(1-\nu^2)K_I^2}{\lambda\ \sigma_y\ E} \quad \text{(for small-scale yielding approximations)} \qquad (2.8)$$

where σ_y is the yield stress and λ is a constant. K_I is the stress intensity factor and the factor $(1-\nu^2)$ can be deleted for plane stress

situations.

It is noted that earlier analyses in literature produced a varying range of values for λ: Calculations by Burdekin and Stone [46], Bilby et al. [47], Rice [21] using the Dugdale model and small-scale yielding considerations, and the experimental work of Robinson and Tetelman [23] show $\lambda \sim 1$; Wells' [42] analysis, $\lambda = \pi/4$; deformation plasticity analysis (small deformation theory) by Hutchinson-Rice-Rosengren [2,3] shows $\lambda = 1.27$. The result obtained by Rice and Johnson [45] which considers the finite deformation effects near the crack-tip using a rigid-plastic slip line theory (for small-scale yielding) yields $\lambda = 1.48$. Finite element analysis by Hayes and Turner [48] and by Levy et al. [49] yields λ values of 2 and 2.14, respectively.

A direct measurement of COD is certainly difficult and virtually impossible in a routine test. It can be obtained indirectly by measuring K_I and using Equation (2.8), or by using some measurable displacement data from experiments in conjunction with derived relations. Thus, there exist some definitions of COD as related to the measurable crack-mouth opening displacements (or clip gage displacement CGD) through calibration obtained from experiments on standard test specimens, such as by Robinson and Tetelman [23], the British CODA panel [25], and by Wells [26].

Based on measurement of COD using silicone rubber infiltration techniques, Robinson and Tetelman [23] proposed a calibration curve between COD and CGD of cracked three-point bend specimens given by:

$$B_o + B_1(\text{COD}) + B_2(\text{COD})^2 + B_3(\text{COD})^3 + B_4(\text{COD})^4 = 0 \qquad (2.9)$$

where

$$B_o = 0.03684\ (CGD)$$

$$B_1 = 3.899\ (CGD) - \left(\frac{a+z}{w-a}\right) - 0.03684$$

$$B_2 = -\ 16.34\ (CGD) - 3.899$$

$$B_3 = 27.24\ (CGD) + 16.34$$

$$B_4 = -\ 27.24$$

W is the specimen width, a is the crack length, and z is the height of the knife edges above the specimen surface. Equation (2.9) can be solved using standard computer programs thereby giving on-load COD values directly from measurements of on-load clip gage displacement and specimen geometry only.

A linear relationship between COD and V_M(CGD) recommended in CODA [25] is

$$COD = \left[\frac{0.33(w-a)}{0.33w + 0.67a}\right] V_M \qquad (2.10)$$

A modification to the above, suggested by Wells [26] is given by:

$$COD = \frac{0.45\ (w-a)}{0.45w + 0.55a}\left[\frac{V_M^2\, E}{4\gamma\sigma_y w(1-\nu^2)}\right] \quad ; \quad V_M \leq \frac{2\gamma\sigma_y w(1-\nu^2)}{E} \qquad (2.11)$$

$$COD = \frac{0.45(w-a)}{0.45w + 0.55a}\left[V_M - \frac{\gamma\sigma_y w(1-\nu^2)}{E}\right] ; \; V_M > \frac{2\gamma\sigma_y w(1-\nu^2)}{E} \qquad (2.12)$$

where $\gamma = 1.54$ for the present specimen, $a/w = 0.5$.

The Equation (2.11) is such that COD varies as $V_M^2(CGD^2)$ up to the point of attainment of significant plasticity* in the net-section ligament, and afterwards linearly with $V_M(CGD)$.

In Chapter VII, based on these various definitions of COD, an attempt was made to obtain COD from the computed results and to examine its correlation with the J-integral. Also, an appropriate suggested value of λ in Equation (2.8) is given.

It is worthwhile to discuss the applicability of the COD criterion. Robinson and Tetelman [23] recently proposed the use of two initiation detection methods to determine critical $(COD)_C$ for measurements of K_{IC} using "small" specimens. Since the structure fails at the same $(COD)_C$, Equation (2.8) can be used to determine K_{IC}. Since the fracture toughness can be determined from a $(COD)_C$ measurement taken on a small specimen, the large expensive valid ASTM K_{IC} specimens would not be necessary.

However, since Equation (2.8) is not applicable to materials with high toughness, a K_{IC} cannot be determined. Yet the COD may be used to rank high toughness materials in accordance with their fracture resistance. Thus, this concept as well as the J-integral can be used to establish a basis for material selection and procurement.

---

*This appears to be corroborated by theoretical arguments: (a) in the linear elastic analysis (or a small-scale yielding approximation) the CGD is proportional to the load, and then to the stress intensity factor K, i.e., $CGD = \beta K$, where β is a constant, (b) in the small-scale yielding range, from equation (2.8), $COD = K_I^2(1-\nu^2)/(\lambda\sigma_y E)$ and thus $COD = (CGD)^2(1-\nu^2)/(\beta^2\lambda E\sigma_y)$.

CHAPTER III

PLASTICITY RELATIONS

As a first step in the computation procedure, it is important to clarify the elastic-plastic behavior of cracked structures under unloading situations when one studies the mechanism of crack propagation. Under the use of the J_2 incremental flow theory, as known earlier, unique relations do not exist in general between stress and strain components. Therefore, for an elastic-plastic finite element analysis, the stress-strain relations which have been familiar to us in the theory of elasticity must be replaced by relations between increments of stress and strain in developing theories of plasticity. That is,

$$d\sigma_{ij} = E^{t}_{ijk\ell}\, d\epsilon_{k\ell} \tag{3.1}$$

where $d\sigma_{ij}$ and $d\epsilon_{ij}$ are the incremental stresses and incremental total strains respectively. $E^{t}_{ijk\ell}$ is the current constitutive property, as modified by plasticity. Moreover, during an infinitesimal increment of stress, changes of strain are assumed to be divided into elastic and plastic parts, thus,

$$d\epsilon_{ij} = d\epsilon^{e}_{ij} + d\epsilon^{p}_{ij}$$

Hooke's law gives

$$d\sigma_{ij} = E_{ijk\ell}\, d\epsilon^{e}_{k\ell} \tag{3.2}$$

where $E_{ijk\ell}$ is the well-known constant elasticity compliance tensor. In matrix notation, (3.1) and (3.2) can be rewritten as:

$$\{d\sigma\} = [E]^t \{d\epsilon\}$$

and

$$\{d\sigma\} = [E] \{d\epsilon^e\}$$

For two-dimensional elastic problem, [E] is shown as:

$$[E] = \begin{bmatrix} \frac{E}{1-\nu^2} & \frac{E\nu}{1-\nu^2} & 0 \\ & \frac{E}{1-\nu^2} & 0 \\ \text{-sym-} & & \frac{E}{2(1+\nu)} \end{bmatrix} \qquad \text{(plane stress)}$$

$$= \begin{bmatrix} \frac{E(1-\nu)}{(1+\nu)(1-2\nu)} & \frac{\nu E}{(1+\nu)(1-2\nu)} & 0 \\ & \frac{(1-\nu)E}{(1+\nu)(1-2\nu)} & 0 \\ \text{-sym-} & & \frac{E}{2(1+\nu)} \end{bmatrix} \qquad \text{(plane strain)}$$

To describe the plastic behavior of a material correctly, one must choose: (1) an initial yield criterion, (2) a flow rule, and (3) a hardening rule. Yamada et al. [50] and Miyamoto et al. [51] derived the matrix $[E]^t$ based on the Hencky-Mises-Huber yield criterion and Drucker's normality flow rule [52,53]. However, Yamada et al.'s approach was restricted to the problem made of isotropically

hardening material. Miyamoto et al. dealt with kinematically hardening material, as proposed by Prager [19] and then modified by Ziegler [20], and carried out plane stress analysis only.

Now, the derivation of $[E]^t$ in this current research can be briefly stated as follows:

(1) The Hencky-Mises-Huber yield criterion, which describes a smooth surface in stress space and be represented by a simple mathematical function, is still chosen as the initial yield condition. That is

$$f(\sigma_{ij}) = \frac{3}{2}\,\sigma'_{ij}\sigma'_{ij} - \sigma_y^2 = 0 \;;$$

$$\sigma'_{ij} = \sigma_{ij} - \frac{1}{3}\,\sigma_{kk}\,\delta_{ij}$$

where σ_{ij}, σ_y, σ'_{ij} are the stress tensor, yield stress and deviatoric stress respectively. With consideration limited to plane stress situations ($\sigma_z = \sigma_{yz} = \sigma_{xz} = 0$), the Hencky-Mises-Huber function is represented as

$$f(\sigma_{ij}) = \sigma_x^2 + \sigma_y^2 - \sigma_x\sigma_y + 3\tau_{xy}^2 - \sigma_y^2 = 0 \quad .$$

However, for a plane strain case (viz $\epsilon_z = \gamma_{xz} = \gamma_{yz} = 0$, $\sigma_z = \nu(\sigma_x + \sigma_y)$) a different Huber-Mises-Hencky yield criteria obtained, say,

$$f(\sigma_{ij}) = \sigma_x^2 + \sigma_y^2 + \sigma_z^2 - \sigma_x\sigma_y - \sigma_x\sigma_z - \sigma_y\sigma_z + 3\tau_{xy}^2 - \sigma_y^2 = 0$$

(2) The flow rule, which is based on Drucker's postulate for work-hardening materials, is a constitutive relation between increments

of plastic strain $d\epsilon_{ij}^{P}$ on the one hand and stress and stress increments on the other [53]. The Drucker's normality flow rule, represented in tensor form, is written here as

$$d\epsilon_{ij}^{P} = d\lambda \frac{\partial f(\sigma_{ij},\alpha_{ij})}{\partial \sigma_{ij}} \tag{3.3}$$

where $f(\sigma_{ij},\alpha_{ij})$ represents the loading function, used to determine subsequent yielding from some plastic state; α_{ij} is a measure of the degree of work hardening. The positive scalar quantity $d\lambda$ can be determined by the assumption that the vector $cd\epsilon_{ij}^{P}$, shown in Figure 6, is the projection of $d\sigma_{ij}$ on the exterior normal to the loading surface at the instantaneous stress state. Thus, we have

$$(d\sigma_{ij} - cd\epsilon_{ij}^{P}) \frac{\partial f}{\partial \sigma_{ij}} = 0$$

$$d\lambda = \frac{1}{c} \frac{\dfrac{\partial f}{\partial \sigma_{ij}} \, d\sigma_{ij}}{\dfrac{\partial f}{\partial \sigma_{k\ell}} \dfrac{\partial f}{\partial \sigma_{k\ell}}} \tag{3.4}$$

The parameter c corresponds to the slope of the uniaxial stress σ_{ij} versus plastic strain ϵ_{ij}^{P} in tension (or compression).

(3) As to the hardening rule, there are mainly two versions in use. The isotropic hardening rule, given by Hill and Hodge [52,54], assumes that during plastic flow the loading surface expands uniformly about the origin in stress space, maintaining the same shape, center location, and orientation as the yield surface. Figure 5 illustrates, on the basis of a simplification to a two dimensional plot, the yield

and loading surfaces when stress state shifts from point 1 to point 2. Unloading and subsequent reloading in the reverse direction result in yielding at the stress state represented by point 3. The path 2-3 will be elastic, and 0-2 is equal to 0.3. σ_1 and σ_2 are the principal stresses.

Another rule, so-called kinematic hardening rule [19,20], assumes that during plastic deformation the loading surface translates as a rigid body in stress space, maintaining the size, shape, and orientation of the yield surface. As a consequence of assuming a rigid translation of the loading surface, kinematic hardening rule predicts an ideal Bauschinger effect [55,56,57] for completely reversed loading conditions; i.e., the magnitude of the increase of yield stress in one direction results in a decrease of yield stress of the same magnitude in the reverse direction. However, as shown in Figure 5, isotropic hardening rule provides that the material will exhibit an increase in the compressive yield stress equal to the increase in the tensile yield stress. Thus, this theory does not account for the Bauschinger effect exhibited by most structural materials. Furthermore, since the plastic deformation is actually an anisotropic process, the isotropic hardening theory is rejected in this research.

A similar pictorial illustration of kinematic hardening rule is provided in Figure 5. Denoting the translation of the center of the yield surface by α_{ij}, we may represent the loading function in the form $f(\sigma_{ij}-\alpha_{ij})$; the subsequent yield condition is given as

$$f(\sigma_{ij} - \alpha_{ij}) = 0 \quad . \tag{3.5}$$

The increment of translation of the loading surface $d\alpha_{ij}$, as given by Ziegler [20]. is computed at each loading step and summed to determine the total translation α_{ij}. It is assumed that $d\alpha_{ij}$ is directed along the radius vector connecting the center of the loading surface to the instantaneous stress state in stress space (Figure 6). Thus,

$$d\alpha_{ij} = d\mu(\sigma_{ij} - \alpha_{ij}) \tag{3.6}$$

The scalar $d\mu$ can be determined by the condition that the stress state must remain on the translated loading surface during plastic deformation. For infinitesimal increments, this condition can be represented as

$$(d\sigma_{ij} - d\alpha_{ij}) \frac{\partial f}{\partial \sigma_{ij}} = 0 \tag{3.7}$$

Substituting Equation (3.6) into Equation (3.7), we have

$$d\mu = \frac{\frac{\partial f}{\partial \sigma_{mn}} d\sigma_{mn}}{(\sigma_{k\ell} - \alpha_{k\ell}) \frac{\partial f}{\partial \sigma_{k\ell}}}$$

and

$$d\alpha_{ij} = \frac{(\sigma_{ij} - \alpha_{ij}) \frac{\partial f}{\partial \sigma_{k\ell}} d\sigma_{k\ell}}{(\sigma_{mn} - \alpha_{mn}) \frac{\partial f}{\partial \sigma_{mn}}} \tag{3.8}$$

Also, using Equation (3.3) and Equation (3.4), the flow rule now becomes

$$d\epsilon_{ij}^{P} = \frac{1}{c}\frac{\partial f}{\partial \sigma_{ij}} \frac{\dfrac{\partial f}{\partial \sigma_{mn}} d\sigma_{mn}}{\dfrac{\partial f}{\partial \sigma_{k\ell}}\dfrac{\partial f}{\partial \sigma_{k\ell}}} \tag{3.9}$$

Next, $d\epsilon_{ij}^{e} = d\epsilon_{ij} - d\epsilon_{ij}^{P}$. Through Equations (3.2), (3.5) and (3.9), after some manipulations, the relation between the incremental stresses $d\sigma_{ij}$ and incremental total strains $d\epsilon_{ij}$ can be easily obtained. For purpose of brevity and completion, both the end results of plane stress and plane strain cases are quoted as follows:

(1) for plane stress case

$$\begin{Bmatrix} d\sigma_x \\ d\sigma_y \\ d\tau_{xy} \end{Bmatrix} = \begin{bmatrix} \frac{E}{1-\nu^2} - \frac{S_1^2}{S} & \frac{E\nu}{1-\nu^2} - \frac{S_1 S_2}{S} & -\frac{S_1 S_3}{S} \\ & \frac{E}{1-\nu^2} - \frac{S_2^2}{S} & -\frac{S_2 S_3}{S} \\ \text{sym} & & \frac{E}{2(1+\nu)} - \frac{S_3^2}{S} \end{bmatrix} \begin{Bmatrix} d\epsilon_x \\ d\epsilon_y \\ d\gamma_{xy} \end{Bmatrix} \tag{3.10}$$

where

$$S_1 = \frac{E}{1-\nu^2}\left(\frac{\partial f}{\partial \sigma_x} + \nu \frac{\partial f}{\partial \sigma_y}\right)$$

$$S_2 = \frac{E}{1-\nu^2}\left(\nu \frac{\partial f}{\partial \sigma_x} + \frac{\partial f}{\partial \sigma_y}\right)$$

$$S_3 = \frac{E}{1+\nu}\frac{\partial f}{\partial \tau_{xy}}$$

$$S = CQ + S_1 \frac{\partial f}{\partial \sigma_x} + S_2 \frac{\partial f}{\partial \sigma_y} + 2S_3 \frac{\partial f}{\partial \tau_{xy}}$$

$$Q = \left(\frac{\partial f}{\partial \sigma_x}\right)^2 + \left(\frac{\partial f}{\partial \sigma_y}\right)^2 + 2\left(\frac{\partial f}{\partial \tau_{xy}}\right)^2$$

$$\frac{\partial f}{\partial \sigma_x} = 2(\sigma_x - \alpha_x) - (\sigma_y - \alpha_y)$$

$$\frac{\partial f}{\partial \sigma_y} = 2(\sigma_y - \alpha_y) - (\sigma_x - \alpha_x)$$

$$\frac{\partial f}{\partial \tau_{xy}} = 3(\tau_{xy} - \alpha_{xy})$$

(2) plane strain case

$$\begin{Bmatrix} d\sigma_x \\ d\sigma_y \\ d\tau_{xy} \end{Bmatrix} = \begin{bmatrix} \frac{E(1-\nu)}{(1+\nu)(1-2\nu)} - \frac{S_1^2}{S} & \frac{\nu E}{(1+\nu)(1-2\nu)} - \frac{S_1 S_2}{S} & -\frac{S_1 S_3}{S} \\ & \frac{(1-\nu)E}{(1+\nu)(1-2\nu)} - \frac{S_2^2}{S} & -\frac{S_2 S_3}{S} \\ \text{——— sym. ———} & & \frac{E}{2(1+\nu)} - \frac{S_3^2}{S} \end{bmatrix} \begin{Bmatrix} d\epsilon_x \\ d\epsilon_y \\ d\gamma_{xy} \end{Bmatrix} \qquad (3.11)$$

where

$$S_1 = \frac{E}{(1+\nu)(1-2\nu)} \left\{ (1-\nu) \frac{\partial f}{\partial \sigma_x} + \nu \frac{\partial f}{\partial \sigma_y} \right\}$$

$$S_2 = \frac{E}{(1+\nu)(1-2\nu)} \left\{ \nu \frac{\partial f}{\partial \sigma_x} + (1-\nu) \frac{\partial f}{\partial \sigma_y} \right\}$$

$$S_3 = \frac{E}{(1+\nu)} \frac{\partial f}{\partial \tau_{xy}}$$

$$S = CQ + S_1 \frac{\partial f}{\partial \sigma_x} + S_2 \frac{\partial f}{\partial \sigma_y} + 2S_3 \frac{\partial f}{\partial \tau_{xy}}$$

$$Q = \left(\frac{\partial f}{\partial \sigma_x}\right)^2 + \left(\frac{\partial f}{\partial \sigma_y}\right)^2 + 2\left(\frac{\partial f}{\partial \tau_{xy}}\right)^2$$

$$\frac{\partial f}{\partial \sigma_x} = \frac{3}{2}\left[(\sigma_x - \alpha_x) - (\sigma_y - \alpha_y)\right]$$

$$\frac{\partial f}{\partial \sigma_y} = \frac{3}{2}\left[(\sigma_y - \alpha_y) - (\sigma_x - \alpha_x)\right]$$

$$\frac{\partial f}{\partial \tau_{xy}} = 3(\tau_{xy} - \alpha_{xy})$$

Whenever the initial stresses σ_{ij}, the total translation α_{ij}, and $\partial f/\partial \sigma_{ij}$ are given on the state C_N, and the incremental stresses $d\sigma_{ij}$ from state $C_N \rightarrow C_{N+1}$ are known, then $d\alpha_{ij}$ from state $C_N \rightarrow C_{N+1}$ can be evaluated by (3.8). This follows that $\alpha_{ij}^{(N+1)} = \alpha_{ij}^{(N)} + d\alpha_{ij}$ and $[E^t]$ can be obtained. It is to be noted that all the state variables, such as stresses, strains, displacements and the total yield surface translations are taken as zero at the initial undeformed state C_o.

CHAPTER IV

FORMULATION OF FINITE ELEMENT MODELS FOR ELASTIC-PLASTIC, FINITE DEFORMATION PROBLEMS

In the present chapter, finite element models for a nonlinear cracked problem with geometrical and material nonlinearity are to be formulated. The deformation of the cracked body is characterized by the features that not only its displacements are finite, but also its strains are no longer small, and the material behavior is elastic-plastic.

The first section is devoted to the formulation of an incremental theory by combining the Eulerian and Lagrangean approaches. A detailed survey of this continuously updated incremental theory which provides a basis for the formulation of the finite element method is also presented in detail.

In the second and third sections, the variational formulation of the finite element method is created with emphasis on the modification of the conventional variational principle. Since the most commonly used compatible displacement finite element model in each element cannot represent the asymptotic singular behaviors in the vicinity of the crack-tip, an alternative finite element formulation is needed. In such a formulation, one should be able to incorporate the exact asymptotic form of solution for singular stresses and strains in elements near the crack-tip and maintain the inter-element continuity of displacements and tractions between the near field elements with

singular basis and the far field regular elements. One such formulation used in this work is the hybrid displacement finite element model. However, in the far field region, the compatible displacement finite element model is still employed for sake of simplicity.

In the fourth section, several general incremental numerical methods which have been developed in dealing with nonlinear problems using finite element method are discussed. For the present finite deformation investigations, the so-called "tangent modulus method" is found to be most appropriate.

Lastly, the calculation procedure limited to the stationary crack case is summarized in the last section of this chapter.

A Continuously Updated Lagrangean Incremental Theory

Assuming the loading path of the nonlinear cracked problem can be divided into a number of equilibrium states

$$C_o, C_1, C_2 \cdots C_N \cdots$$

where C_o is the initial undeformed state, while C_N is an arbitrary intermediate state. It is assumed that all the state variables, such as stresses, strains, displacements and the total yield surface translations, together with the loading history, are known up to the C_N state. The interest is then to formulate an updated Lagrangean incremental theory for determining all the state variables in the current state, say C_{N+1} state, under an assumption that the C_{N+1} state is incrementally close to the C_N state and all the governing equations may be linearized with respect to the incremental quantities. In this

theory, all the state variables are defined with respect to the reference state, say C_N state.

Let the position vectors of an arbitrary material point of the structure in the C_0, C_N and C_{N+1} states be denoted by $\underset{\sim}{R}^{(0)}$, $\underset{\sim}{R}^{(N)}$ and $\underset{\sim}{R}^{(N+1)}$ respectively. $x_i, X_i^{(N)}$ and $X_i^{(N+1)}$ are the corresponding different Cartesian coordinate variables, thus

$$\underset{\sim}{R}^{(0)} = x_i \hat{e}_i$$

$$\underset{\sim}{R}^{(N)} = X_i^{(N)} \hat{e}_i = (x_i + U_i)\hat{e}_i$$

$$\underset{\sim}{R}^{(N+1)} = X_i^{(NH)} \hat{e}_i = (X_i^{(N+1)} + \Delta U_i)\hat{e}_i$$

where $\hat{e}_i$ are the base vectors of the rectangular Cartesian coordinates, while U_i are the total displacement component from C_0 to C_N. ΔU_i denote the incremental displacement components from C_N to C_{N+1}. Let the true (Eulerian) symmetric stress tensor in C_N be $\tau_{ij}^{(N)}$, measured per unit area in C_N and in the metric of the fixed Cartesian system. The new stress in C_{N+1}, due to the additional incremental loading, will be represented by the Kirchhoff-Trefftz stress tensor $S_{ij(N)}^{(N+1)}$, which is measured per unit area in C_N but in the deformed-metric in C_{N+1}. Thus

$$S_{ij(N)}^{(N+1)} = \tau_{ij}^{(N)} + \Delta S_{ij} \tag{4.1}$$

where the Truesdell stress increment ΔS_{ij} can be determined by the elastic-plastic constitutive law (3.10) and (3.11), using the appropriate notations, say

$$\Delta S_{ij} = E^{t}_{ijk\ell}\, \Delta g_{k\ell} \tag{4.2}$$

Here, $\Delta g_{k\ell}$ denotes the total incremental Green strain tensor from C_N state to C_{N+1} state, with reference to the metric in C_N. It is defined as

$$\Delta g_{ij} = \frac{1}{2}\,(\Delta U_{i,j} + \Delta U_{j,i} + \Delta U_{k,i}\Delta U_{k,j}) \tag{4.3}$$

where a comma "," denotes a covariant differentiation with respect to coordinates $X_i^{(N)}$. Since ΔU_i is assumed small for <u>each</u> load increment, Δg_{ij} can be linearized as follows:

$$\Delta g_{ij} \sim \Delta \epsilon_{ij} = \frac{1}{2}\,(\Delta U_{i,j} + \Delta U_{j,i})$$

We denote the body forces by $\bar{F}_i^{(N)}$, and the surface tractions on S_σ by $\bar{T}_i^{(N)}$ in the C_N state. It is noted here that $\bar{T}_i$ are defined per unit area and $\bar{F}_i$ are defined per unit volume of the C_N state. On the other hand, we define the body forces $\bar{F}_i^{(N)} + \Delta\bar{F}_i$ and the surface tractions $\bar{T}_i^{(N)} + \Delta\,\bar{T}_i$ on S_σ in the C_{N+1} state, where it is also understood that all these quantities are defined per unit volume and per unit area of the C_N state. Thus, the principle of virtual work then states,

$$\int_V [(\tau_{ij}^{(N)} + \Delta S_{ij})\delta\Delta g_{ij} - (\bar{F}_i^{(N)} + \Delta\bar{F}_i)\delta\Delta U_i]dV$$

$$- \int_{S\sigma} (\bar{T}_i^{(N)} + \Delta\bar{T}_i)\delta\Delta U_i \, dS = 0 \tag{4.4}$$

where

$$\Delta U_i = \Delta\bar{U}_i \qquad \text{on} \qquad Su$$

and where a bar " − " denotes a prescribed quantity. ΔS_{ij} and Δg_{ij} are given by Equations (4.2) and (4.3). In Equation (4.4), the volume v, and the surfaces S_σ and S_u refer to the known reference state C_N, and a "δ" denotes variations. $\delta\Delta U_i$ vanishes on S_u. Equation (4.4) can be written as

$$\int_V [\Delta S_{ij}\delta\Delta g_{ij} + \frac{1}{2}\tau_{ij}^{(N)}\delta(\Delta U_{k,i}\Delta U_{k,j}) - \Delta\bar{F}_i\delta\Delta U_i]dV - \int_{S_\sigma}\Delta\bar{T}_i\delta\Delta U_i dS$$

$$= \int_V (-\tau_{ij}^{(N)}\delta\Delta\epsilon_{ij} + \bar{F}_i^{(N)}\delta\Delta U_i)dV + \int_{S_\sigma}\bar{T}_i^{(N)}\delta\Delta U_i\, dS$$

Since ΔS_{ij}, Δg_{ij} and $\tau_{ij}^{(N)}$ are symmetric, using Equation (4.2), the above equation can be rearranged as

$$\delta\Big\{\int_V \Big[\frac{1}{2}E^t_{ijk\ell}\,\Delta g_{ij}\,\Delta g_{k\ell} + \frac{1}{2}\tau_{ij}^{(N)}\,\Delta U_{k,i}\Delta U_{k,j} - \Delta\bar{F}_i\Delta U_i\Big]dV - \int_{S_\sigma}\Delta\bar{T}_i\Delta U_i dS\Big\}$$

$$= \delta\Big\{\int_V (-\tau_{ij}^{(N)}\Delta\epsilon_{ij} + \bar{F}_i^{(N)}\,\Delta U_i)dV + \int_{S_\sigma}\bar{T}_i^{(N)}\,\Delta U_i\, dS\Big\} \qquad (4.5)$$

If it is assumed that the known "initial" stress state ($\tau_{ij}^{(N)}$, $\bar{F}_i^{(N)}$, $\bar{T}_i^{(N)}$) in C_N is in equilibrium, then the right hand side of Equation (4.5) can be shown to be identically equal to zero. However, in general, because of the numerical computation errors and the inherent approximations involved in piecewise-linear-incremental process, state C_N will not be in true equilibrium. In such cases, the right hand side of Equation (4.5) is retained to provide the so-called "equilibrium check" [18,31]. Thus, we can formulate the functional $\Delta\pi$, the vanishing

of the first variation of which yields Equation (4.5). Thus,

$$\Delta\pi = \int_V \left[\frac{1}{2} E^t_{ijk\ell} \Delta g_{ij} \Delta g_{k\ell} + \frac{1}{2} \tau^{(N)}_{ij} \Delta U_{k,i} \Delta U_{k,j} - \Delta \bar{F}_i \Delta U_i \right] dV$$

$$- \int_{S_\sigma} \Delta \bar{T}_i \Delta U_i dS - \epsilon_m \qquad (4.6)$$

where

$$\epsilon_m = \int_V (-\tau^{(N)}_{ij} \Delta e_{ij} + \bar{F}^{(N)}_i \Delta U_i) dV + \int_{S_\sigma} \bar{T}^{(N)}_i \Delta U_i \, dS \quad .$$

Next, by the use of divergence theorem [58], the first and second term of (4.5) can be divided into four and two terms respectively. Those are

$$\delta \int_V \frac{1}{2} E^t_{ijk\ell} \Delta g_{ij} \Delta g_{k\ell} \, dV$$

$$= \int_{S_\sigma} n_j \Delta S_{ij} \delta \Delta U_i dS - \int_V \Delta S_{ij,j} \delta \Delta U_i dV$$

$$+ \int_{S_\sigma} n_i \Delta S_{ij} \Delta U_{k,j} \delta \Delta U_k \, dS - \int_V (\Delta S_{ij} \Delta U_{k,j})_{,i} \delta \Delta U_k \, dV \qquad (4.7)$$

and

$$\delta \int_V \frac{1}{2} \tau_{ij}^{(N)} \Delta U_{k,i} \Delta U_{k,j} \, dV$$

$$= \int_{S_\sigma} n_i \tau_{ij}^{(N)} \Delta U_{k,j} \delta \Delta U_k \, dS - \int_V (\tau_{ij}^{(N)} \Delta U_{k,j})_{,i} \delta \Delta U_k dV \qquad (4.8)$$

where n_i is the direction cosine of the surface S_σ normal. Substitute (4.7) and (4.8) into (4.5), assuming the right hand side of (4.5) vanishes, $\delta \Delta \pi = 0$ yields the incremental equilibrium equations and surface traction conditions:

$$\Delta S_{kj,j} + [(\Delta S_{ij} + \tau_{ij}^{(N)}) \Delta U_{k,j}]_{,i} + \Delta \bar{F}_k = 0 \qquad (4.9)$$

and

$$\Delta \bar{T}_k = n_j \Delta S_{kj} + [\Delta S_{ij} + \tau_{ij}^{(N)}] \Delta U_{k,j} \, n_i \quad \text{on } S_\sigma \quad . \qquad (4.10)$$

Now, certain simplifications can be made, in order to facilitate the above developments for numerical calculations. One can assume that the incremental displacement ΔU_i and the incremental Truesdell stress ΔS_{ij} are of order $O(\epsilon)$, whereas the initial stresses $\tau_{ij}^{(N)}$ are of order $O(1)$. Thus, Equations (4.9) and (4.10) can be simplified as

$$\Delta S_{kj,j} + (\tau_{ij}^{(N)} \Delta U_{k,j})_{,i} + \Delta \bar{F}_k = 0 \quad . \qquad (4.11)$$

$$\Delta \bar{T}_k = n_j \Delta S_{kj} + \tau_{ij}^{(N)} \Delta U_{k,j} \, n_i \qquad \text{on } S_\sigma \qquad (4.12)$$

and the last two terms of Equation (4.7) can be neglected. Likewise, Equations (4.3) and (4.2) become

$$\Delta g_{ij} = \frac{1}{2} (\Delta U_{i,j} + \Delta U_{j,i}) + O(\epsilon^2) \sim \Delta \epsilon_{ij} \tag{4.13}$$

and

$$\Delta S_{ij} \sim E^{t}_{ijk\ell} \, \Delta \epsilon_{k\ell} \quad . \tag{4.14}$$

From Equations (4.11) to (4.14), it is clear that the incremental functional (4.6) reaches the form

$$\Delta \pi = \int_V \left[\frac{1}{2} E^{t}_{ijk\ell} \, \Delta \epsilon_{k\ell} \Delta \epsilon_{ij} + \frac{1}{2} \tau^{(N)}_{ij} \Delta U_{k,i} \Delta U_{k,j} - \Delta \bar{F}_i \Delta U_i \right] dV$$

$$- \int_{S_\sigma} \Delta \bar{T}_i \Delta U_i \, dS - \epsilon_m \tag{4.15}$$

where $\Delta U_i = \Delta \bar{U}_i$ on S_u.

Finite Element Models

In a continuum, two most commonly used variational principles are: (a) Principle of minimum potential energy, which can be derived directly from the principle of virtual work and for which the only field variables, the displacements, must be continuous within the domain. (b) Principle of minimum complementary energy for which the only field variables, the stresses, must be in equilibrium. Based on the application of those variational principles, two broad finite element categories have been defined. The first, based on the principle of minimum potential energy, approximates the displacement field. This is termed the displacement method and satisfies the displacement compatibility between adjacent elements alone. The second approach stems from the principle of minimum complementary energy and an assumed stress

field. It satisfies only the equilibrium requirement.

In the finite element method as applied to solid mechanics, the solid continuum is considered as an assemblage of nonoverlapping subdomains V_m (finite elements) which have piecewise smooth inter-element boundaries. The solution procedure is first to seek an approximate solution within each element and to characterize the behavior of the element by a finite number of unknown parameters. A suitable procedure is then employed to combine the relations for the individual elements into a system of equations to be used to solve these parameters.

The elaborate illustrations in this dissertation are restricted to the displacement method. In this respect, two various displacement models will be demonstrated in the following portions.

(1) Compatible Displacement Finite Element Model

The principle of minimum potential energy may be stated as the vanishing of the variation of the total potential energy functional $\Delta\pi$ (from C_N state to C_{N+1} state) expressed by Equation (4.15). When a solid is divided into a finite number of discrete elements Am, the potential energy functional (4.15) may be written as (for two-dimensional case):

$$\Delta\pi_{CD} = \sum_m \left\{ \int_{A_m} \left[\frac{1}{2} E^t_{ijk\ell} \Delta\epsilon_{k\ell} \Delta\epsilon_{ij} + \frac{1}{2} \tau^{(N)}_{ij} \Delta U_{k,i} \Delta U_{k,j} - \Delta\bar{F}_i \Delta U_i \right] dA \right.$$

$$\left. - \int_{S_{\sigma_m}} \Delta\bar{T}_i \Delta U_i dS - \epsilon_m \right\}$$

Where Am is the area of the mth element ($m = 1,2,\ldots$) in the C_N state and S_{σ_m} is the portion of the boundary of the mth element over which the surface tractions ΔT_i are prescribed. Again, $\Delta\epsilon_{ij}$ is written in terms of the derivatives of the displacement ΔU_i by (4.13) and the displacement functions ΔU_i should satisfy the continuity conditions not only within the element but also across the interelement boundaries. The Euler equations and boundary conditions corresponding to $\delta\Delta\pi_{CD} = 0$, assuming $\epsilon_m = 0$, are obviously the equilibrium conditions given by Equations (4.11) and (4.12).

In the finite element formulation the incremental displacement functions ΔU_i are represented approximately over each element, say the mth element, by shape functions (See Chapter V) and undetermined incremental displacements at a finite number of nodal points of this element. The shape functions must be such that when the displacements at the nodes along the interelement boundary of two neighboring elements are compatible, the displacements along the corresponding interelement boundaries are also compatible. In matrix form the assumed displacements may be expressed as

$$\{\Delta U_i\} = [D]\ \{\Delta q\} \tag{4.16}$$

Where [D] is a matrix of shape functions and $\{\Delta q\}$ is a column matrix of element incremental nodal displacements. Now, the corresponding strain displacement relation is

$$\{\Delta\epsilon_{ij}\} = [B]\ \{\Delta q\} \tag{4.17}$$

[D] and [B] are provided in Chapter V.

Substituting Equations (4.16) and (4.17) into $\Delta\pi_{CD}$ and neglecting the body forces terms, we obtain

$$\Delta\pi_{CD} = \sum_{m} \frac{1}{2} \lfloor \Delta q \rfloor ([K^R] + [K_g^R])\{\Delta q\} - \lfloor \Delta q \rfloor \{F_2^R\} - \lfloor \Delta q \rfloor (\{F_4^R\} + \{C_e^R\}) \quad (4.18)$$

In this expression

$\lfloor\ \rfloor$, $[\ ]^T$ = transpose of $\{\ \}$ and $[\ ]$ respectively

$$[K^R] = \int_{Am} [B]^T [E]^t [B]\, dA$$

$$[K_g^R] = \int_{Am} ([W_1]^T [\tau^{(N)}][W_1] + [W_2]^T [\tau^{(N)}][W_2])\, dA$$

$$\{F_2^R\} = \int_{S_{\sigma_m}} [D]^T \{\Delta\bar{T}\}\, dS$$

$$\{F_4^R\} = \int_{S_{\sigma_m}} [D]^T \{\bar{T}\}\, dS$$

$$\{C_e^R\} = \int_{Am} [B]^T \{\tau^{(N)}\}\, dA$$

Here, the matrix $[W_1]$ and $[W_2]$ are defined such that

$$\begin{Bmatrix} \Delta U_{1,1} \\ \Delta U_{1,2} \end{Bmatrix} = [W_1]\ \{\Delta q\}$$

and

$$\begin{Bmatrix} \Delta U_{2,1} \\ \Delta U_{2,2} \end{Bmatrix} = [W_2] \{\Delta q\}$$

(2) Hybrid Displacement Finite Element Model

In formulating a compatible model difficulties may often occur in constructing the continuous displacement functions within the element as well as at the interelement boundary. Thus, for simplicity in finite element analysis, one must seek a modified variational principle in which the above interelement continuity requirement need not be satisfied a priori but will be enforced posteriori through the variational principle. Here, the model has been termed "hybrid" due to the fact that a different field variable, ΔU_{ip}, is assumed at the interelement boundary in addition to the interior displacements ΔU_i which are assumed in Am [59,60].

The basis of the hybrid displacement model and its use in linear fracture mechanics have been discussed in detail in [14,15]. For clarity, compared to the compatible model, the advantage of the hybrid displacement model in dealing with crack problems can be summarized as:

(a) The correct type of displacement singularities can be included in the singular elements around the crack-tip.

(b) The inter-element compatibility conditions are still satisfied.

(c) The correct type of boundary displacement distributions can be assumed for the singular elements around the crack tip.

(d) Stress distribution conditions at crack boundary can be satisfied easily.

Now, by introducing a Lagrange multipliers $T_{i\rho}$, the approach in [14,15,16] is modified for the incremental formulation of the elastic-plastic problem based on finite deformation assumption, using the continuously updated Lagrangean approach presented in section 1. The Lagrange multipliers $T_{i\rho}$ can be recognized as the interelement boundary tractions but are independent for the two neighboring elements. The incremental energy functional (4.15) becomes

$$\Delta\pi_{HD}(\Delta U_i;\Delta U_{i\rho};T_{i\rho}) = \sum_m \Big\{ \int_{Am} \Big[\frac{1}{2} E^t_{ijk\ell} \Delta\epsilon_{k\ell} \Delta\epsilon_{ij} + \frac{1}{2} \tau^{(N)}_{ij} \Delta U_{k,i} \Delta U_{k,j} - \Delta\bar{F}_i \Delta U_i \Big] dA - \int_{\partial_{Am}} T_{i\rho}(\Delta U_i - \Delta U_{i\rho}) dS - \int_{S_{\sigma m}} \Delta\bar{T}_i \Delta U_{i\rho}\, dS - \epsilon^*_m \Big\} \tag{4.19}$$

again,

$$\epsilon^*_m = \int_{Am} (-\tau^{(N)}_{ij} \Delta U_{i,j} + \bar{F}^{(N)}_i \Delta U_i) dA + \int_{S_{\sigma m}} \bar{T}^{(N)}_i \Delta U_i \, dS$$

where $\Delta U_{i\rho}$ denotes the independently assumed increments of element boundary displacements which are inherently compatible from C_N state to C_{N+1} state. All other notations are defined the same as before.

The first variation of the functional $\Delta\pi_{HD}$ for the three

independent unknown variables, ΔU_i, $\Delta U_{i\rho}$ and $T_{i\rho}$, yields the following equation

$$\delta\Delta\pi_{HD}(\Delta U_i;\Delta U_{i\rho};\ T_{i\rho}) = \sum_m \Big\{ \int_{Am} [-(E^t_{ijk\ell}\Delta\epsilon_{k\ell})_{,j}$$

$$- (\tau^{(N)}_{kj}\Delta U_{i,j})_{,k} - \Delta\bar{F}_i - \tau^{(N)}_{ij,j} - \bar{F}_i]\delta\Delta U_i dA$$

$$+ \int_{\partial Am} [(E^t_{ijk\ell}\Delta\epsilon_{k\ell} + \tau^{(N)}_{ij})n_j$$

$$+ \tau^{(N)}_{kj}\Delta U_{i,j}n_k - T_{i\rho}]\delta\Delta U_i dS$$

$$- \int_{\partial Am} (\Delta U_i - \Delta U_{i\rho})\delta\ T_{i\rho}\ dS + \int_{\partial Am} T_{i\rho}\delta\Delta U_{i\rho} dS$$

$$- \int_{S_{\sigma m}} \bar{T}^{(N)}_i \delta\Delta U_i dS - \int_{S_{\sigma m}} \Delta\bar{T}_i \delta\Delta U_{i\rho} dS \Big\}$$

Where n_j are the direction cosines of the outward boundary surface normal. It is noted that arbitrary $\delta\Delta U_{i\rho}$ are admissible on ∂Am, however, $\delta\Delta U_{i\rho} = 0$ on S_{u_m}, where S_{u_m} is the portion of ∂Am over which the displacement is prescribed. From calculus of variations, the Euler equation and natural boundary condition corresponding to $\delta\Delta\pi_{HD} = 0$ lead to:

$$(E^t_{ijk\ell}\Delta\epsilon_{k\ell})_{,j} + (\tau^{(N)}_{kj}\Delta U_{i,j})_{,k} + \Delta\bar{F}_i + [\tau^{(N)}_{ij,j} + \bar{F}^{(N)}_i] = 0 \text{ in Am} \quad (4.20)$$

$$(E^{t}_{ijk\ell}\Delta\epsilon_{k\ell} + \tau^{(N)}_{ij})n_j + \tau^{(N)}_{kj}\Delta U_{i,j}\, n_k = T_{i\rho} \qquad \text{at } \partial Am \qquad (4.21)$$

$$\Delta U_i = \Delta U_{i\rho} \qquad \text{at } \partial Am \qquad (4.22)$$

and

$$\bar{T}^{(N)}_i + \Delta\bar{T}_i = T_{i\rho} \qquad \text{at } S_{\sigma_m} \qquad (4.23)$$

In the Equations (4.20) and (4.21) the partial differentiation is made with respect to the Cartesian coordinate, $X^{(N)}_i$. Equation (4.20) refers to the equilibrium of the total Kirchhoff-Trefftz stress $S^{(N+1)}_{ij(N)}$ in C_{N+1} state. If state C_N was in true equilibrium, the last two bracketed terms in Equation (4.20) would be equal to zero. However, as mentioned before, the state C_N may not be truly equilibrated and the last two terms in Equation (4.20) leads to the "equilibrium check". Equation (4.21) states that the tractions derived from the assumed incremental interior displacement match the independently assumed boundary tractions $T_{i\rho}$ in C_{N+1} state. Equation (4.22) is the statement of interelement displacement compatibility that is enforced in the variational principle by the term $\int_{\partial A_m} T_{i\rho}(\Delta U_{i\rho} - \Delta U_i)$ of Equation (4.19). The fact that the Lagrange multiplier tractions $T_{i\rho}$ are equal to the prescribed tractions $\bar{T}^{(N)}_i + \Delta\bar{T}_i$ at S_{σ_m} in C_{N+1} state is displayed by Equation (4.23). In other words, Equation (4.23) would force $T_{i\rho}$ to be equal to the applied boundary tractions on S_{σ_m}. Thus, for crack problems, since $T_{i\rho}$ are independently assumed, the stress distribution condition on the crack surface can be easily satisfied.

Next, making the finite element approximations, the incremental interior displacement is assumed as (in matrix form)

$$\{\Delta U_i\} = \{\Delta U_i^S\} + \{\Delta U_i^{RB}\} = [U]\{\beta_s\} + [U_R]\{\beta_R\} \qquad \text{in Am} \tag{4.24}$$

where $[U]$ are the interpolation functions which do not contain any rigid body modes and have only straining mode in displacements, $[U_R]$ are the interpolation functions which contain only rigid body modes; β_s and β_R are unknown independent parameters. The corresponding linearized incremental total strains $\Delta\epsilon_{ij}$ are

$$\{\Delta\epsilon_{ij}\} = \frac{1}{2}\{\Delta U_{i,j} + \Delta U_{j,i}\} = [W_s]\{\beta_s\} \tag{4.25}$$

Note that the term corresponding to $\{\beta_R\}$ disappeared because it is pure rigid body modes and does not produce any strain terms. Similarly, the element boundary displacement $\Delta U_{i\rho}$ and the element boundary tractions $T_{i\rho}$ are assumed as

$$\{\Delta U_{i\rho}\} = [L]\{\Delta q\} \qquad \text{at } \partial \text{ Am} \tag{4.26}$$

and

$$\{T_{i\rho}\} = [R]\{\alpha\} \qquad \text{at } \partial \text{ Am} \tag{4.27}$$

Again, α are unknown independent parameters and Δq are the increments of nodal displacements for each load step. The functions $[R]$ are arbitrary whereas $[L]$ are functions at ∂Am that uniquely interpolate for $\Delta U_{i\rho}$ at ∂Am in terms of the relevant Δq. $[U]$, $[U_R]$, $[L]$ and $[R]$ will be discussed more elaborately in the next chapter.

Then, when Equations (4.24) to (4.27) are substituted into Equation (4.19), the Equation for $\Delta\pi_{HD}$ can be written as follows

$$\Delta\pi_{HD} = \sum_{m}\Big(\tfrac{1}{2}\,\lfloor\beta_s\rfloor[H]\{\beta_s\} + \tfrac{1}{2}\,\lfloor\beta_s\rfloor[C_g]\{\beta_s\} - \lfloor\beta_s\rfloor\{F_1\} - \lfloor\alpha\rfloor[P]\{\beta_s\} + \lfloor\alpha\rfloor[G]\{\Delta q\} - \lfloor\Delta q\rfloor\{F_2\} + \lfloor\beta_s\rfloor\{C_e\} - \lfloor\beta_s\rfloor\{F_3\} - \lfloor\beta_s\rfloor\{F_4\} + \tfrac{1}{2}\,\lfloor\beta_R\rfloor[C_g^{RB}]\{\beta_R\} + \lfloor\beta_R\rfloor[C_e^{RB}]\{\beta\} - \lfloor\beta_R\rfloor\{F_1^{RB}\} - \lfloor\alpha\rfloor[P^{RB}]\{\beta_R\} - \lfloor\beta_R\rfloor\{F_4^{RB}\} - \lfloor\beta_R\rfloor\{F_3^{RB}\}\Big) \qquad (4.28)$$

In this expression

$$[H] = \int_{Am} [W]^T[E]^t[W]dA$$

$$[P] = \int_{\partial Am} [R]^T[U]dS$$

$$[G] = \int_{\partial Am} [R]^T[L]dS$$

$$[C_g] = \int_{Am} \Big([W_1]^T[\tau_{ij}^{(N)}][W_1] + [W_2]^T[\tau_{ij}^{(N)}][W_2] \Big)\, dA$$

$$\{C_e\} = \int_{Am} [W]^T\{\tau_{ij}^{(N)}\}dA$$

$$\{F_1\} = \int_{Am} [U]^T \{\Delta \bar{F}_i\} dA$$

$$\{F_2\} = \int_{S_{\sigma_m}} [L]^T \{\Delta \bar{T}_i\} dS$$

$$\{F_3\} = \int_{Am} [U]^T \{\bar{F}_i^{(N)}\} dA$$

$$\{F_4\} = \int_{S_{\sigma_m}} [U]^T \{\bar{T}_i^{(N)}\} dS$$

$$[P^{RB}] = \int_{\partial Am} [R]^T [U_R] dS$$

$$[C_e^{RB}] = \int_{Am} \left(\{W_1^{RB}\} (\tau_{22}^{(N)}) \lfloor W_1^S \rfloor + \{W_2^{RB}\} (\tau_{11}^{(N)}) \lfloor W_2^S \rfloor \right) dA$$

$$[C_g^{RB}] = \int_{Am} \left(\{W_1^{RB}\} (\tau_{22}^{(N)}) \lfloor W_1^{RB} \rfloor + \{W_2^{RB}\} (\tau_{11}^{(N)}) \lfloor W_2^{RB} \rfloor \right) dA$$

$$\{F_1^{RB}\} = \int_{Am} [U_R]^T \{\Delta \bar{F}_i\} \, dA$$

$$\{F_3^{RB}\} = \int_{Am} [U_R]^T \{\bar{F}_i^{(N)}\} \, dA$$

$$\{F_4^{RB}\} = \int_{S_{\sigma_m}} [U_R]^T \{\bar{T}_i^{(N)}\} dS$$

where

$$\begin{Bmatrix} \Delta U^s_{1,1} \\ \Delta U^s_{1,2} \end{Bmatrix} = [W_1]\{\beta_s\} \; ; \qquad \begin{Bmatrix} \Delta U^s_{2,1} \\ \Delta U^s_{2,2} \end{Bmatrix} = [W_2]\{\beta_s\}$$

$$\Delta U^s_{1,2} = \lfloor W^s_1 \rfloor \{\beta_s\} \; ; \qquad \Delta U^s_{2,1} = \lfloor W^s_2 \rfloor \{\beta_s\}$$

and

$$\Delta U^{RB}_{1,2} = \lfloor W^{RB}_1 \rfloor \{\beta_R\} \; ; \qquad \Delta U^{RB}_{2,1} = \lfloor W^{RB}_2 \rfloor \{\beta_R\}$$

Now, consider some of the terms which correspond to the rigid body modes, say,

$$- \{\beta_R\}\{F_1^{RB}\} - \lfloor \alpha \rfloor [P^{RB}]\{\beta_R\} - \lfloor \beta_R \rfloor \{F_3^{RB}\} - \lfloor \beta_R \rfloor \{F_4^{RB}\}$$

Since body forces are not going to be considered in the present work, $\{F_1\}$, $\{F_3\}$, $\{F_1^{RB}\}$ and $\{F_3^{RB}\}$ would be zero. $\lfloor \alpha \rfloor [P^{RB}] \{\beta_R\}$ can be represented alternatively as

$$\lfloor \alpha \rfloor [P^{RB}]\{\beta_R\} = \int_{\partial Am} \Delta U_i^{RB} \, T_{i\rho} \, dS = \int_{\partial Am} \Delta U_i^{RB} \, \sigma^S_{ij} \, n_j \, dS$$

where σ^{S}_{ij} are the pseudo stresses. Using the Green's theorem [58], one has

$$\int_{\partial Am} \Delta U_i^{RB} \sigma^{S}_{ij} \, n_j \, dS = \int_{Am} \Delta U^{RB}_{i,j} \, \sigma^{S}_{ij} \, dA + \int_{Am} \Delta U_i^{RB} \, \sigma^{S}_{ij,j} \, dA$$

The first term in the above expression is vanished because ΔU_i^{RB} are rigid body displacement. The expression $\sigma^{S}_{ij,j}$ of the second term is the equation of equilibrium for the stresses derived from two dimensional (Airy) stress functions (see the last section of Chapter V), which are inherently satisfied. Thus the term $\lfloor \alpha \rfloor \, [P^{RB}] \, \{\beta_R\}$ is vanished. Similarly, the term $\lfloor \beta_R \rfloor \, \{F_4^{RB}\}$ can be set to zero. Now the equation (4.28) can be written as

$$\begin{aligned} \Delta\pi_{HD} = \sum_m \Big(& \tfrac{1}{2} \lfloor \beta_s \rfloor [H] \{\beta_s\} + \tfrac{1}{2} \lfloor \beta_s \rfloor [C_g] \{\beta_s\} - \lfloor \alpha \rfloor [P] \{\beta_s\} \\ & + \lfloor \alpha \rfloor [G] \{\Delta q\} - \lfloor \Delta q \rfloor \{F_2\} + \lfloor \beta_s \rfloor \{C_e\} \\ & - \lfloor \beta_s \rfloor \{F_4\} + \tfrac{1}{2} \lfloor \beta_R \rfloor [C_g^{RB}] \{\beta_R\} \\ & + \lfloor \beta_R \rfloor [C_e^{RB}] \{\beta_s\} \Big) \end{aligned}$$

In the above expression, the unknown parameters $\lfloor \alpha \rfloor$, $\lfloor \beta_s \rfloor$ and $\lfloor \beta_R \rfloor$ are independent for each of the elements whereas the parameter $\lfloor \Delta q \rfloor$ (the incremental nodal displacements) is common to the entire system of elements. Now $\Delta\pi_{HD}$ is minimized with respect to independent

parameters $\lfloor\alpha\rfloor$, $\lfloor\beta_s\rfloor$ and $\lfloor\beta_R\rfloor$ to obtain

$$- [P]\{\beta_s\} + [G]\{\Delta q\} = 0$$

$$[H]\{\beta_s\} + [C_g]\{\beta_s\} - [P]^T\{\alpha\} + \{C_e\} - \{F_4\} + [C_e^{RB}]^T\{\beta_R\} = 0$$

$$[C_g^{RB}]\{\beta_R\} + [C_e^{RB}]\{\beta_s\} = 0$$

Thus, the parameters $\{\beta_s\}$, $\{\beta_R\}$ and $\{\alpha\}$ can be expressed in terms of incremental nodal displacement $\{\Delta q\}$ as follows:

$$\{\beta_s\} = [P]^{-1}[G]\{\Delta q\}$$

$$\{\beta_R\} = - [C_g^{RB}]^{-1}[C_e^{RB}][P]^{-1}[G]\{\Delta q\} \tag{4.29}$$

$$\{\alpha\} = [P]^{-T}\left([H] + [C_g] - [C_e^{RB}]^T[C_g^{RB}]^{-1}[C_e^{RB}]\right)[P]^{-1}[G]\{\Delta q\}$$
$$+ [P]^{-T}\{C_e\} - [P]^{-T}\{F_4\}$$

Therefore

$$\lfloor\alpha\rfloor[P]\{\beta_s\} = \lfloor\alpha\rfloor[G]\{\Delta q\} \tag{4.30}$$

Substituting back $\{\beta_s\}$, $\{\beta_R\}$ and Equation (4.30) into $\Delta\pi_{HD}$, the $\Delta\pi_{HD}$ can be expressed in terms of $\{\Delta q\}$ only, very similar to the form of (4.18), that is

$$\Delta\pi_{HD} = \sum_m \frac{1}{2}\lfloor\Delta q\rfloor\left([K] + [K_g]\right)\{\Delta q\} - \lfloor\Delta q\rfloor\{\Delta Q\} - \lfloor\Delta q\rfloor\{\Delta Q_c\} \tag{4.31}$$

where

$$[K] = ([P]^{-1}[G])^{T}[H]([P]^{-1}[G])$$

$$[K_g] = ([P]^{-1}[G])^{T}([C_g] - [C_e^{RB}]^{T}[C_g^{RB}]^{-T}[C_e^{RB}])([P]^{-1}[G])$$

$$\{\Delta Q\} = \{F_2\}$$

$$\{\Delta Q_c\} = ([P]^{-1}[G])^{T}(\{F_4\} - \{C_e\})$$

Also, combining Equations (4.24), (4.25) and (4.29), the incremental interior displacements and incremental total strains can be attained in terms of the incremental nodal displacements $\{\Delta q\}$. That is

$$\{\Delta U_i\} = [U][P]^{-1}[G]\{\Delta q\} - [U_R][C_g^{RB}]^{-1}[C_e^{RB}][P]^{-1}[G]\{\Delta q\} \qquad (4.32)$$

$$\{\Delta \epsilon_{ij}\} = [W]\{\beta_s\} = [W][P]^{-1}[G]\{\Delta q\} \qquad (4.33)$$

Thus, as a result, Equation (4.2) can be expressed in an appropriate matrix form:

$$\{\Delta S_{ij}\} = [E]^{t}\{\Delta \epsilon_{ij}\} = [E]^{t}[W][P]^{-1}[G]\{\Delta q\} \qquad (4.34)$$

Combination of Compatible Displacement and Hybrid Displacement Finite Element Model

In fracture mechanics, in general, one can visualize the domain of the crack problem to be divided into two regions, (a) a small region

near the crack-tip where the singular, near field solution is predominant, and (b) a region away from the crack tip where no singularity exists. In the present finite element analysis, the compatible displacement and hybrid displacement finite element model are employed to study those two regions respectively.

In region (a), with the element shape defined, the dominant singular behaviour for strains and stresses near the crack-tip for strain-hardening materials, of the now well known Hutchinson-Rice-Rosengren type [2,3,4], is embedded in each of these near crack-tip "singular" elements. Continuity of displacements and tractions between these "singular" elements and the neighboring "regular" elements was enforced through a hybrid displacement finite element model, as was discussed earlier. In region (b), however, because of the simplicity and less cost for computer usage, a compatible displacement finite element model is introduced.

Thus, combining Equations (4.18) and (4.31), the total energy functional for the whole domain of the crack problem $\Delta\pi$ is

$$\Delta\pi = \Delta\pi_{HD} \text{ (for region (a))} + \Delta\pi_{CD} \text{ (for region (b))}$$

$$= \sum_{m=1}^{P} \left(\frac{1}{2} \lfloor \Delta q \rfloor ([K] + [K_g])\{\Delta q\} - \lfloor \Delta q \rfloor \{\Delta Q\} - \lfloor \Delta q \rfloor \{\Delta Q_c\} \right)$$

$$+ \sum_{m=p+1}^{M} \left(\frac{1}{2} \lfloor \Delta q \rfloor ([K^R] + [K_g^R])\{\Delta q\} - \lfloor \Delta q \rfloor \{\Delta Q^R\} - \lfloor \Delta q \rfloor \{\Delta Q_c^R\} \right)$$

where

p = the total number of singular elements

M = the total number of elements in the whole domain

$$\{\Delta Q^R\} = \{F_2^R\}$$

and

$$\{\Delta Q_c^R\} = \{F_4^R\} + \{C_e^R\}$$

All other notations have been defined in the last two subsections. Now by expressing the element incremental nodal displacement $\{\Delta q\}$ in terms of independent generalized global incremental displacements $\{\Delta q^*\}$ of the structure considered, the expression for $\Delta\pi$ becomes

$$\Delta\pi = \frac{1}{2} \lfloor \Delta q^* \rfloor ([K^*] + [K_g^*])\{\Delta q^*\} - \lfloor \Delta q^* \rfloor \{\Delta Q^*\} - \lfloor \Delta q^* \rfloor \{\Delta Q_c^*\} \quad (4.35)$$

Next, by using the stationary condition of $\Delta\pi$ in (4.35) with respect to $\{\Delta q^*\}$ leads to the following incremental equations for the cracked structures:

$$([K^*] + [K_g^*])\{\Delta q^*\}_N^{N+1} = \{\Delta Q^*\} + \{\Delta Q_c^*\} \quad (4.36)$$

where $\{\Delta q^*\}_N^{N+1}$ denotes the values of $\{\Delta q^*\}$ from C_N state to C_{N+1} state. $[K^*]$, $[Kg^*]$, $\{\Delta Q^*\}$ and $\{\Delta Q_c^*\}$ are the global matrices which are obtained by assembling the corresponding element matrices. $([K^*] + [Kg^*])$ is the updated tangent stiffness matrix from C_N state to C_{N+1} state which includes the effect of prior plastic yielding and finite geometry changes.

$\{\Delta Q^*\}$ is the incremental load vector, and $\{\Delta Q_C^*\}$ corresponds to the nodal force imbalance terms to check the equilibrium of C_N state. It is to be noted that $\{\Delta Q_C^*\}$ are initially taken as zero and at the end of iteration for each load increment it finally converges to zero.

Incremental Numerical Methods

In dealing with nonlinear problems, involving plasticity, and using the finite element method, there are three general incremental methods which have been developed. These are (a) the initial strain method; (b) the initial stress method; and (c) the tangent modulus method.

"The initial strain method" [61] treats the plastic strains at each incremental load step as initial strains for the next load step. In this method, plasticity effects are taken into account as pseudo loads, and the elastic stiffness matrix is used throughout the entire loading process. The advantage of this method is that for small deformation problems the governing stiffness matrix need be built and inverted only once. We note that the initial strain method fails to converg for perfect plasticity or for a very small degree of work hardening because the total strain increments are only the plastic components in these cases [62].

An alternative approach formulated to overcome such difficulty is "the initial stress method" (or residual force method) [63,64]. This method appears to be suitable for general plastic behavior because it relies on the fact that a unique stress exists for an increment of strain. Using the method, we treat the elastic-plastic problem first as an elastic problem. Because of the nonlinearity, the stress

increment will not generally be the correct stress increment necessary to equilibrate. Therefore, at every stage, we determine the difference between the true stress levels corresponding to the appropriate strains and that corresponding to the elastic solution. The difference is used as an initial (corrective) stress, and a correction load vector is calculated. If the difference is below a certain limit, the process is stopped.

The tangent modulus method [17,18] is based on the incremental stress-strain laws of plasticity. In this method, plasticity effects are accounted for in the stiffness matrix, which is updated at each load step. For each load increment, corresponding to a new stiffness matrix, the problem in the flow theory of elastic-plastic analysis is the same as the elastostatic problem. Thus, the numerical solution of this problem consists of a series of solutions each of which is equivalent to a solution of an elastostatic problem.

For finite deformation problems, the stiffness matrix has to be updated to account for changes of geometry. So in finite deformation elastic-plastic problem, tangent modulus method is most appropriate.

As mentioned in section 2, an "equilibrium check" is considered in the present work. Thus, together with tangent modulus numerical method, the equilibrium check is employed at any point in the present incremental solution process, with an updated stiffness matrix even in iteration stage, to reduce any cumulative error in nodal point equilibrium. It is the fact that the equilibrium check can prevent the computed load-displacement behavior from straying from the true equilibrium path.

Calculation Procedure

In the first increment of the present elastic-plastic incremental solution procedure, setting an unit applied load (p = 1 lb.) and a power hardening coefficient (n = 1), an initial linear elastic computation can be first carried out. In this linear elastic case, as was mentioned earlier, $\{\Delta Q_C^*\}$ (Equation (4.36)) is taken as zero and the application of iteration process is not necessary. At this stage, a numerical integration procedure involving singularity is required to construct the element stiffness matrix [K] (See Appendix C).

In the second increment of the solution procedure, the load chosen is that which permits a specific material point (adjacent to the crack-tip) to be on the point of yielding. Since the yield zone can be specifically small, the whole structure is still assumed approximately in pure elastic state. Thus, the constant elasticity compliance tensor [E] (Equation (3.2)) is taken and the results are stored on magnetic tape for the next increment to determine the field values of interest.

Now, for the state after the second increment, say C_N state, the applied loadings are divided into finite increments and the important plasticity effect should be included. Once the stress point has reached yielding in the structure, the updated elastic-plastic constitutive law (Equation (3.1)) instead of Equation (3.2) is used to determine Truesdell stress increments ΔS_{ij}. Then, one can construct the updated tangent stiffness $([K^*] + [K_g^*])$ and form the final algebraic equation (4.36), based on the regular Gaussian integration (Appendix C) and the results available in the previous state. As long as the incremental nodal

displacements $\{\Delta q\}_{N-1}^{N}$ are computed by solving the algebraic linear simultaneous equations represented by Equation (4.36) (See Appendix C), $[E]^t$, $\{\Delta\epsilon_{ij}\}$ and ΔS_{ij} can be determined directly through Equations (3.10), (3.11) and (4.33). Again, these results are stored on magnetic tape for subsequent processing. One can then calculate the "equilibrium check" due to non-equilibrium and see if it is small. Once the equilibrium check is not small, the current equilibrium check is reloaded as new applied load for next iteration and the new updated tangent stiffness is reconstructed. Meanwhile, the convergent property of the equilibrium check needs to be carefully studied during iteration. The iteration procedure is thus repeated until the equilibrium check converges to a very small quantity. The true (Euler) stress $\tau_{ij}^{(N)}$ are finally computed and treated as initial stresses in C_N.

For the next load step, now, C_{N+1} state will be the new reference state. Thus, if the iteration procedure is again satisfactorily achieved, the true (Euler) stresses in C_{N+1} ($\tau_{ij}^{(N+1)}$) need to be computed and treated as initial stresses in C_{N+1}. As a result, one needs to convert the Kirchhoff-Trefftz stresses $S_{ij}\,{}^{(N+1)}_{(N)}$ (Equation (4.1)) to the Euler stresses $\tau_{ij}^{(N+1)}$ by the following relations:

$$\tau_{ij}^{(N+1)} = \frac{1}{\mathrm{Det}\left[\dfrac{\partial X_i^{(N+1)}}{\partial X_j^{(N)}}\right]} \frac{\partial X_i^{(N+1)}}{\partial X_k^{(N)}} \frac{\partial X_j^{(N+1)}}{\partial X_\ell^{(N)}} S_{k\ell}\,{}^{(N+1)}_{(N)}$$

For two dimensional problems, since ΔU_i is small for each increment, the above equation can be written in a more explicit form:

$$\begin{Bmatrix} \tau_{11} \\ \tau_{22} \\ \tau_{12} \end{Bmatrix}^{(N+1)} = (1-\Delta\epsilon_{11}-\Delta\epsilon_{22}) \begin{bmatrix} (1+\Delta\epsilon_{11})^2 & (\Delta U_{1,2})^2 & 2\Delta U_{1,2}(1+\Delta\epsilon_{11}) \\ (\Delta U_{2,1})^2 & (1+\Delta\epsilon_{22})^2 & 2\Delta U_{2,1}(1+\Delta\epsilon_{22}) \\ (\Delta U_{2,1})(1+\Delta\epsilon_{11}) & (\Delta U_{1,2})(1+\Delta\epsilon_{22}) & (1+\Delta\epsilon_{11})(1+\Delta\epsilon_{22}) \\ & & + (\Delta U_{1,2})(\Delta U_{2,1}) \end{bmatrix} \begin{Bmatrix} S_{11} \\ S_{22} \\ S_{12} \end{Bmatrix}^{(N+1)}$$

The solution then continues by progressively increasing the applied loads and determining an elastic-plastic solution at each increment. Some more detailed descriptions, such as crack propagation procedure and the so-called "knee correction", are provided in Chapter VI and Appendix C respectively.

CHAPTER V

ELEMENT DESIGN AND ASSUMED INTERPOLATION FUNCTIONS

In the preceding chapter the basic formulations of both a compatible displacement model and a hybrid displacement finite element model used to analyze the elastic-plastic finite deformation crack problems were presented. This chapter is denoted to the detailed description of all the field functions and interpolation functions for both regular as well as singular elements. The basic element design and the related calculation quantities such as the necessary transformation laws are also presented.

Regular Elements

(1) Element Design

In two-dimensional analyses the simplest element shapes are obviously a triangle and a rectangle which are defined by three or four nodes respectively. However, due to the limitation of a straight boundary for the element, both of these elements present the simplest possible forms of approximation and are of limited accuracy.

Thus, the basic shape of the regular element chosen here is a quadrilateral, the sides of which can be distorted in a prescribed parabolic shape with one additional node involved in each side (Figure 10). Consequently, there are four corner nodes and four midside nodes for each element. The curved shape of the element is described as the

isoparametric quadrilateral [65].

(2) Isoparametric Transformations

The term "isoparametric" here means that the transformations can be employed to use the same interpolation functions to define the element shape as to define incremental displacements within the element. Those transformations enable one to transform a general quadrilateral element whose four corners have the physical, Cartesian coordinates $(x_i, y_i, i = 1,\ldots,4)$ and whose boundary lines are general quadratic curves into a square element whose nondimensional coordinates ξ and η are such that $-1 \le \xi \le 1$ and $-1 \le \eta \le 1$ [65]. The transformation procedures are necessary for the determination of the element matrices by numerical integration with respect to the nondimensional coordinates ξ and η.

For an eight-node quadrilateral element, the coordinate transformation from the isoparametric system to the physical system follows a quadratic transformation of

$$x = \sum_{i=1}^{8} N_i(\xi,\eta)\, x_i$$

$$y = \sum_{i=1}^{8} N_i(\xi,\eta)\, y_i$$

where (x,y) is the global Cartesian coordinate and (x_i, y_i) is the coordinate of node i. $N_i(\xi,\eta)$ are called the shape functions and are defined as (Figure 10):

Corner nodes:

$$N_i(\xi,\eta) = \frac{1}{4}(1 + \xi\xi_i)(1 + \eta\eta_i)(\xi\xi_i + \eta\eta_i - 1)$$

Midside nodes with $\xi_i = 0$:

$$N_i(\xi,\eta) = \frac{1}{2}(1 - \xi^2)(1 + \eta\eta_i)$$

Midside nodes with $\eta_i = 0$:

$$N_i(\xi,\eta) = \frac{1}{2}(1 - \eta^2)(1 + \xi\xi_i)$$

Now, to define the interior incremental displacements, one also assumes that the same shape functions $N_i(\xi,\eta)(i = 1,2,\ldots,8)$ can be again employed. Thus,

$$\Delta u_x(\xi,\eta) = \sum_{i=1}^{8} N_i(\xi,\eta)\ \Delta q_{2i-1}$$

$$\Delta u_y(\xi,\eta) = \sum_{i=1}^{8} N_i(\xi,\eta)\ \Delta q_{2i}$$

where Δq_i represents the nodal values of incremental displacement components. In a compact matrix form, the Equation (4.16) is thus defined as:

$$\{\Delta u_i\} = \begin{Bmatrix} \Delta u_x \\ \\ \Delta u_y \end{Bmatrix} = [D]\ \{\Delta q\}$$

in this expression,

$$\lfloor \Delta q \rfloor = \lfloor \Delta q_1, \Delta q_2, \ldots, \Delta q_{15}, \Delta q_{16} \rfloor$$

and

$$[D] = \begin{bmatrix} N_1, & 0, & N_2, & 0, & \ldots, & N_8, & 0 \\ 0, & N_1, & 0, & N_2, & \ldots, & 0, & N_8 \end{bmatrix}_{2 \times 16}$$

Using the present compatible finite element procedures, in order to obtain the strains (and therefore stresses) and evaluate the element matrices, one needs the derivatives of the shape functions, and the transformation laws between $(X_1^{(N)}, X_2^{(N)})$ and (ξ, η) which are given as follows:

(i) Derivatives of the shape functions

Corner nodes:

$$N_{i,\xi} = \frac{1}{4} \xi_i (1 + \eta\eta_i)(2\xi\xi_i + \eta\eta_i)$$

$$N_{i,\eta} = \frac{1}{4} \eta_i (1 + \xi\xi_i)(\xi\xi_i + 2\eta\eta_i)$$

Midside nodes with $\xi_i = 0$:

$$N_{i,\xi} = -\xi(1 + \eta\eta_i)$$

$$N_{i,\eta} = \frac{1}{2} \eta_i (1 - \xi^2)$$

Midside nodes with $\eta_i = 0$:

$$N_{i,\xi} = \frac{1}{2}\,\xi_i(1 - \eta^2)$$

$$N_{i,\eta} = -\,\eta(1 + \xi\xi_i)$$

(ii) The differentiations with respect to $X_1^{(N)}$ and $X_2^{(N)}$ can be changed to those with respect to ξ and η, in matrix notation

$$\begin{Bmatrix} \dfrac{\partial}{\partial X_1^{(N)}} \\ \dfrac{\partial}{\partial X_2^{(N)}} \end{Bmatrix} = [J]^{-1} \begin{Bmatrix} \dfrac{\partial}{\partial \xi} \\ \dfrac{\partial}{\partial \eta} \end{Bmatrix} = \begin{bmatrix} J_{11}^* & J_{12}^* \\ J_{21}^* & J_{22}^* \end{bmatrix} \begin{Bmatrix} \dfrac{\partial}{\partial \xi} \\ \dfrac{\partial}{\partial \eta} \end{Bmatrix}$$

Where [J] denotes the Jacobian matrix of the coordinate transformation

$$[J] = \begin{bmatrix} \dfrac{\partial X_1^{(N)}}{\partial \xi} & \dfrac{\partial X_2^{(N)}}{\partial \xi} \\ \dfrac{\partial X_1^{(N)}}{\partial \eta} & \dfrac{\partial X_2^{(N)}}{\partial \eta} \end{bmatrix}$$

(iii) Integration with respect to $dX_1^{(N)}$ and $dX_2^{(N)}$ can similarly be changed to integration with respect to $d\eta$ and $d\xi$, with a simplification of the limits of integration, which now are simply from -1 to +1.

For area element

$$dX_1^{(N)}\, dX_2^{(N)} = \det [J]\, d\xi\, d\eta$$

For line element

$$dS = \sqrt{(dX_1^{(N)})^2 + (dX_2^{(N)})^2} = \sqrt{\left(\frac{\partial X_1^{(N)}}{\partial \xi}\right)^2 + \left(\frac{\partial X_2^{(N)}}{\partial \xi}\right)^2} \quad d\xi \text{ on } d\eta = 0$$

$$= \sqrt{\left(\frac{\partial X_1^{(N)}}{\partial \eta}\right)^2 + \left(\frac{\partial X_2^{(N)}}{\partial \eta}\right)^2} \quad d\eta \text{ on } d\xi = 0$$

Lastly, after some manipulation, the following interpolation functions ([B] in equation (4.17)) can be obtained.

$$\{\Delta\epsilon_{ij}\} = \begin{matrix} \Delta\epsilon_{xx} \\ \Delta\epsilon_{yy} \\ \Delta\gamma_{xy} \end{matrix} = [B]\{\Delta q\} \qquad \text{(Equation (4.17))}$$

and

$$[B] = \begin{bmatrix} (J_{11}^* N_{1,\xi} + J_{12}^* N_{1,\eta}) & 0 & \cdots & (J_{11}^* N_{8,\xi} + J_{12}^* N_{8,\eta}) & \cdots \\ 0 & (J_{21}^* N_{1,\xi} + J_{22}^* N_{1,\eta}) & \cdots & 0 & \cdots \\ (J_{21}^* N_{1,\xi} + J_{22}^* N_{1,\eta}) & (J_{11}^* N_{1,\xi} + J_{12}^* N_{1,\eta}) & \cdots & (J_{21}^* N_{8,\xi} + J_{22}^* N_{8,\eta}) & \cdots \end{bmatrix}_{3\times 16}$$

Singular Elements

(1) Element Design

As discussed in the preceding chapter, one needs to assume in each singular element around the crack tip (a) the element interior

displacement field ΔU_i; (b) the element boundary displacement field $\Delta U_{i\rho}$; and (c) the equilibrated element boundary traction field $T_{i\rho}$. Here, the singular element is chosen as a six-noded sector of a circle centered at the crack tip, as shown in Figure 11. Further, φ is the global angular coordinate and θ is the local angular coordinate with respect to the element's symmetric axis, and r is the distance from the crack tip.

(2) Assumed Element Interior Displacement

The element interior displacement which contains pure rigid body modes can be readily assumed as follows:

$$\Delta U_r = \beta_1 \cos\varphi + \beta_3 \sin\varphi$$

$$\Delta U_\varphi = -\beta_1 \sin\varphi + \beta_2 r + \beta_3 \cos\varphi$$

and

$$\lfloor \beta_R \rfloor = \lfloor \beta_1, \beta_2, \beta_3 \rfloor$$

Thus, $[U_R]$ in Equation (4.24) is determined.

Likewise, the regular and singular parts of element interior displacement field corresponding to pure strain modes are assumed to be

$$\Delta U_r = \beta_1 r + 2\beta_2 r\theta + \beta_3 r\theta^2 + \beta_5 r^2 + \beta_6 r^2\theta + \beta_{10}\cos\varphi r^{\frac{1}{n+1}} + \beta_{11}\cos\varphi r^{\frac{1}{n+1}}\theta$$

$$+ \beta_{12}\cos\varphi r^{\frac{1}{n+1}}\theta^2 + \beta_{13}\sin\varphi r^{\frac{1}{n+1}} + \beta_{14}\sin\varphi r^{\frac{1}{n+1}}\theta + \beta_{15}\sin\varphi r^{\frac{1}{n+1}}\theta^2$$

$$\Delta U_{\varphi} = \beta_2 r + \beta_4 r\theta + \beta_7 r\theta^2 + \beta_8 r^2 + \beta_9 r^2\theta - \beta_{10}\sin\varphi r^{\frac{1}{n+1}} - \beta_{11}\sin\varphi r^{\frac{1}{n+1}}\theta$$
$$- \beta_{12}\sin\varphi r^{\frac{1}{n+1}}\theta^2 + \beta_{13}\cos\varphi r^{\frac{1}{n+1}} + \beta_{14}\cos\varphi r^{\frac{1}{n+1}}\theta + \beta_{15}\cos\varphi r^{\frac{1}{n+1}}\theta^2$$

It can be readily seen that the displacements are free from rigid body motion and the singular part of the displacement field, when considered in Cartesian components, varies quadradically in θ. n is the power hardening coefficient.

From the strain-displacement relations in polar coordinates, one obtains

$$\{\Delta\epsilon_{ij}\} = \begin{Bmatrix} \Delta\epsilon_{rr} \\ \Delta\epsilon_{\theta\theta} \\ \Delta\gamma_{r\theta} \end{Bmatrix} = \begin{Bmatrix} \frac{\partial \Delta U_r}{\partial r} \\ \frac{\Delta U_r}{r} + \frac{1}{r}\frac{\partial \Delta U_{\varphi}}{\partial \varphi} \\ \frac{1}{r}\frac{\partial \Delta U_r}{\partial \varphi} + \frac{\partial \Delta U_{\varphi}}{\partial r} - \frac{\Delta U_{\varphi}}{r} \end{Bmatrix} = [W_s]\{\beta_s\} \quad \text{(Equation (4.25))}$$

here $[\beta_s] = [\beta_1, \beta_2, \ldots, \beta_{15}]$. $[W_s]$ can then be evaluated directly. It should be noted that the proper Hutchinson-Rice-Rosengren type strain singularity in $r(r^{-n/n+1})$ has been embedded in the singular part of displacement field.

Thus a total of 18 functions are assumed for the element interior displacement field, out of which three are rigid body modes and the other fifteen produce strains.

(3) Assumed Element Boundary Displacement

As discussed in the previous chapter, the element boundary displacements $\{\Delta U_{i\rho}\}$ should be the same at common boundaries of neighboring elements and should be interpolated in terms of nodal displacements on the common boundaries.

The proper $r^{\frac{1}{n+1}}$ type displacement is now built into the boundary displacements along the element boundaries AB and AC. However, the type $\Delta U_{i\rho} = a + b\theta + c\theta^2$ is assumed along BC (See Figure 11).

Along AB, AC:

$$\Delta U_{i\rho} = a + br^{\frac{1}{n+1}} + cr$$

Along BC:

$$\Delta U_{i\rho} = a + b\theta + c\theta^2$$

where coefficients a, b and c are to be determined from the three nodal displacements along the respective segment of the boundary. For instance, consider the x component of $\Delta U^{AB}_{i\rho}$, these coefficients a, b and c can be expressed as (in matrix notation)

$$\begin{Bmatrix} a \\ b \\ c \end{Bmatrix} = \begin{bmatrix} 1, & r_1^{\frac{1}{n+1}}, & r_1 \\ 1, & r_2^{\frac{1}{n+1}}, & r_2 \\ 1, & r_3^{\frac{1}{n+1}}, & r_3 \end{bmatrix}^{-1} \begin{Bmatrix} \Delta q_1 \\ \Delta q_3 \\ \Delta q_5 \end{Bmatrix}$$

Where r_1, r_2 and r_3 are the distances measured from the crack-tip to each nodal point considered on AB. Thus, the interpolation functions [L] in Equation (4.26) can be obtained.

(4) Assumed Boundary Tractions

The independently assumed Lagrangean multipliers tractions $\{T_{i\rho}\}$, mathematically speaking, can be assumed in any convenient form. However, the relevant natural boundary conditions (4.21) dictate that the boundary tractions generated from the assumed incremental element interior displacements $\{\Delta U_i\}$ must match the assumed boundary tractions $\{T_{i\rho}\}$ at the interelement boundaries. These assumed incremental displacement fields $\{\Delta U_i\}$, in addition to satisfying Equation (4.21), must also satisfy the equilibrium equations (4.20) through the variational principle. Thus, a better approximation is assured if the assumed $\{T_{i\rho}\}$ are generated from an equilibrated stress field.

For two dimensional analysis, in the absence of body forces, such a stress field can be derived from an assumed Airy stress function Φ. The relationships between the stresses and the Airy stress function are given as follows (in polar coordinates)

$$\sigma_{rr} = \frac{1}{r}\frac{\partial \Phi}{\partial r} + \frac{1}{r^2}\frac{\partial^2 \Phi}{\partial \varphi^2}$$

$$\sigma_{\theta\theta} = \frac{\partial^2 \Phi}{\partial r^2}$$

$$\sigma_{r\theta} = \frac{1}{r^2}\frac{\partial \Phi}{\partial \varphi} - \frac{1}{r}\frac{\partial^2 \Phi}{\partial r \partial \varphi}$$

where $\frac{\partial}{\partial\varphi} = \frac{\partial}{\partial\theta}$. Since $T_{i\rho} = \sigma_{ij} n_j$, n_j are the direction cosines of a normal to the boundary, the proper singularity for the assumed traction $\{T_{i\rho}\}$ is a $r^{-\frac{1}{n+1}}$ type. It follows that the assumed Airy stress function Φ contains $r^{\frac{2n+1}{n+1}}$ terms along with regular polynomial terms. Another necessary condition in the proper choice of the Airy stress function Φ is that the matrix [P] in Equation (4.29)

$$[P] = \int_{\partial A_m} [R]^T [U] \, dS$$

(where $\{\Delta U^s\} = [U]\{\beta_s\}$ and $\{T_{i\rho}\} = [R]\{\alpha\}$) should be square and non-singular, and hence, can be inverted. Therefore, the total number of α's is forced to equal to β_s's. Consequently, the assumed Airy stress function is given below:

$$\Phi = \alpha_1 r^2 + \alpha_2 r^2\theta + \alpha_3 r^2\theta^2 + \alpha_4 r^2\theta^3 + \alpha_5 r^3 + \alpha_6 r^3\theta + \alpha_7 r^3\theta^2 + \alpha_8 r^3\theta^3$$

$$+ \alpha_9 r^4 + \alpha_{10} r^4\theta + \alpha_{11} r^4\theta^2 + \alpha_{12} r^4\theta^3 + \alpha_{13} r^{\frac{2n+1}{n+1}} + \alpha_{14} r^{\frac{2n+1}{n+1}}\theta$$

$$+ \alpha_{15} r^{\frac{2n+1}{n+1}}\theta^2$$

[R] is now well defined.

CHAPTER VI

STABILITY OF CRACK GROWTH

Stable crack growth is an apparently common phenomenon in fracture processes. In fact, plane strain fracture in thick specimens under small-scale yielding conditions, which is preceded by unnoticeable stable crack growth, seems to belong to a special case. But in thin sheet materials under plane stress fracture situations, much more extensive stable growth usually occurs. Thus, a realistic analysis of fracture must include not only models for initiation of crack growth, but also models for subsequent stable crack growth and, especially, for its terminal loss of stability.

The studies summarized in Chapter II provide a useful background for description of the problem of a stationary crack subjected to monotonically increasing load. But if cracks extend in a stable quasi-static fashion and the path-dependent nature of plastic stress-strain relations cause a very different deformation field at a moving crack-tip (versus a stationary crack-tip), there is no similar background that has yet been acquired. The aim of this chapter is thus to devise a rigorous finite element model which can be extended for the description of stably growing cracks.

In this chapter, a simple macroscopic model of the fracture process and some comments on existing analyses of stable crack growth are first provided. Then, a general energy balance for crack extension

in a form valid even for the incremental theory of plasticity is presented. The global energy release rate G^* together with the so-called "crack separation energy rate" G^{Δ} [74,75,76,77] are thoroughly studied. Lastly, a rigorous finite-element modeling of the study of global energy release rate G^*, based on an available experimental J-Δa curve, is described in detail. The necessary introduction of hereditary properties in a propagating crack problem where unloading occurs in the plastic region behind the advancing crack-tip has also been discussed as well as the inclusion of routines for relaxation of cohesive crack-tip nodal forces.

Study of Stable Crack Growth

Typically, cracks do not abruptly begin to propagate in elastic-plastic solids. Instead it is usual that the initiation of crack extension is followed by stable growth under a continuous increase of the applied load, or at least of the load point displacement. Ultimately, the required increase for continuing stable crack growth falls to zero, and unstable propagation ensues.

The complete situation of crack initiation, stable crack growth, and quasi-static propagation can be shown schematically as in Figure 12 where load is represented as a function of the current crack length for a typical case of ductile crack propagation.

In the figure a is the current crack length, a_o being the initial crack length, and p is the external load. The case of a stationary crack with initial crack length a_o is represented by region I where p_c (point A in Figure) is the load for initiation of crack growth. The

region of stable crack growth, where an infinitesimally small increase of the external load causes only a corresponding small increase of the crack length, is represented by region II in the figure where a_i is the crack length at instability (point B in Figure). After a transition phase, region III in Figure 12, a limiting steady-state situation, is approached as indicated by region IV. The heavy lines are characteristics for the onset of growth and instability respectively. Thus, as was pointed out in Chapter II, the J_{IC} criterion is no more than a ductile criterion for defining point A in the above Figure.

Experimental summaries for the existence of stable crack growth have been given by Broek [27] for crack growth in thin aluminum sheets and by Link and Muntz [28] for bending test specimens in medium-strength steels. An experimental study of the detailed flow of material and energy round a stably growing crack-tip which would be of interest for evaluation of the fracture tests on a small-scale was made by Bergkvist and Anderson [29]. Although interesting details of the flow were revealed, Bergkvist and Anderson concluded that it is very difficult to interpret the results in terms of a fracture criterion. The phenomenon of stable crack growth has been studied theoretically, only in the case of the anti-plane shear mode (Mode III), where the flow equations for an ideally-plastic material may be solved by means of numerical integration under the assumption of a critical mean strain ahead of the crack-tip as a simple fracture criterion. These methods has been devised by McClintock et al. [72,73]. For the other two modes (Mode I and Mode II), however, a very little amount of work has been

done. Although Anderson [78,79] and Kfouri and Miller [74,75] have presented finite element methods to analyze growing cracks, the results do not yet seem sufficiently refined to serve as a basis for understanding the crack-tip stress field in any detail and there is still much to be learned.

Energy Balance for Crack Extension

A simple fracture characterizing parameter which accurately corresponds to the realistic fracture phenomenon, without a detailed description of crack-tip processes, is highly desirable. Since stable crack growth is considered to be a continuous process, one's first inclination in devising such an approach might be to generate an energy balance, in a manner suitable to crack growth in an elastic-plastic continuum. This energy balance can be briefly stated as: crack extension can occur as soon as the energy release due to crack growth equals to the energy which is consumed in the production of a new zone of plastically deformed material at the tip of the advanced crack.

A general energy balance for fracture, under the assumptions of small deformations, was presented by Rice [76] in a form valid for any continuous body sustaining a crack. The energy balance takes the familiar form:

$$G - P = 2\gamma$$

where G is the energy release rate, P the plastic work rate estimated from continuum considerations, and the surface energy term γ is interpreted as the work per unit area required to create new surface.

Rice [76] suggested that is is not necessary to separately assess G and p during crack extension and to write explicit formulae for G and P, as the fracture criterion requires only that their difference G-P be known. Thus, an examination with particular attention to the role of surface energy term γ was given. As a result, it was shown that if stresses vary continuously during crack extension everywhere in the crack body except at the crack-tip, an elastic-perfectly plastic material (non-work hardening) carrying bounded stresses results in $G = P$ for all levels of applied load, so that crack extension involves no energy surplus and fracture cannot occur. For a perfectly elastic material, certainly, the platic work rate P is equal to zero (no plastic dissipation). Therefore, Rice [76] confirmed that as one passes through varying degrees of hardening behavior from the perfect elasticity to the perfect plasticity limiting cases, the difference G-P passes from G to zero.

The quantitative studies of the surface energy term γ, based on the simplest finite element approach, were made by Kfouri et al. [74,75]. It will be convenient for purposes of clarity to introduce the term "crack separation energy rate" $G^{\Delta}(=2\gamma)$ as adopted by Kfouri et al. [74,75]. In the sense of finite-element method, G^{Δ} is defined as the energy release per unit crack area based on a finite crack growth increment Δa, calculated as the work of quasi-statically unloading the finite-element adjacent to the crack, of size Δa, while constant stress is maintained on the specimen [74]. Thus, suppose a crack is allowed to extend by an amount Δa and that the work absorbed is Δw, then G^{Δ} will

be defined as $\frac{\Delta w}{\Delta a}$.

The finite element procedure devised by Kfouri and Miller [74,75] to obtain an estimate of G^{Δ} is as follows:

(1) From an initial solution for the given loads and constraints, the equivalent nodal reaction R_A at the crack tip node A is obtained.

(2) The constraint on the vertical displacement, δ_A, of the crack-tip node A is relaxed and relaxation is performed by negative force increments at the crack-tip node ΔR_A until the original crack-tip nodal force R_A is completely released. Thus, a free crack surface is extended, but not opened, to the next node.

(3) The nodal force R_A is removed and the corresponding vertical displacement δ_A for each increment determined. As a result, the value of G^{Δ} is twice the area under the R_A-δ_A curve divided by the distance between adjacent nodes (Δa).

Thus, to evaluate the value of G^{Δ}, it is very necessary to determine the nodal force at the crack-tip (R_A) accurately. However, since the distributions of the nodal force in the uncracked ligament (and therefore the extrapolated nodal force at the crack-tip) are inherently geometry dependent (see Figure 47 and Figure 51), another characterizing parameter which is not determined solely by the deformation field at the crack tip is required at least when the present hybrid displacement finite-element model is employed. To this end, the global energy release rate G^{*}, which is essentially equal to G^{Δ}, is introduced

in this work. Further discussions about G^{Δ} will be provided in the next chapter.

The purpose of the following work is to re-examine the energy balance. To obtain the global energy changes after initiation of crack growth, a solution for the plane cracked-body problem with changing internal boundary (subcritical crack growth) and changing elasic-plastic boundary coupled with an elastic-plastic strain hardening assumption is needed. Now, consider an arbitrarily shaped plane solid of unit thickness having a straight, through-the-thickness crack of length a (Figure 13), and consider an instant of time at which slow stable crack extension is taking place. Let U_f represent the work performed by the applied forces in reaching the current deformed state, and $U = U_e + U_p$ the strain energy of the deformation, where U_e is the elastic portion, and U_p is the plastic part of the total strain energy U. Applying the first law of thermodynamics, the global energy balance required in the fracture process can be written in the form:

$$\dot{U}_f + Q = \dot{E} + \dot{K} + \dot{\Gamma}$$

where Q is the heat rate, E the internal energy, K the kinetic energy, Γ the fracture surface energy, and the dot denotes differentiation with respect to time t. Since the process is assumed to be slow and adiabatic, $Q = \dot{K} = 0$ and $\dot{E} = U = U_e + U_p$. As a result, the above relation becomes:

$$\frac{\partial(U_f - U_e - U_p)}{\partial a} = G^* = \frac{\partial \Gamma}{\partial a} \qquad (6.1)$$

Note that $\frac{\partial}{\partial t} = \frac{\partial}{\partial a}\frac{\partial a}{\partial t} \cdot \frac{\partial \Gamma}{\partial a}$ is the material surface energy density which is assumed to be an experimentally determined quantity at the given temperature. The left side of Equation (6.1) may be interpreted as the net energy available to generate new crack surfaces and it retains this identity regardless of the extent of stable crack growth.

Until the point of the onset of crack growth, under monotonic loading, a deformation theory of plasticity can be considered valid. The deformation theory is essentially equivalent to nonlinear theory of elasticity. Hence under the deformation theory of plasticity, without the presence of any unloading, one can formally observe the equivalence of $U_e + U_p$ (sum of elastic and plastic energies) to a hypothetical nonlinear elastic strain energy $\bar{U}_e$. Thus, under the use of deformation theory one can write

$$\frac{\partial}{\partial a}\left[U_f - U_e - U_p\right] = \frac{\partial}{\partial a}\left[U_f - \bar{U}_e\right]$$

But $(\bar{U}_e - U_f)$ for a nonlinear elastic body is nothing but the total potential energy of the system. Recalling the equivalence of J to $-\frac{\partial V}{\partial a}$ (equation 2.2), one can then write,

$$\frac{\partial}{\partial a}\left[U_f - U_e - U_p\right] = -\frac{\partial V}{\partial a} = J \qquad (6.2)$$

up to the point of onset of initial crack growth (i.e. the point A in Figure 12). Thus, when stable crack growth does not occur, and a deformation theory of plasticity is a valid approximation, the critical value of J as an initiation criterion is physically equivalent to a

critical value of G^*. However, as was emphasized in Chapter II, under the use of the deformation theory of plasticity, the J-integral is interpreted as "the potential energy difference between two identically loaded bodies having neighboring crack size" [32] and no actual new crack surface created. Consequently, the numerical proof of the equivalence of G^* to J in Equation (6.2) loses its meaning. When stable crack growth occurs with attendant unloading near the crack-tip, and the use of an incremental flow theory is imperative, Equation (6.2) is no longer valid.

It is significant that since Equation (6.1) is based only on a global energy balance, it is apparently not restricted to fracture mechanics theories based on a deformation theory. Thus, as long as the surface energy density $\frac{\partial \Gamma}{\partial a}$ for each crack growth size is experimentally determined, the energy balance (Equation (6.1)) can be served as a valid fracture criterion for an extending crack in an arbitrary hardening elastic-plastic material. To the author's best knowledge, however, those experimental values of $\frac{\partial \Gamma}{\partial a}$ were never recorded and hence providing a complete scheme of stable crack growth for ductile materials based on the present development is impossible. It can be stated that the formulation of an acceptable fracture criterion associated with stable crack growth is still an open subject. Due to limitation of time, the scope in this dissertation was limited to the understanding of the properties of G^* for an extending crack.

Study of Crack Growth Process

It is desirable to provide a procedure for evaluating the global

energy release rate G^* for the crack growth process. To assure the analyses of crack growth phenomenon, an experimental J resistance curve constructed by plotting the J data versus the measured crack extension Δa as suggested by Landes and Begley [37] is thus proposed to study the stability of the crack growth process in this dissertation. This is shown schematically in Figure 14. Notice that the J value calculated by Equation (2.3) does not give an exact value for the case of an advancing crack. However, this does not present any problem since these inexact values of J are originally used only for extrapolation purposes (to pick the J_{IC} measurement point) and the error thereby generated is negligible.

For a given experimental J - Δa resistance curve, a virgin specimen containing a crack of initial length a_o will be loaded monotonically, and a finite-element incremental solution will be obtained based on the assumptions described earlier. Since no unloading is present, the criterion $J = J_{IC}$ can be used for the initiation of crack growth. From the dependence of J on the loading parameter P ($J = J(p)$), one can obtain P_c at the onset of crack growth initiation. It is noted that the apparent small crack extension $\Delta a = \Delta a_o$ as shown in Figure 14 is caused by the stretch zone formation instead of actual crack extension due to material separation. Thus, the extrapolated J_{IC} value taken at the intersection of the J resistance curve with the crack-tip blunting line is consistent with that taken at the vertical line, $\Delta a = 0$.

To simulate an available experimental J resistance curve using the computer program developed, first of all an appropriate value of ΔJ

needs to be prescribed (See Figure 14). Then the crack-tip node will be released and made to advance by an amount Δa while keeping the load parameter constant. At the end of the crack-tip advance the quantity $\frac{\Delta}{\Delta a}(U_f - U_e - U_p)$, which is numerically nothing but the global energy G^* at crack growth Δa_1, will be computed. Next, by using Equation (2.3), say

$$J = \frac{2A}{Bb}$$

one has (See Figure 15)

$$\Delta J \sim \frac{2}{Bb}(A_2 - A_1)$$

$$\sim \frac{2P_c}{Bb}(\Delta\delta_1 + \Delta\delta_2)$$

and

$$\Delta\delta_2 \sim \frac{\Delta JBb}{2P_c} - \Delta\delta_1 \qquad (6.3)$$

Again, B is the thickness of the cracked specimen, and b is the uncracked ligament. $\Delta\delta_1$ denotes the incremental load-point displacement caused by crack extension. $\Delta\delta_2$ is the approximate incremental load point displacement of interest which can be used to determine the incremental applied load ΔP for next load step. This procedure was termed as the so-called "Displacement Control Loading Process" (See Appendix C). After applying ΔP on the specimen, a new J value corresponding to crack growth Δa_2 in Figure 14 is recomputed by Equation (2.3). That is:

$$J = \frac{2A_2}{Bb_2}$$

Note that b_2 is the uncrack ligament corresponding to crack growth Δa_2. This process will be continued until a coincident J resistance curve is constructed and, simultaneously a G^* -Δa relation will be generated (See also Figure 54). An estimate of the P-δ relation during crack extension is given schematically in Figure 15.

It is worthwhile to reiterate that G^* is interpreted as the net energy "available" for fracture and its calculation is not restricted to the deformation theory of plasticity. Thus, as a crack starts extending while keeping the load parameter constant, a higher value of G^* will make the crack extend more readily. Studying the computed G^* -Δa relation, one may obtain much useful information about stable crack growth. Some results will be discussed in detail in the last section of Chapter VII.

Finite Element Representation of Crack Growth

Anderson [78,79] and Kfouri and Miller [74,75] have presented finite element solutions for growing cracks under plane stress and plane strain conditions, respectively. Since the singular behavior of elements at the crack-tip is not included (the elements used are the simplest constant strain elements), the accurate behavior at the crack-tip which would be of interest for evaluation of the fracture tests can not be generated and any summary is bound to be incomplete. The necessity to develop a much more precise finite element analysis which can give

reliable predictions of the extent of the plastic zone for each crack growth is obvious. The present hybrid displacement finite element model, with high-order isoparametric elements in the regular region and circular-sector shaped "embedded-singularity" elements near the crack-tip (yet satisfy the conditions of inter-element displacement and traction continuities), is therefore devised and should be of value for further extension of the knowledge of ductile fracture including the phenomenon of stable crack growth. The details of the finite-element representation of crack growth, such as element design, detailed procedures, and fitting functions are described as follows:

(1) Element Design

The same crack-tip sector singular elements as those employed in the study of crack growth initiation are suggested here. The distance between the apex node and its middle node, as shown in Figure 17, is designed to be the desired extension of the crack Δa. This distance is small compared to the crack length a and is equal to about 1 percent $\sim$ 2.5 percent of the crack length.

As long as the crack propagates, the sector elements are all shifted together by the distance Δa toward the direction of crack growth. The surrounding regular elements, which do not necessarily cover the entire regular region, must be rearranged due to the shifting of the singular elements. Thus, the element mesh needs to be changed for each stage during the whole period of crack growth.

(2) Modeling of Crack Growth Process

The crack growth process as pictorially indicated in Figure 14

can be elaborately described and roughly divided into four steps ((a) - (d)):

(a) Before the crack propagates, an accurate, well-developing fitting procedure is required to interpolate all the data on twenty-five Gaussian points (Appendix C) in each "old" element onto the new data points in fictitious rearranged elements. Those fitted data, which include all the field variables such as displacements, strains, stresses, translation of yield surface, strain energy, etc. are subsequently stored in a temporary tape. Now, as shown in Figure 17, the apices of the rearranged elements are centered ahead of the crack-tip A, say at point C.

As long as the fitting procedure is followed as shown in Figure 17, the Gaussian point D in an old element will "move" to the corresponding point D' in a rearranged element, the question may well be asked as to how some suitable points are determined such that the data at point D' can be fitted by them accurately.

To interpolate the data in the old element mesh onto the new element mesh, a simple but accurate linear fitting function is used in the present work. As a motivation, for example, in terms of the two-dimensional rectangular Cartesian coordinate system the undetermined fitting function can be expressed as a linear combination of polynomials. That is:

$$(a + bx)(c + dy)$$

where a, b, c, and d are the four arbitrary coefficients to be

determined. Therefore, to find the data at a fitted point in the rearranged element by the linear interpolation polynominals (for two dimensional analyses), the data on four nearest surrounding points in the old element are required. Further, because of the inherent inter-element discontinuity of stresses and strains, those four chosen Gaussian points must be located in the same element.

Fitting Procedures. Since the data of four old Gaussian points in the same element are required to interpolate the data at the fitted point, say D' (See Figure 17), each "old" element with twenty-five Gaussian points can be readily separated into sixteen regions with each region containing four Gaussian points (See Figure 18). Those inter-region boundaries are defined by the local isoparametric coordinates (ξ,η) or polar coordinates (r,θ) of Gaussian points, depending on regular or singular elements those Gaussian points are in.

The "movement" from point D to point D' in general covers the following four cases:

(i) from a regular element to a singular element,

(ii) from a singular element to a singular element,

(iii) from a regular element to a regular element,

(iv) from a singular element to a regular element.

Referring to Figure 17, the first two cases can be readily dealt with by transforming the Cartesian coordinates $(x_{D'}, y_{D'})$ of D' into the polar coordinates $(r_{D'}, \theta_{D'})$ with respect to the old crack-tip A. The appropriate element and region to be used to fit the data at point D' in the singular element are thus determined by classifying the values

of $(r_{D'}, \theta_{D'})$. However, for the last two cases, one has

$$x'_D = \sum_{i=1}^{8} N_i(\xi,\eta)x_i$$

$$y'_D = \sum_{i=1}^{8} N_i(\xi,\eta)y_i$$

where the shape functions $N_i(\xi,\eta)$ are polynomials of (ξ,η) and defined in Chapter V. x_i and y_i $(i = 1,\ldots,8)$ are the nodal Cartesian coordinates of the old regular element. Now, to find the isoparametric coordinates (ξ,η) of point D' with respect to the old element and to determine the suitable region in the old regular element, it is required that the two nonlinear simultaneous equations in two unknowns (ξ,η) be solved. These solutions can be easily achieved by modifying the well-known Newton-Raphson iteration method. Assume

$$E(\xi,\eta) = x'_D - \sum_{i=1}^{8} N_i(\xi,\eta)x_i = 0$$

$$F(\xi,\eta) = y'_D - \sum_{i=1}^{8} N_i(\xi,\eta)y_i = 0$$

Let $\xi_o = 0$, $\eta_o = 0$ be the initial values. Define:

$$E_\xi = \frac{\partial E}{\partial \xi} \; ; \qquad E_\eta = \frac{\partial E}{\partial \eta}$$

$$F_\xi = \frac{\partial F}{\partial \xi} \quad ; \qquad F_\eta = \frac{\partial F}{\partial \eta} \quad .$$

Then the iteration becomes

$$\xi_{i+1} = \xi_i - \left\{ \frac{E\,F_\eta - F\,E_\eta}{E_\xi F_\eta - E_\eta F_\xi} \right\}_i$$

$$\eta_{i+1} = \eta_i - \left\{ \frac{F\,E_\xi - E\,F_\xi}{E_\xi F_\eta - E_\eta F_\xi} \right\}_i \quad .$$

The subscript i indicates that these functions are evaluated for $\xi = \xi_i$ and $\eta = \eta_i$. The iteration are repeated until the results are satisfied.

Fitting Functions. As was mentioned above, an appropriate fitting function need be devised. As shown in Figure 19, suppose the values of the field variable f_i of regular elements are known at all the given four points with isoparametric coordinates (ξ_i, η_i), $i = 1,\ldots,4$, respectively. Then the approximating functions, $g_1(\eta)$ and $g_2(\eta)$, can be found by interpolating f_i as

$$g_1(\eta) = (f_2 - f_1) \frac{\eta - \eta_1}{\eta_2 - \eta_1} + f_1 \tag{6.4}$$

$$g_2(\eta) = (f_4 - f_3) \frac{\eta - \eta_3}{\eta_4 - \eta_3} + f_3 \tag{6.5}$$

Similarly, by interpolating $g_1(\eta)$ and $g_2(\eta)$, the approximate fitting function $f(\xi,\eta)$, having the same values as f_i at given corresponding points, is constructed as follows:

$$f(\xi,\eta) = (g_2(\eta) - g_1(\eta)) \frac{\xi - \xi_1}{\xi_3 - \xi_1} + g_1(\eta) \tag{6.6}$$

Substituting Equations (6.4) and (6.5) into Equation (6.6), after some manipulation, one has:

$$\begin{aligned} f(\xi,\eta) = {} & f_1\left[\left(\frac{\eta - \eta_1}{\eta_2 - \eta_1} - 1\right)\frac{\xi - \xi_1}{\xi_3 - \xi_1} - \frac{\eta - \eta_1}{\eta_2 - \eta_1} + 1\right] \\ & + f_2\left[\frac{\eta - \eta_1}{\eta_2 - \eta_1}\left(1 - \frac{\xi - \xi_1}{\xi_3 - \xi_1}\right)\right] + f_3\left(1 - \frac{\eta - \eta_3}{\eta_4 - \eta_3}\right)\frac{\xi - \xi_1}{\xi_3 - \xi_1} \\ & + f_4 \frac{\eta - \eta_3}{\eta_4 - \eta_3}\frac{\xi - \xi_1}{\xi_3 - \xi_1} \end{aligned} \tag{6.7}$$

It is noted that ξ_1 and ξ_2 in Equation (6.7) essentially represent the same ξ locations, that is, $\xi_1 = \xi_2$. Moreover,

$$\xi_3 = \xi_4 \,, \quad \eta_1 = \eta_3 \quad \text{and} \quad \eta_2 = \eta_4$$

Therefore, Equation (6.7) can be simplified as

$$\begin{aligned} f(\xi,\eta) = {} & f_1\{A(\xi)[B(\eta) - 1] - B(\eta) + 1\} + f_2\{B(\eta)[1 - A(\xi)]\} \\ & + f_3\{[1 - B(\eta)]A(\xi)\} + f_4[A(\xi)B(\eta)] \end{aligned} \tag{6.8}$$

where

$$A(\xi) = \frac{\xi - \xi_1}{\xi_3 - \xi_1}$$

$$B(\eta) = \frac{\eta - \eta_1}{\eta_2 - \eta_1}$$

For singular sector elements, the same fitting polynomial f as expressed in Equation (6.8) is achieved, except that isoparametric coordinates (ξ,η) are replaced by polar coordinates (θ,r). Here, $f(r,\theta)$ can be used to find the approximate data at any fitted point in the rearranged singular element near the crack-tip region.

(b) Define the singularity location at the new crack-tip C. The stiffness matrix is then recalculated for the rearranged mesh while keeping the same power singularity based on the new fitted data which were stored in the tape. In order to minimize the numerical errors which occurred due to the fitting process, the whole cracked body should be equilibrated before releasing the old crack-tip node A. To assure this, the convergence of the residual forces during iterations need be carefully investigated. Also, for each iteration procedure, such as in the static crack case, an updated stiffness matrix is required.

(c) In terms of finite-element simulation, after obtaining the equilibrium conditions for the cracked body, crack growth can be represented as the relaxation of the nodal forces at the node representing the old crack-tip. In this dissertation, the relaxation is performed

directly by applying a negative reaction at the old crack-tip node A and eliminating the residual force by successive iterations. The role of unloading process occurred in the plastic region behind the advancing crack-tip need be satisfactorily demonstrated (See Appendix C).

(d) At the end of the crack-tip release, the quantity $G^* = \frac{\Delta(U_f - U_e - U_p)}{\Delta a}$ will be calculated. It is noted that all the parameters (U_f, U_e and U_p) should be computed based on the data obtained before the fitting procedures are done. By prescribing the increment of J to be ΔJ, and by using Equation (6.3), an increment of external load Δp can be easily obtained and applied. A new J value of crack growth Δa is thereby achieved.

Lastly, repeat steps (a) - (d) until the whole procedure is finished. The flow chart of crack growth computer program by the present finite element procedure is provided in the Appendix B.

CHAPTER VII

PROBLEM SOLUTIONS

In this chapter, three mode I cracked specimens (three-point bend, center-cracked and compact tension types) are chosen to study the initiation of crack growth. They supply a direct means of checking the available experimental results [34]. To investigate the behaviors of crack growth, however, Kfouri et al.'s center-cracked plane strain tension specimen [74,75] together with two compact tension specimens made of different materials are solved.

In the first section, based on the earlier mentioned assumptions and the analysis procedure developed, it is proposed to obtain the functional relationship computationally between the J-integral and displacement δ. Comparing this J in an arbitrary problem with the experimentally determined J_{IC} (which then becomes a material property) governing the initiation of crack growth, the situation can thus be assessed whether the crack in the given case is on the verge of growing or not.

In the second section, the relationship between the J-integral and crack-tip opening displacement (COD) for ductile materials is explored and compared with that obtained by others [23,25,26].

In order to provide a realistic analysis for fracture, the remainder of this chapter is devoted to investigate the phenomenon of crack growth. The focus for this section is the calculations of global energy release rate G^* in the presence of crack extension. The results

summarized by Kfouri and Miller [75] for elastic-plastic linear hardening material are thoroughly reviewed and the predictive inadequacy is compensated. A first analysis of global energy release rate G^* for an extending crack in arbitrary hardening material is also presented in this section. An attempt is finally made to provide the relation G^* versus Δa (crack growth) which should be useful in the investigation of stable crack growth. However, due to the lack of an acceptable *fracture criterion associated* with stable crack growth and the extensive experimental data, it is presently not possible to predict fracture from the global energy balance as developed in the previous chapter. Detailed discussions are thus given.

The Initiation of Crack Growth

(1) Three-Point Bend Specimen

The Problem. A three-point bend specimen made of Ni-Cr-Mo-V rotor steel is analyzed in this work and is inserted in Figure 21. Since the system is symmetrical, it is only necessary to analyze a half portion whose finite element mesh is idealized for the present geometry of dimensions W = 0.474", L = 1.57", W/a = 0.5, thickness B = 0.394" and 0.788" (See Figure 21). Figure 21 shows the element breakdown for half of the structure with circular-sector shaped "singular" elements surrounded by "regular" eight-node isoparametric quadrilateral elements. The number of elements and nodes are 40 and 137, respectively. The region of greatest interest is obviously the uncracked ligament ahead of the crack-tip. Appropriate prescribed displacement boundary conditions are provided.

The uniaxial stress-strain behavior of Ni-Cr-Mo-V steel is assumed to be of the Ramberg-Osgood form shown in Figure 22. Young's modulus of elasticity E is taken at 30 X 10^6 psi, and the plastic modulus B equals 183, 031 psi. The power hardening coefficient is taken as 22.19, and the material yields at 120,000 psi. Poisson's ratio, ν, is 0.3.

Results and Discussions. The presently developed finite-element model does not involve the thickness of the bend bar specimen except for the "either-or" choice of plane stress or plane strain. Based on the arguments of Bucci et al. [34], for the dimensions of the present specimen, plane stress conditions were invoked.

First, in the assumed field functions for the "singular element" as detailed in Chapter V, one can set the power hardening coefficient $n = 1$, and then the assumptions correspond to an approximation for the asymptotic solutions for displacements/stresses in the linear elastic case. Thus, in the first increment of the present incremental solution procedure (setting $n = 1$) the linear elastic solution can be computed. In the linear elastic case, the value of the normalized elastic stress intensity factor as calculated directly from the built-in asymptotic stress/displacement field in the present procedure was found to be $K_I/p = 12.15(\text{in})^{-3/2}$. This is in excellent agreement with Bucci et al.'s result of $K_I/p = 12.81(\text{in})^{-3/2}$ for similar geometry. The path independent J-integral for this linear elastic case was also directly computed around four different paths as shown in Figure 21. The average value of J for these four paths was found to be 0.5401×10^{-5} lb-in/in^2 per

unit load which corresponds to a value $K_I/p = 12.56(in)^{-3/2}$. Thus, it is found that the stress-intensity factor evaluation from the J-integral is also highly accurate in the present approach.

Then, the load required for the specific point (near the crack-tip) to be on the point of yielding was determined. The solution thus continued by progressively increasing the applied load and determining an elastic-plastic solution at each increment. These solutions were stored on magnetic tape for subsequent processing to determine the field values of interest.

Figure 23 shows the computed load versus load-point displacement (δ) and the load versus half crack-mouth-opening (V) curves. Also shown for comparison purpose are (i) the p versus δ curve based on linear-elastic theory, and (ii) the p versus δ estimation given by Bucci et al. [34].

Figure 24 displays the directly computed relationship between the J-integral and load point displacement δ. The J-integral was calculated using Equation (2.6) over four different paths and the average value was plotted. In the present finite-deformation analysis the value of J was found to be almost path-independent. (The maximum variation was just two percent while computed at the highest load level.) Also shown in Figure 24 for comparison purposes are: (i) the J-integral estimation based on a linear-elastic analysis, (ii) the J-integral given by Bucci et al. [34], and (iii) the Westinghouse experimental data [34] for bend specimens of thickness 0.394" and 0.788" respectively, and (iv) the estimation of J from the presently compute p versus δ curves using the

empirical formula (2.3). The excellent correlation between the present finite deformation results and the referenced experimental results can be noticed. As reported in [34] for both the single and double thickness bend bars, Westinghouse experimentally determined displacement δ at fracture ranged between 0.022 and 0.024 inches for a/w ratios of magnitude comparable to 0.5. Under the present finite-deformation analysis for the above mentioned experimentally determined fracture displacements, the computed J is almost halfway in between the Westinghouse experimental results (See Figure 24). For the same critical δ range, the estimates of Bucci et al. [34] for J is about six to ten percent higher.

As is seen in Figure 24, based on the present finite deformation analysis, the computed critical value of J, J_{IC}, is about 1000 in-lb/in^2. Even though the question of precise measurement point for J_{IC} does not appear to have been addressed to in the 1971 work of Begley and Landes [32,33], from the excellent agreement of these results with the present results based on the modeling of a non-growing, stationary crack, it may be deduced that there was no noticeable stable crack growth in the experiments [32,33]. Also, because of the reasonable agreement (with maximum seven percent difference) between the present computed results and the empirical formula (2.3) of Rice et al. [38], it can be concluded that the estimate of Equation (2.3) can be used with reasonable accuracy in the experimental measurement of J from a single specimen (three-point bend) test data.

Notice that in the present procedure the J-integral paths go

through the middle of the quadratic isoparametric regular elements where a much smoother stress and strain data can be expected. It is also worth noting that in the small-deformation analysis, even though path-independence was noted for paths 2, 3 and 4 (Figure 21), this was not the case for path 1, which is adjacent to the crack-tip (the path 1 value J different by about five to seven percent from those of paths 2-4) [69]. However, in the present finite deformation analysis, more accurate path-independence was noticed for all the paths 1-4 (with only $\pm$ two percent variation), and the path-independence for path 1 was sometimes better than that for the other path at higher load levels. It is speculated that since finite-geometry changes are more important near the crack-tip, the use of the equation (2.6) for J under finite deformations lead to this more accurate path independence for the contour immediately adjacent to the crack-tip. Thus, finite deformation assumptions as used in the present analysis play an important role in dealing with elastic-plastic fracture mechanics.

Figure 25 shows the yield zones in the specimen, and Figure 26 shows the crack surface deformation profiles for various load levels. Figure 27 and Figure 28 show the distribution of the effective strain and effective stress ahead of the crack-tip in the uncracked ligament respectively. Here, the effective strain and effective stress are defined as follows:

$$\sigma_{ef} = \sqrt{\sigma_x^2 + \sigma_y^2 - \sigma_x\sigma_y + 3\sigma_{xy}^2}$$

$$\epsilon_{ef} = \int d\ \epsilon_{ef}^p + \sigma_{ef}/E$$

where the plastic effective strain increment $d\varepsilon^p_{ef}$ can be determined as (for plane stress case)

$$d\varepsilon^p_{ef} = (1 + \nu^2 + \nu)(d\varepsilon_x^2 + d\varepsilon_y^2) - 2(1 - \nu^2 - \nu)d\varepsilon_x d\varepsilon_y + 3d\varepsilon_{xy}^2$$

The relative path independence of the computed J-integral (modified for the present finite deformations) indicates that it is indeed a valid parameter to be used in a ductile fracture initiation criterion.

(2) Center-Cracked Specimen

The Problem. The center-cracked specimen which is analyzed in this work is shown in Figure 29. As is clear in Figure 29, the finite element mesh represent quadrant 1 of the specimen geometry which is sufficient for the calculation procedure. The present geometry of dimensions are 2b = 1", 2D = 2.25", B(thickness) = 1" and a/b = 0.5. The chosen test piece was presented by 50 elements and 171 nodes. It is also to be observed from the mesh that there is a gradual gradient in element size towards the crack-tip.

The material considered for the present configuration is Ni-Cr-Mo-V steel. Thus, the same Ramberg-Osgood form as that shown in Figure 22 is again adopted.

Results and Discussions. Similarly, based on the arguments of Bucci et al. [34], the analysis was performed using a plane stress assumption. An initial elastic computation was first carried out and eight more load increments were then progressively increased and solved. The path-independent nature of the J integral was successfully

demonstrated for each increment around five different paths as shown in Figure 29. The maximum variation was found to be about four percent for all paths. The average value of J for these five paths (for linear elastic case) was found to be 0.3733×10^{-7} lb-in/in^2 per unit load which corresponds to a value $K_I/p = 1.06(\text{in})^{-3/2}$. This is in excellent agreement with that calculated directly from the built-in asymptotic stress/displacement field of $K_I/p = 1.07(\text{in})^{-3/2}$.

Figure 30 shows the results for gage-point displacement δ (at point G in Figure 29) variation with applied load p. Also shown, for comparison, are the curves based on linear-elastic analysis as well as the approach of Landes et al. [33,34].

Figure 31 shows the variation of the value of the J-integral with the gage-point displacement δ. The J-integral was calculated, using Equation (2.6), and averaged over the five paths for each load. Also shown for comparison purposes are: (i) estimation of J based on linear-elastic theory (essentially a "small-scale yielding" approximation), (ii) estimation of J given by Landes et al. [33,34,71], and, (iii) the Westinghouse experimental data. Again, J versus δ agreement of actual experiment and the present finite-deformation analysis are quite good.

Referring to Figure 31, it is worthwhile to mention that all J values presented in Landes et al. [33,34] for center-cracked specimens should be twice the values presented. These "self-compensating" errors are now recognized by these authors [71]. These involved a missing factor of two in determining J from compliance measurements and a

measurement point for J_{IC} at maximum load, which had been observed to coincide with the onset of crack growth in their three-point bend specimens but had been assumed, incorrectly, to do so in the present tension specimen as well. In [71], Landes et al. also note that their recent experimental results show that when the toughness measurement point is clearly defined, center-cracked panels and bend specimens for the same material yield the same J_{IC} toughness level. Thus, it is concluded that J_{IC} is indeed independent of specimen geometry.

Figure 32 shows the growth of the yield zone in the test piece at several stages of loading. Figure 33 displays how the crack profile deforms throughout the loading history.

(3) Compact Tension Specimen

The Problem. Using the present procedure, detailed analyses were performed for the case of a compact tension specimen for which experimental results had also been reported by Bucci et al. [34]. Because of the symmetry, only the upper half plane was used to analyze this problem. The present geometry of dimensions are W = 2", 2H = 2.4", and a/w = 0.5 (See Figure 34). The finite element idealization is illustrated in Figure 34, with 30 elements, 103 nodes and 196 degrees of freedom.

The material is A533B steel. As is shown in Figure 35, the experimental stress-strain curve was fitted by two Ramberg-Osgood type curves. In the first curve the mathematical yield point is lower than that in the experiment, but the strain hardening is well represented; whereas, in the second curve the mathematical yield point is roughly the

same as that in the experiment, but it is almost a non-hardening type of approximation.

The effects of the mathematical modeling of the true uniaxial stress-strain curve was studied by Atluri and Nakagaki [69]. No significant differences were found for the gross results for load-point displacements and J for these two types of material characterizations. One reason for this may perhaps be attributed to the compensating feature of these two approximations as described above. Thus, because of the expensive computer time, the fitted curve in the present analysis was taken to be that corresponding to material characterization 1 in Figure 35.

Results and Discussions. Again, for the present compact tension specimen geometries, based on the arguments of Bucci et al. [34], plane stress conditions were invoked. Even though the loading of the compact tension specimen in the actual experiment involves a pin-hole in the specimen, the effect of this pin has not been simulated in the present numerical procedure. Instead, a point loading has been assumed.

The linear elastic solution showed that the value of the normalized elastic stress intensity factor evaluated from the J-integral (0.1632×10^{-5} lb-in/in^2) $K_I/p = 6.90(\text{in})^{-3/2}$ was also in excellent agreement with that reported by Bucci et al. [34] ($K_I/p = 6.79(\text{in})^{-3/2}$) and that calculated directly from the built-in asymptotic stress/displacement field ($K_I/p = 6.61(\text{in})^{-3/2}$). The direct evaluation of J was carried out and averaged along three different paths at each load level as shown in Figure 34. Throughout the loading history each value

of J was within 1.3 percent of the mean.

Figure 36 shows the computed load versus load-line displacement (P versus V_L) and the load versus the half crack mouth opening (P versus V) curves. Also displayed for comparison purposes are (i) the P versus V_L curve based on linear-elastic theory, and (ii) the p versus V_L curve given by Bucci et al. [34].

Figure 37 shows the directly computed average value of J versus load-line displacement V_L (at point L in Figure 34) curve along with J versus V_L estimates based on (i) a linear-elastic analysis, (ii) the computed p versus load-line displacement and using the empirical formula (2.3) of Rice et al. [38], and (iii) the computed p versus load-line displacement curve and using the empirical formula (2.4) of Merkle and Corten [39]. The experimental results [32,33,34] for J_{IC} using the present one-inch thick specimen as well as for G_{IC} using a 12 inch thick specimen are also shown. For the present one-inch thick specimen a/w = 0.5, the crack-mouth opening V_M at fracture was found experimentally to be 0.07 inch, which corresponds to load-line critical displacement $V_L \sim 0.023$ inch. From the presently computed J versus V_L curve in Figure 37, it can be seen that the computed $J_{IC} \sim 1190$ in-lb/in^2 which is about 16 percent higher than the reported [32,33,34] experimental $J_{IC} \sim 1030$ in-lb/in^2. In the 1971 work of [32,33], however, the precise measurement point of J_{IC} was not clearly defined and the phenomenon of possible stable crack growth prior to fracture does not appear to have been accounted for until the 1973 work of Landes and Begley [37]. Thus, the fact that the J value (and hence J_{IC}) computed by using

a stationary-crack model such as the present case is always higher than in experimental specimens undergoing subcritical crack growth can easily be explained as in [37,70]. From the present results it is felt that there was some subcritical crack growth on the present compact tension specimen prior to fracture in the experiments of Begley and Landes 1971 [32,33]. Some results about the finite element simulation of crack growth are to be presented in detail in the last section of this chapter.

From the Figure 37 it can also be seen that the present directly computed J correlates excellently with the empirical formula (2.4) of Merkle and Corten [39], whereas the empirical relation (2.3) of Rice et al. provides an underestimate by about 12 percent. Thus, in experimentally measuring J from a single compact tension specimen test data, it is advisable to use the relation (2.4) rather than (2.3).

Figure 38 shows the yield zones at various load levels. The crack profile at each load level is illustrated in Figure 39. To test the singular nature of strains near the crack-tip, the effective strain in a tip element at along $\theta = 60^{\circ}$ (See Figure 1) is plotted in Figure 40. It shows an almost exact singular-strain behavior at all load levels, i.e., $\varepsilon \sim r^{-n/n+1}(n = 6.971)$. Finally, based on the present finite-deformation analysis, Figure 41 displays how the "singular" crack-tip elements deform at the load level, p = 21,974 lbs.

The Relation Between the J and COD Concepts

The various earlier cited calibrations for COD from CGD for a three-point bend specimen are shown in Figure 42. As expected, the

CODE [25] relation and the "extrapolation of linear portion of the crack surface" give linear relations between COD and CGD, where as the calibration suggested by Wells [26] and Robinson and Tetelman [23] give a nonlinear relation between COD and CGD in the small-scale-yielding range and a linear relation when the plastic-yield zones start growing in the net section ligament (large-scale plasticity). Moreover, there is a reasonable agreement between the COD value corresponding to a particular CGD value using the first three of the above calibrations, whereas that given by the calibration curve of Robinson and Tetelman [23] is lesser by a factor of $1.5 \sim 2.0$. Using the information in Figure 23 (which also shows the CGD values corresponding to given load-point displacement, δ, values), Figure 24 (J versus δ curve), and Figure 42 (CGD versus COD curve), the data is reduced to show the variation of J with COD (using the above cited different definitions for COD) in Figure 43. Also shown for comparison purposes is the straight line $J = \sigma_y(\text{COD})$; where σ_y is taken to be 147.5 ksi, halfway between the 0.2 percent offset yield stress and the ultimate stress (Figure 22) (for weakly hardening materials, this is justifiable [37]).

As can be expected, the relation between COD and J is almost linear when the calibrations of Wells [26] and [23]* are used (because of the variation $\text{COD} \sim \text{CGD}^2$ in the small-scale-yielding range in these calibrations) whereas the COD versus J relation is significantly nonlinear in the small-scale yielding range when the CODA [25] and linear

*The small degree of nonlinearity in the J versus COD curve for COD values 0.5 to 1.5 x 10^{-3} in. (.013 - .04 mm) may perhaps be spurious when one notes that the error band in the experimental measurement of COD in this region appears to be about 25-35 percent [23].

extrapolation methods are used. It can be argued [39] that for COD to be a valid fracture criterion, COD = $J/(\lambda\sigma_y)$ (or $J = \lambda\sigma_y$COD) for weakly-hardening materials such as the present.

It can be seen from Figure 43, that the essentially linear relation between J and COD, using Wells' [26] calibration value for COD can be stated by the equation $J \simeq 1.4\ \sigma_y$ COD ($\sigma_y = 147.5$ ksi as noted earlier). Whereas, Hays and Turner [48] using the same definition of COD for a similar three-point bend specimen find, from their finite element analysis, $J = 2\sigma_y(\text{COD})$. It is interesting to note that Rice and Johnson [45], considering the finite deformation effects near the crack-tip and using a rigid-plastic slip line theory, find for the small-scale-yielding range, $J \simeq 1.485\sigma_y(\text{COD})$, which is excellent agreement with the present finite-deformation analysis result, as above, using Wells' [26] calibration for COD. Again the predominantly linear portion of J versus COD relation from the COD calibrations of [23] can be stated, as seen from Figure 43, to be $J \sim 1.8\sigma_y$COD, while the linear extrapolation values of COD correspond to $J \sim 1.38\sigma_y$COD and thus the value of λ (in $J = \lambda\sigma_y$COD) in the present computations using various COD definitions is in the range $1.4 \sim 1.8$ (See Figure 43).

As for the compact tension specimen, using the computed crack surface deformation profiles (Figure 39), p versus V relation (Figure 36), J versus V_L curve (Figure 37) data is reduced to the form of J versus COD curve, which is shown in Figure 44. For want of a better definition, COD for the compact tension specimen is taken by extrapolating the linear portion of crack-surface profile near to the crack-tip.

From Figure 44, it can be seen that the computed J versus COD curve can be stated approximately as $J = 1.44\sigma_y COD$. This value of $\lambda = 1.44$ is once again in excellent agreement with the preductions of Rice and Johnson [45] and Hutchinson-Rice-Rosengren [2,3]. Similar procedure was made for the center-cracked specimen and the computed J versus COD curve (Figure 45) can be stated approximately as $J = 1.21\sigma_y COD$. Thus from the two present analyses of bend type specimens (three-point bend and compact tension specimens), with the exception of the result for the three-point bend specimen using the calibration of [23], it may be inferred that $J = 1.4\sigma_y COD$. As for the tension type crack problems, such as the present center-cracked specimen, it may be inferred that $J = 1.2\sigma_y COD$. Thus, there is a direct correlation between J and COD.

However, in analyzing in-service situations of arbitrary ductile fracture problems using elastic-plastic finite element analysis procedures such as the present, the question still remains as to how to directly compute COD based on a consistent definition. To this end, attempts were made in the present computations to take COD to be crack opening at the point where the elastic-plastic boundary intersects the crack-profile or to define COD to be the diameter of an inscribed circle near the crack-tip. These attempts,unfortunately, do not lead us to any rational conclusions.

Some Comments and Results about G^*

The results summarized in earlier sections are, together, rather encouraging for the problem of the initiation of crack growth from those stationary "plane fracture" problems at large-scale yielding based on

the J-integral. As has been emphasized earlier, however, since the stable crack growth problem is of great importance to the fracture of the more ductile metals, a parallel effective development for stably growing cracks is highly desirable in this section.

There has, thus far, been little attempt to study the phenomenon of crack growth for cases of large scale yielding. The current trend in those limited publications [75,76] is directed to a description of the crack separation energy rate G^{Δ} in stable crack growth. Since G^{Δ} is a geometry dependent parameter at least when the present hybrid displacement finite-element model is employed, the global energy release rate G^{*} which is not determined solely by local stresses and deformations near the crack-tip is developed and used in this work instead of G^{Δ}. Hence, if the fracture step size Δa and the global energy release rate G^{*} can be taken to be characteristic of the material, then a definite fracture criterion is supplied to predict the instability of crack growth. Therefore, in this section, the investigations will include the following two parts:

(1) to study the variation of G^{*} and J with decreasing values of parameter S at various levels of applied stress σ_p. S is a parameter which is proportional to the ratio of growth step size Δa to plastic zone size. In the case of small scale yielding the plastic zone size is proportional to $(K_I/\sigma_y)^2$ or to $(\sigma_p/\sigma_o)^2$ a and S can be given as

$$S = \frac{\Delta a}{\left[a \cdot \left(\frac{\sigma_p}{\sigma_y}\right)^2\right]}$$

or

$$S = \frac{\Delta a}{\left(\frac{K_I}{\sigma_y}\right)^2}$$

Now when the plastic zone is small, i.e., when S is large the elastic solution dominates over the range of Δa and so the linear elastic fracture mechanics solutions are justifiable. As S decreases this will be less true and the linear solutions will be inapplicable.

To do this, the same center-cracked plane strain tension specimen as studied in Kfouri et al. [74,75] was again solved based on the present finite-element procedure. Comparing the results with those presented in Reference [75], some extensive discussions were made. The role of unloading effect in the plastic region near the advancing crack-tip was noted and the equivalence between global energy release rate G^* and crack separation energy rate G^Δ was proved computationally. Further, these analyses were also extended to solve a compact tension specimen made of arbitrary hardening material.

(2) To display a rough scheme of crack extension by using the G^* concept and simulating an available experimental J-Δa resistance curve [30].

Variation of G^* and J with Decreasing Values of Parameter S

Kfouri et al.'s Center-Cracked Specimen. The center-cracked tension specimen solved by Kfouri et al. [74,75] is inserted in Figure 46. The geometry of dimensions are 2b = 1.6", 2d = 1.6" and a/b = 0.125. Figure 46 also represents the finite element mesh for a symmetric

quadrant of the specimen with 49 elements and 170 nodes. The region of interest is the segment in close proximity to the crack and this segment is magnified in Figure 49. Material properties are: $E = 30 \times 10^6$ psi, Poisson's ratio $\nu = 0.3$, yield stress 44,940 psi and a linear strain hardening with plastic modulus $B_o = 716{,}982$ psi plane strain conditions are assumed.

The equivalence between G^* and G^Δ was demonstrated. Since the tangent modulus method was employed in this work, the values of G^Δ were evaluated by applying an arbitrary negative force at the crack-tip until the original crack-tip nodal force was relaxed instead of using the step-wise process illustrated in the previous chapter. Moreover, by using the present hybrid displacement finite element model, due to the inherent discrepancy of nodal force distribution within singular crack-tip elements, the original nodal force at the crack-tip node which is used to determine G^Δ should be modified by an appropriate extrapolation procedure (as shown in Figure 47). These procedures were carried out and the maximum difference between G^* and G^Δ was found to be 8.8 percent.

Figure 48 shows the variation of $G^*(G^\Delta)$ and J with decreasing values of S. The results obtained by Kfouri et al. [75] are also shown for comparison purposes. In Reference [75], without a detailed description of plasticity, it was recognized that the elastic-plastic analyses were proceeded by an incremental, compatible displacement finite-element model. The elements used were the simplest of the family of isoparametric quadrilateral elements. An inappropriate incremental numerical

method, initial stress method, was used while geometry changes were included. Further, it is also noted that, as shown in Reference [75], the important role of the unloading process occurred in the plastic region behind an advancing crack-tip was apparently ignored. Thus, to provide an accurate solution in the study of stably growing cracks, the results summarized by Kfouri et al. [75] need be modified.

As illustrated in Figure 48, the values of G^*(or G^Δ) and J were normalized by a factor K_I^2, where $K_I^2 = 1.785\ \sigma_p(\sqrt{a})$ [75]. The energy balance examined by Rice [76] can be rewritten as (See the previous chapter):

$$G - P = 2\gamma = G^\Delta = G^* \quad .$$

As was already shown in Chapter II, the elastic energy release rate G is equal to $\frac{(1-\nu^2)K_I^2}{E}$ (for plane strain case) and the above formula can be represented alternatively as

$$\frac{1-\nu^2}{E}\left(1 - \frac{P}{G}\right) = \frac{G^\Delta}{K_I^2} = \frac{G^*}{K_I^2}$$

For pure elastic cases, since G = J and p = 0 (no plastic dissipation), one has

$$G^\Delta = G$$

and

$$\frac{G^\Delta}{K_I^2} = \frac{G^*}{K_I^2} = \frac{J}{K_I^2} = \frac{1-\nu^2}{E}$$

In the truly brittle region, the present finite-element solutions together with that obtained by Kfouri et al. [75] are both in excellent agreement with the value $\frac{1-\nu^2}{E} = 3.03 \times 10^{-8}$ (psi)$^{-1}$ (See Figure 48). In the brittle to ductile region, the values of G^*/K_I^2 and G^Δ/K_I^2 were calculated at various applied loads while the same crack growth increment Δa was maintained. As $S > 0.1$, as shown in Figure 48, the trend of the variation of normalized G^* and J based on the present analyses is in agreement with that obtained by Kfouri et al. [75]. However, since the recoverable dissipated energy attained in the unloading region (the shaded region in Figure 49) was not accounted for in Reference [75], the values of G^Δ/K_I^2 and J/K_I^2 (with a higher plastic work rate p) are therefore lower than that obtained by the present elastic-plastic finite deformation analysis. Moreover, it is noted that the dotted curve in Figure 48 was constructed by Kfouri et al. [75] using a twice smaller crack-tip element mesh. Thus, an accurate solution obtained by the present analysis procedure which is essentially much more sophisticated than that used by Kfouri et al. [75] is confirmed.

When the crack growth Δa was extremely small fraction of yield zone size ($S < 0.1$), as would be expected to be representative of highly ductile materials, the finite element results were not carried out even in Reference [75]. In this truly ductile region, a rigorous model for plasticity is really required. Based on the present rigorous elastic-plastic, finite deformation, hybrid displacement finite-element model, the behaviors of large-scale plasticity were first demonstrated accurately in this work.

Again, the significant role of unloading during crack extension was displayed in Figure 49, where a rearranged element mesh near the crack-tip was also drawn. The energy recovered due to unloading will cause a plastic work rate p which is less than that evaluated at neglecting unloading conditions. Thus, for cases where plastic yielding is on a large scale in comparison to geometric dimensions, as indicated by Rice [76], the functional dependence of plastic work rate p on applied loads may be appreciably altered and consequently the dependence of $\frac{P}{G}$ on applied loads is not expected to be a monotonic increasing function of applied loads. These comments can be verified here at least for the present linear hardening material. As $S < 0.07$, the results for G^*/K_I^2 in Figure 48 do increase drastically with decreasing values of S.

The variation of J/G^* was also plotted in Figure 50 with decreasing values of S. An uncertain region is again found when $S < 0.06$ (See Figure 50). The complicated relation between J and G^* discourages one to devise a parameter which could be related to J in a simple way and, somehow, allow a similarly simple approach to crack growth as does J for the initiation of crack growth.

Compact Tension Specimen. It has become evident that the prediction [76] of a vanishing energy supply to the crack-tip in the limit of continuous crack growth with vanishing Δa is restricted to elastic-perfectly plastic materials (non-hardening). As for the case of linear hardening material, the results have already been presented above. Unfortunately, however, no work has been published so far for an

arbitrary hardening material and, thus, the purpose of the following work is to extend the investigation of G^* to this material.

The geometry dimensions, finite element mesh and material properties of the present compact tension specimen (made of A533B Steel) were given in Figure 34 and Figure 35 respectively. The plane stress assumptions were again used here.

The equivalence between G^* and G^Δ was proved with a maximum variation 7.4 percent. The scheme which displayed extrapolations at the crack-tip was shown in Figure 51. As shown in Figure 47 and Figure 51, since the distributions of the nodal force in the uncracked ligament are apparently geometry dependent, the global energy release rate G^* appears to be a better definition at least when the present hybrid displacement finite-element model is used.

The variation of G^*/K_I^2, J/K_I^2 and J/G^* was plotted in Figure 52 and Figure 53 with decreasing values of S respectively. Here K_I and S are given as follows:

$$K_I = \frac{P}{B\sqrt{W}} \left[29.6 \left(\frac{a}{W}\right)^{1/2} - 185.5\left(\frac{a}{W}\right)^{3/2} + 655.7\left(\frac{a}{W}\right)^{5/2} - 1017.0\left(\frac{a}{W}\right)^{7/2} + 638.9\left(\frac{a}{W}\right)^{9/2} \right] \qquad \text{(Reference [34])}$$

and

$$S = \frac{\Delta a}{\left(\frac{K_I}{\sigma_y}\right)^2}$$

where p is the applied load (lbs), thickness B = 1", W = 2" and a = 1". It is interesting to find that, even in the large scale yielding region ($S < 0.14$), the variation of G^*/K_I^2 and J/G^* has the same trend as that obtained by solving Kfouri et al.'s center-cracked specimen for linear hardening material. Thus, the results presented here are the first computation about the variation of G^* (or G^Δ) for arbitrarary hardening materials. It is not necessary to reiterate the discussions which were already made earlier.

Using G^* Concept to Study Crack Growth Phenomenon

In order to provide an actual analysis of crack growth, based on the procedure discussed elaborately in Chapter VI, the experimental J-Δa resistance curve [30] of a one-inch compact tension specimen for Ni-Cr-Mo-V rotor steel was stimulated by the present finite-element analysis procedure. The geometry dimensions and finite element idealization were exactly the same as that illustrated in Figure 34, except the width = 2.5" and the crack length = 1.115". The material properties were given in Figure 22. Plane stress assumptions were invoked.

As a start, the specimen was first loaded monotonically until the point of the initiation of crack growth, where the critical value of J measured by the empirical formula (2.3) [38] was taken as $J_{IC} \sim 640$ (lbs-in/in^2). Taking $\Delta J = 120$ (lbs-in/in^2) and $\Delta a = 0.0175$", the experimental J-Δa was finally simulated (See Figure 54).

As was displayed in Figure 54, the variation of the global energy release rate G^* with increasing values of crack extension Δa can be noticed. G^* increased slowly and smoothly until the crack

extension Δa reached 0.035" (point S_1 in Figure 54). The values of G^* then varied unstably until the experimental J-Δa curve was simulated (point S_3 in Figure 54). To study the significant role of G^* during crack extension, it is interesting to plot the corresponding load versus crack extension (p versus a) curve as shown in Figure 55. Comparing Figure 55 with Figure 12, some encouraging observations can be drawn as follows.

(1) If the region of stable crack growth is ended at point S_o (point B in Figure 12), apparently, S_o will be located between point S_1 and S_2 (See Figure 55). At this point, the required increase of the applied load or at least of the load point displacement for stable crack growth falls to zero. The dashed line in Figure 55 represents the assumed path undertaken by stable crack growth and may be determined approximately by taking smaller increments of J and a for each crack growth step.

(2) The region S_o-S_3 represents the transition phase (region III in Figure 12) and point S_3 is no more than the point which leads a limiting steady-state situation (region IV in Figure 12).

It is emphasized that, however, the observations mentioned above are cited by simulating "one" available experimental J-Δa curve only. Thus, to create an universal function $G^*(\Delta a)$ which could be used for predicting fracture in ductile materials, some more extensive experimental data must be analyzed by the same finite-element simulation procedure as described above. Unfortunately, those extensive experimental data are so far unavailable. Further, due to the lack

of an acceptable fracture criterion associated with stable crack growth, providing a complete scheme of crack growth is presently impossible.

Fracture Criteria for Stably Growing Cracks

Palmer and Rice [80] have observed that an integral which will be termed J' is path-independent for stationary or growing cracks in any material (elastic or elastic-plastic or viscoelastic, etc.). The integral J' has a simple interpretation for crack models with a cohesive zone at the tip, within which separation begins when some critical stress level, say σ_c, is reached and there is a restraining stress $\sigma(\delta)$ during separation which falls to zero at some critical separation δ_c. Thus, for a crack which has been monotonically loaded to the initiation of growth, or which is at any stage during a subsequent process of continuous stable growth, the integral J' can be rewritten as [80]:

$$J' = \int_0^{\delta_c} \sigma(\delta) d\delta \quad .$$

However, since the details of the near crack tip field must be known (to evaluate J'), the integral J' is less useful than it may at first appear.

In fact, from this dissertation, it is clear that only very few tentative approaches have been made to the stable crack growth problem, and that much remains to be done.

CHAPTER VIII

CONCLUSIONS AND FUTURE RECOMMENDATIONS

Conclusions

This dissertation provides a rigorous finite deformation, embedded singularity, incremental elastic-plastic finite element procedure which has been demonstrated to be a highly efficient and accurate means to analyze plane problems of ductile fracture under large-scale yielding conditions, with arbitrary geometrical domains and under arbitrary loading conditions. The material properties are characterized as elastic-plastic behavior with arbitrary strain hardening. Based on the results reported in the previous chapter, several conclusions can be drawn that are relevant to the general problem of fracture in the case of large scale plasticity:

(1) The tangent modulus method was employed in the present incremental solution process, with an updated stiffness matrix even in iteration, to reduce the cumulative error in nodal point equilibrium. Due to the high efficiency and accuracy, the tangent modulus method is indeed an attractive incremental numerical method especially in dealing with finite deformation elastic-plastic problem.

(2) Twenty-five Gaussian integration points were considered in each of the high-order isoparametric elements in the numerical evaluation of the stiffness matrix and the elastic-plastic constitutive law was adjusted at each point depending on the stress level at the

respective point. Thus, in the present formulation, part of the element can remain elastic while the rest undergoes plasticity.

(3) Excellent correlations were found for the computed J versus δ relation, the critical J value and the reported experimental values whenever there was insignificant stable crack growth.

(4) By using the modified definition of the J integral to account for finite deformations, a more accurate path-independence for J is maintained even for the contour closest to the crack-tip. Thus, to develop the J_{IC} fracture criterion, a finite deformation analysis seems to be a better choice as compared with a small deformation theory.

(5) The empirical formula (2.3) of Rice, et al. [38] to compute J, from a single specimen test data for p versus δ curve, appears to be valid in the case of a deep-cracked bend bar. However, for deep cracked compact tension specimens, the relation (2.3) underestimates J by about 12 percent. The empirical relation (2.4) of Merkle and Corten [39] which accounts for not only the bending effect, but also that of axial force, was found to be more accurate for deep-cracked compact tension specimens.

(6) From the point of view of a more meaningful applications of the J-integral concept to in-service situations, a more precise measurement point for J_{IC} to characterize crack growth initiation must be defined in the experiments.

(7) It appears that the COD is directly correlated with J. Wells' [26] calibration for COD from CGD appears to be most consistent since it implies $\text{COD} \sim \text{CGD}^2$ in the small-scale yielding range, and

COD $\sim$ CGD in the large-scale yielding range. The reported numerical results for bend type specimens suggest $J \sim 1.4\sigma_y COD$ for moderately hardening materials, where σ_y is taken to be halfway between yield stress and the ultimate stress. This result appears to be consistent with that of Rice and Johnson [45] who also account for finite geometry changes near the crack-tip and use a rigid plastic slip line theory. As for tension type cracked specimen, $J \sim 1.2\sigma_y COD$ is suggested.

(8) From the point of view of finite element analysis of in-service situations, the J-integral is unambiguously defined and can be calculated routinely, even though it may be somewhat of an abstract quantity. On the other hand, even though it is a physically appealing quantity, COD is ambiguous in it's definition. Attempts to correlate the various calibration definitions of COD (from CGD) for the test specimens with essentially near-tip quantities such as, the crack opening at points where the elastic-plastic boundary intersects the crack-profile near the crack-tip did not lead us to any rational conclusions.

(9) Since the J-integral and COD approaches to elastic-plastic fracture were both based on a model which allowed large-scale yielding, those approaches provided a considerable advance in the important engineering problem of chracterizing plane strain fracture toughness of materials using inexpensive and small fracture test specimens. The large expensive valid ASTM (American Society for Testing Materials) K_{IC} specimens would not be necessary.

(10) A rigorous finite element model of crack propagation,

involving the translation of entire "singular" near-tip elements and consideration of global energy balance, was successfully created. The effect of unloading process occurred in the plastic region behind the advancing crack-tip was satisfactorily demonstrated.

(11) The equivalence between the global energy release rate G* and crack separation energy rate G^{Δ} was proved computationally. Since the nodal force extrapolation at the crack-tip was shown geometry dependent, G* appears to be a better definition at least when the present hybrid displacement finite-element model is employed.

(12) The variation of normalized G* and J with decreasing values of parameter S was first studied for arbitrary hardening material. In large-scale yielding region, the trend of normalized G^{*} was inconsistent with the prediction made by Rice [76] for non-hardening material. This surprising result may be explained by the significant large-scale plasticity effect which was first carried out accurately in this work.

(13) In the absence of an acceptable fracture criterion associated with stable crack growth, it is presently not possible to provide a complete scheme of stable crack growth without using the extensive experimental data.

(14) The hybrid-displacement finite-element procedure was found to be advantageous in solving large-scale yield cracked problems with strain-hardening material, for the reasons: (i) it allows for the Hutchinson-Rice-Rosengren strain/stress singularities to be incorporated near the crack-tip and yet satisfy the conditions of inter-element displacement and traction continuities in a rigorous fashion. Thus the mathematical convergence of the solution (to this highly nonlinear

problem) is assured, (ii) the conditions of vanishing traction on the crack-surface can be satisfied easily, (iii) using the high-order isoparametric elements and taking the J-integral path through the middle of the elements (rather than through element boundaries) allows for a more accurate computation of J, (iv) by using the present definition of J (as modified for finite deformations), an accurate path-independence for J was noted even for the path closest to the crack-tip.

Future Recommendations

Several feasible extensions of this work which are recommended for future investigations are summarized as follows:

(1) In many situations, the crack follows a curved path and the influence of Mode II fracture is not always negligible. The current theory of fracture in this work is inadequate in dealing with such a practical fracture problem. Consequently, the failure behaviors of the general damaged structures should be solved based on mixed-mode fracture theories*. Though there was no study made on the solution of Mode II fracture, with some effort, the sophisticated finite-element procedure developed in this work can be extended to deal with two-dimensional, elastic-plastic, mixed-mode fracture problems.

(2) The present method can also be extended, with some modifications, to three-dimensional elastic-plastic fracture problems, which provides a more realistic fracture criterion in practical problems whenever two-dimensional fracture analysis is no longer valid. To do this,

*The term "mixed-mode" is used herein to refer to the mixed Model I and Mode II.

due to the big bandwidth of the merged stiffness matrix, further compacting of the storage of merged stiffness matrix is needed to reduce the required capacity of the computer central memory core.

(3) The present formulation of the large scale yielding problem can be applied to study the phenomenon of fatigue crack closure [82,83]. The determination of the crack closure stress is a necessary step in the understanding of fatigue crack-growth mechanism.

(4) Based on the present achievement, a complete scheme of stable crack growth can be readily made once an acceptable stable crack growth fracture criterion is established.

APPENDIX A

BASIC MODES OF CRACK EXTENSION

Irwin [81] first pointed out that in a solid there are three kinematically admissible crack extension modes shown in Figure 2. These modes, opening, sliding, and tearing, can be proper superposed to obtain any crack.

The three modes of cracking can be described as follows [44]:

Mode I (Opening Mode)

The displacements of the crack surfaces are perpendicular to the plane of the crack.

Mode II (Sliding Mode)

The displacements of the crack surfaces are in the plane of the crack and perpendicular to the leading edge of the crack.

Mode III (Tearing Mode)

Crack surface displacements are in the plane of the crack and parallel to the leading edge of the crack.

APPENDIX B

FLOW CHART OF CRACK GROWTH ANALYSIS BY FINITE ELEMENT PROCEDURE

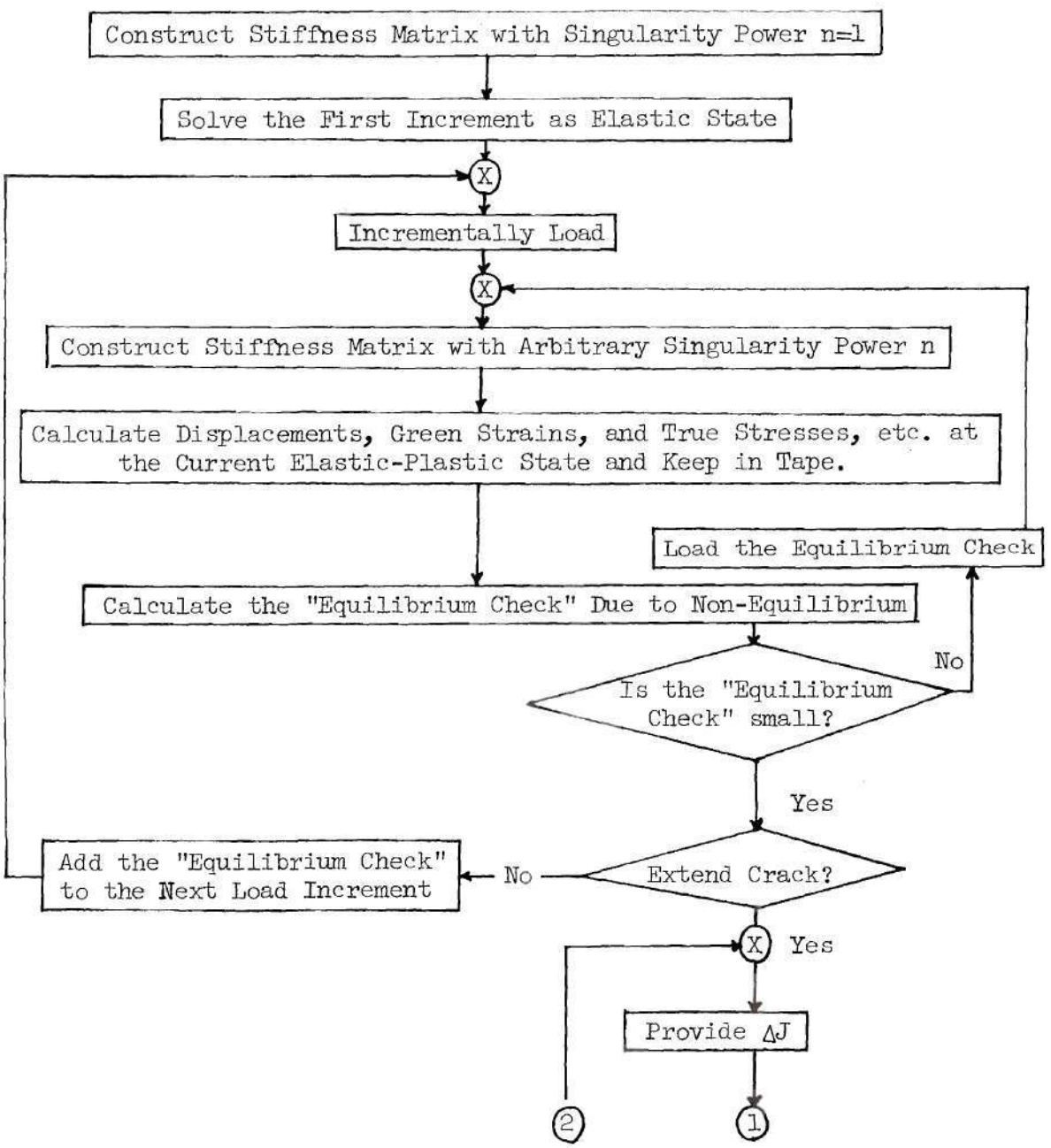

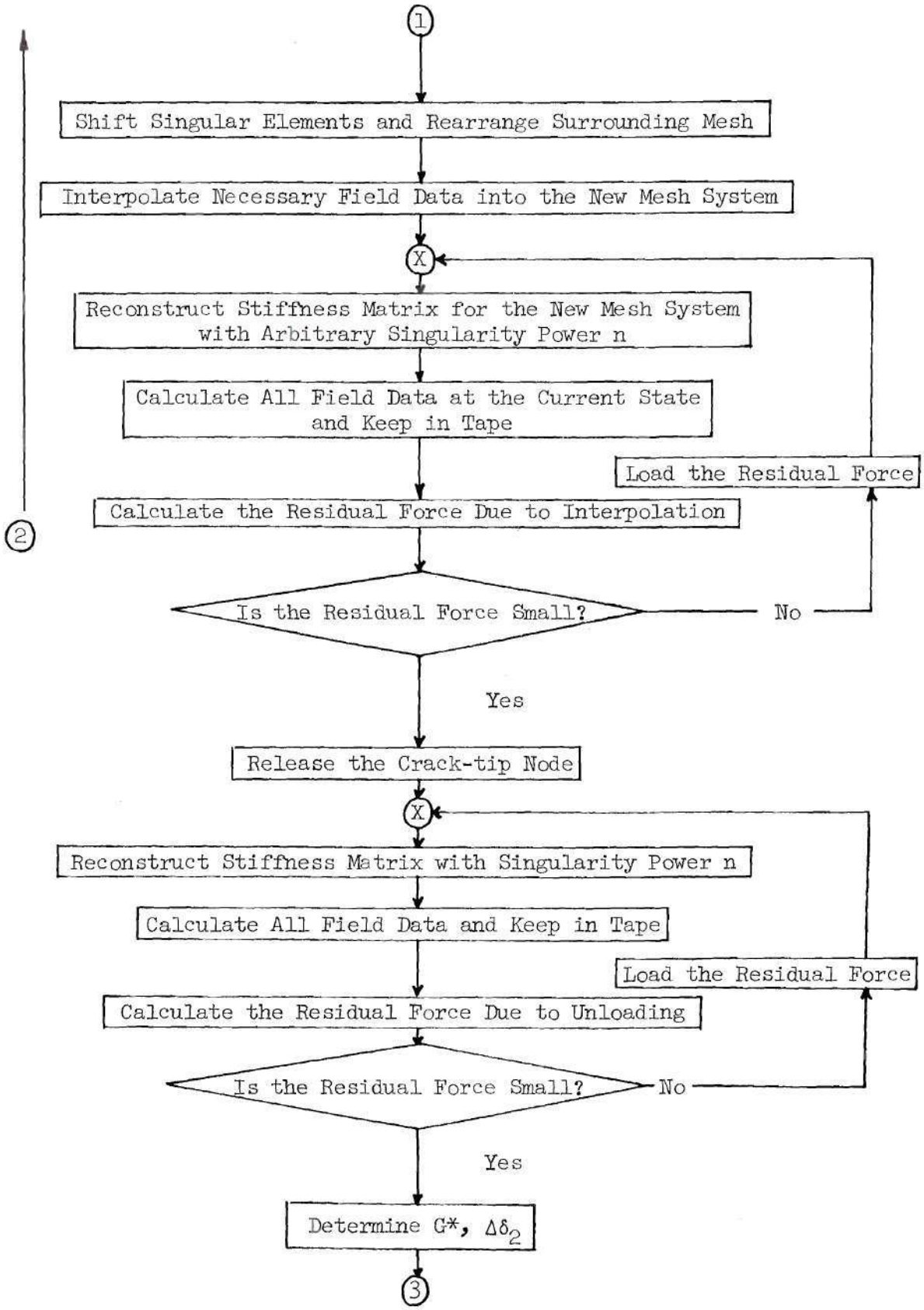
1
Shift Singular Elements and Rearrange Surrounding Mesh
Interpolate Necessary Field Data into the New Mesh System
X
Reconstruct Stiffness Matrix for the New Mesh System with Arbitrary Singularity Power n
Calculate All Field Data at the Current State and Keep in Tape
Load the Residual Force
Calculate the Residual Force Due to Interpolation
2
Is the Residual Force Small?
No
Yes
Release the Crack-tip Node
X
Reconstruct Stiffness Matrix with Singularity Power n
Calculate All Field Data and Keep in Tape
Load the Residual Force
Calculate the Residual Force Due to Unloading
Is the Residual Force Small?
No
Yes
Determine G*, $\Delta\delta_2$
3

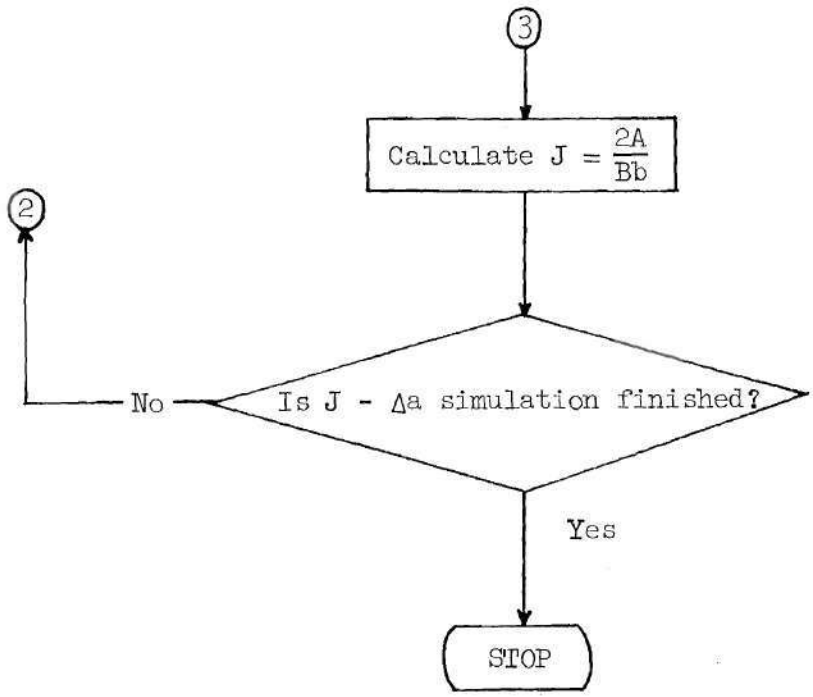
3
Calculate J = 2A/Bb
2
No
Is J - Δa simulation finished?
Yes
STOP

APPENDIX C

SOME DETAILS OF THE SOLUTION PROCEDURE

Gaussian Quadrature Numerical Integration

To perform finite element analysis the matrices defining element properties, e.g., stiffness, etc., must be carried out. To do this, the numerical evaluation required is generally the integration of functions which are of the form (e.g., in two-dimension)

$$I = \int_{-1}^{1}\int_{-1}^{1} f(s,t)\, ds dt \qquad (1)$$

where $f(s,t)$ is the function to be integrated. It is noted that the determinant of the Jacobian matrix [J], as shown in Chapter V, has been included in the function $f(s,t)$.

While the limits of the integration are simple in Equation (1), unfortunately the explicit form of $f(s,t)$ is not. Thus, analytical integration sometimes becomes difficult and numerical quadrature formulae pose the best approach to solving the problem of evaluation of integrals in finite element analysis.

Here, the Gaussian quadrature formulae are used because of their high efficiency. They can approximate the integration very accurately with comparatively small number of points and value of functions associated with these points. By using a Gaussian five-point formula, the integral of (1) can be numerically evaluated as follows [66]:

$$\int_{-1}^{1}\int_{-1}^{1} f(s,t)\,ds\,dt = \sum_{i=1}^{5}\sum_{j=1}^{5} W_i\, W_j\, f(s_i,t_j)$$

where W_i and W_j are the weighting coefficients. $f(s_i,t_j)$ is the value of the function at specified abscissas s_i and t_j. Thus the total number of Gaussian points for area integral would be 25.

Obviously, for a line integral, one has

$$\int_{-1}^{1} f(t)\,dt = \sum_{i=1}^{5} w_i\, f(t_i) \quad .$$

Thus, the total number of Gaussian points for line integral would be 5. The values of the abscissas and weighting coefficients are given below:

i	$s_i(t_i)$			W_i		
1	-0.90617	98459	3866	0.23692	68850	5619
2	-0.53846	93101	0568	0.47862	86704	9937
3	0.00000	00000	0000	0.56888	88888	8889
4	0.53846	93101	0568	0.47862	86704	9937
5	0.90617	98459	3866	0.23692	68850	5619

Numerical Integration Including Singularity

In order to obtain the element stiffness matrix for the singular element, a line integral involving the stress singularity $\sim r^{-\frac{1}{n+1}}$ must be evaluated. For example, to carry out the matrix [P] in Equation

(4.28), one has

$$[P] = \int_{\partial Am} [R]^T [U]\, dS$$

$$= \int_{\partial Am} [R_R]^T [U_R]\, dS + \int_{\partial Am} [R_R]^T [U_S]\, dS$$

$$+ \int_{\partial Am} [R_S]^T [U_S]\, dS + \int_{\partial Am} [R_S]^T [U_R]\, dS \qquad (2)$$

Here, $[R_s]$ denotes the singular part of assumed boundary traction interpolation function $[R]$ which contains a $r^{-\frac{1}{n+1}}$ type singularity. $[U_s]$ contains an assumed $r^{\frac{1}{n+1}}$ type interior incremental displacements. $[R_R]$ and $[U_R]$ represent the regular polynomials of $[R]$ and $[U]$ respectively.

Numerical integration of the first three terms in Equation (2) can be evaluated by using a five-point Gaussian quadrature formula. Although the last term in Equation (2) can be evaluated through the line integration, it was first transformed to a more workable form by removing the singularity $r^{-\frac{1}{n+1}}$ thereby yielding a regular integration. For convenience, the integral is assumed to be integrated along dr, then

$$I = \int_{\partial Am} [R_s]^T [U_R]\, dS$$

$$= \int_0^{r_o} \left[r^{-\frac{1}{n+1}} S(\theta) \right]^T [U_R(r,\theta)]\, dr$$

$$= \int_{o}^{r_o} r^{-\frac{1}{n+1}} [S(\theta)]^T [U_R(r,\theta)]\, dr \qquad (3)$$

where r_o is the radius of the sector singular element. Introducing a transformation

$$r = t^{\frac{n+1}{n}} \qquad (\text{or} \quad t = r^{\frac{n}{n+1}}) \qquad (4)$$

dr can be written as

$$dr = \left(\frac{n+1}{n}\right)\left(r^{\frac{1}{n+1}}\right) dt \qquad (5)$$

and

$$\left(r^{-\frac{1}{n+1}}\right) dr = \left(\frac{n+1}{n}\right) dt \qquad (6)$$

Substituting Equation (6) into Equation (3), it is apparent that the singularity disappeared. That is

$$I = \int_{o}^{r_o^{\frac{n}{n+1}}} \left(\frac{n+1}{n}\right) [S(\theta)]^T [U_R(t,\theta)]\, dt \qquad (7)$$

Next, integration with respect to dt can be changed to integration with respect to dz with a simplification of the limits of integration which now is simply from -1 to +1. Since t: $0 \sim r_o^{\frac{n}{n+1}}$, and let

z: $-1 \sim 1$, the following relationships are obtained:

$$t = \frac{r_o}{2}^{\frac{n}{n+1}} (1 + z) \tag{8}$$

$$dt = \frac{r_o}{2}^{\frac{n}{n+1}} dz \tag{9}$$

Finally, Equation (7) becomes

$$I = \int_{-1}^{1} \left(\frac{n+1}{n}\right) [S(\theta)]^T [U_R(z,\theta)] \left(\frac{r_o}{2}^{\frac{n}{n+1}}\right) dz \tag{10}$$

From Equations (4), (5), (8) and (9), the transformations between r and z are

$$r = \frac{r_o}{2 \cdot 2^{\frac{1}{n}}} (1 + z)^{\frac{n+1}{n}}$$

and $dr = \left(\frac{n+1}{n}\right)\left(\frac{r_o}{2 \cdot 2^{\frac{1}{n}}}\right) (1 + z)^{\frac{1}{n}} dz.$

Thus, Equation (10) can be performed easily by a regular integration using a five-point Gaussian quadrature formula.

Knee Correction

For an elastic-plastic finite element analysis once the stress point has reached yielding in the structure, it is necessary for the computation to proceed without any change except for replacing the elastic stress-strain matrix [E] with the updated elastic-plastic incremental stress-strain matrix $[E]^t$. One can judge the onset of the yielding by the yield condition (3.5):

$$f(\sigma_{ij} - \alpha_{ij}) = 0$$

which is governed by the Ziegler's kinematic hardening rule and the Hencky-Mises-Huber yield criterion.

While a J_2 incremental theory is employed as shown in Figure 9, a virtual stress increment $\Delta\sigma$ is applied to the current C_N state where the elastic stress point of the structure has stress $\sigma^{(N)}$ and total translation $\alpha^{(N)}$. Essentially, the relations between stress and strain involve three components of stress and of strain. However, for simplicity, a simple tension, for example, is given in Figure 9 and the essential quantities are a single stress component σ and the corresponding strain component ϵ. Through the use of the elastic stress-strain matrix [E], it can be seen that a much higher, but incorrect stress σ is obtained although the strain is correct one. Thus, to reach the true stress in C_{N+1} state denoted by P, a corrected procedure, the so-called "Knee Correction", is required.

The scheme of the "Knee Correction" procedure can be explained as follows. Assuming that the stress point yields exactly upon adding

a stress increment $r\Delta\sigma_{ij}$, the multiplier r is then given by the following equation:

$$f(\sigma_{ij}^{(N)} + r\Delta\sigma_{ij} - \alpha_{ij}^{(N)}) = 0 \tag{11}$$

For plane stress case, for example, the explicit form of (11) is then:

$$\begin{aligned}(\sigma_x^{(N)} - \alpha_x^{(N)} + r\Delta\sigma_x)^2 + (\sigma_y^{(N)} - \alpha_y^{(N)} + r\Delta\sigma_y)^2 \\ - (\sigma_x^{(N)} - \alpha_x^{(N)} + r\Delta\sigma_x)(\sigma_y^{(N)} - \alpha_y^{(N)} + r\Delta\sigma_y) \\ + 3(\sigma_{xy}^{(N)} - \alpha_{xy}^{(N)} - r\Delta\sigma_{xy})^2 = \sigma_y^2\end{aligned} \tag{12}$$

where σ_y is the yield stress of the material. Equation (12) can be written as:

$$Ar^2 + Br + C = 0 \tag{13}$$

where

$$A = \Delta\sigma_x^2 + \Delta\sigma_y^2 - \Delta\sigma_x\Delta\sigma_y + 3\Delta\sigma_{xy}^2$$

$$\begin{aligned}B = 2(\sigma_x^{(N)} - \alpha_x^{(N)})\Delta\sigma_x + 2(\sigma_y^{(N)} - \alpha_y^{(N)})\Delta\sigma_y - (\sigma_x^{(N)} - \alpha_x^{(N)})\Delta\sigma_y \\ - (\sigma_y^{(N)} - \alpha_y^{(N)})\Delta\sigma_x + 6(\sigma_{xy}^{(N)} - \alpha_{xy}^{(N)})\Delta\sigma_{xy}\end{aligned}$$

$$\begin{aligned}C = (\sigma_x^{(N)} - \alpha_x^{(N)})^2 + (\sigma_y^{(N)} - \alpha_y^{(N)})^2 - (\sigma_x^{(N)} - \alpha_x^{(N)})(\sigma_y^{(N)} - \alpha_y^{(N)}) \\ + 3(\sigma_{xy}^{(N)} - \alpha_{xy}^{(N)})^2 - \sigma_y^2\end{aligned}$$

Solving Equation (13), we obtain:

$$r = \frac{-B + \sqrt{B^2 - 4AC}}{2A} \tag{14}$$

The formula (14) is also true for plane strain case except using the following definitions of A, B and C. For plane strain case:

$$A = \frac{3}{4}(\Delta\sigma_x - \Delta\sigma_y)^2 + 3\Delta\sigma_{xy}^2$$

$$B = \frac{3}{2}(\Delta\sigma_x - \Delta\sigma_y)[(\sigma_x^{(N)} - \alpha_x^{(N)}) - (\sigma_y^{(N)} - \alpha_y^{(N)})]$$

$$+ 6(\sigma_{xy}^{(N)} - \alpha_{xy}^{(N)})\Delta\sigma_{xy}$$

$$C = \frac{3}{4}[(\sigma_x^{(N)} - \alpha_x^{(N)}) - (\sigma_y^{(N)} - \alpha_y^{(N)})]^2 + 3(\sigma_{xy}^{(N)} - \alpha_{xy}^{(N)})^2 - \sigma_y^2$$

Applying the Knee Correction since the incremental total strain remains the same, we can divide the portion $(1-r)\Delta\varepsilon_{ij}$ into several appropriate intervals. To obtain a better correction some finer intervals near the "Knee" of the stress-strain curve are given. By replacing the constant [E] matrix with the updated $[E]^t$ matrix, smaller slopes and the final answer point p are reached by steps. It is noted that the "Knee Correction" procedure must be taken into account not only in a loading process, but also in an unloading process.

Loading and Unloading Criteria

Once yielding is initiated, the plastic flow may or may not

persist. In general, yielding can occur only if the state of stress satisfied the loading function, say, $f(\sigma_{ij}, \alpha_{ij}) = 0$. Where again α_{ij} represents the total translation of yield surface and is a measure of the degree of strain hardening. If the increment of f is considered, i.e.,

$$df = \frac{\partial f}{\partial \sigma_{ij}} d\sigma_{ij} + \frac{\partial f}{\partial \alpha_{ij}} d\alpha_{ij} \tag{15}$$

where $\frac{\partial f}{\partial \sigma_{ij}}$ is directed along the outer normal to the loading surface $f = 0$. $d\alpha_{ij}$ is a set of incremental translations which vanish in an unloading process. The unloading process, in the present research, happens near the crack-tip region in the study of crack growth stability. By its nature, the stress point will move from a plastic state to an elastic state and the stress-strain behaviors will follow the same relations in the linear theory of elasticity during unloading. These will result in the condition $df < 0$. Hence, by Equation (15), the criterion for unloading from a plastic state can be stipulated as:

$$\frac{\partial f}{\partial \sigma_{ij}} d\sigma_{ij} < 0 \qquad \text{and} \qquad f = 0 \quad .$$

Otherwise, for a strain hardening material, it is said to be loading or neutral loading [67]. Thus,

$$\frac{\partial f}{\partial \sigma_{ij}} d\sigma_{ij} > 0 \qquad \text{and} \quad f = 0 \qquad \text{during loading}$$

$$\frac{\partial f}{\partial \sigma_{ij}} d\sigma_{ij} = 0 \qquad \text{and} \quad f = 0 \qquad \text{during neutral loading}$$

As given in Figure 20, a simple geometric interpretation of these criteria is readily visualized. Point P represents the existing state of stress lying on the loading surface. Now, loading, unloading, or neutral loading take place, according to whether the stress increment vector is directed outward, inward, or along the tangent to the loading surface $f = 0$.

Solving the Linear Simultaneous Equation

In the finite element analysis it is of great importance to solve the final equilibrium equation (4.36) which is essentially a set of linear simultaneous equations yielding high efficiency and good accuracy. For the sake of clarity, the set of equations is represented by the form:

$$[K] \{\Delta q\} = \{\Delta F\} \tag{16}$$

where $[K]$ is the symmetric global stiffness matrix of the whole structure merged from the individual element stiffness matrix, $\{\Delta F\}$ is the load column containing all the applied loads and residual forces associated with all the nodal points, and $\{\Delta q\}$ is the unknown displacement column. Various methods solving linear simultaneous equation have been suggested. However, a Gauss elimination procedure, in which an exact (within round-off accuracy) solution is obtained, is used in the present work because of its simplicity and economic computational time.

In a Gauss elimination procedure, by multiplying a suitable factor the ith (i = 1, ... N; N = total number of unknown variables Δq_i) equation can be used to eliminate the unknown variable Δq_i in all the subsequent equations such that the elements k_{ji} (j = i + 1 ... N) are reduced to zero. This process finally reduces the global stiffness matrix [K] to an upper triangular form which, by applying a back-substitution procedure, yields the solution.

However, since the order of the stiffness equation is usually so high, the traditional procedure needs to be modified with regard to the capacity of the computer. One can take advantage of the symmetry of the global stiffness matrix by restricting operations to the upper triangular portion. Further, by its very nature, the typical global stiffness matrix contains many zero terms; in particular there is a distance from the diagonal beyond which no terms exist (See Figure 7). This distance, the so-called "bandwidth", depends on the way the nodal points are numbered and is numerically equal to the product of the number of degrees of freedom per node and the number which is larger by one than the maximum difference of node numbers in an element. Hence, in order to save space in the central core of the computer, the global stiffness matrix can be stored in a rectangular N x m array as is shown in Figure 8. Here, *m is the length* of the bandwidth.

In practice, as employed in the present work, the total core required at any stage of elimination is 2m x m. After the elimination of the top block (a m x m square matrix), the remaining block will be shifted up to occupy the position of the eliminated matrix (which now

has been deleted) while another block will take up its relevant position in the core accordingly. Similar operations are made for the right hand side load column $\{\Delta F\}$. The required core for the load column $\{\Delta F\}$ is now 2m x 1. Thus, this process makes it possible to solve an unlimited number of equations subject to a maximum bandwidth limitation.

Displacement - Control Loading Process

In the application of boundary conditions, the force boundary conditions are readily taken care of by inserting the amount of the applied loads for the nodal points into the corresponding row of the load column. However, to apply the specified displacement boundary conditions, to global stiffness matrix together with the load column must be modified.

For a low strain hardening capacity material (and thus a large value of power hardening coefficient n), theoretically it provides a very smooth load-displacement curve (especially at high load levels). In other words, at such load levels a small increment of load may correspond to a large displacement. In this case, a better solution can be achieved by using the so-called "displacement-control" loading process by prescribing the displacements at load points instead of adding an increment of loads at load points.

To study the crack propagation, which usually occurs at high load level, the displacement-control loading process has been employed in this dissertation. The overall equilibrium equation (16) can be expressed in an explicit form:

$$\begin{bmatrix} K_{11} & \cdots & K_{1i} & \cdots & K_{1N} \\ \vdots & & \vdots & & \vdots \\ K_{i1} & \cdots & K_{ii} & \cdots & K_{iN} \\ \vdots & & \vdots & & \vdots \\ K_{N1} & \cdots & K_{Ni} & \cdots & K_{NN} \end{bmatrix} \begin{Bmatrix} \Delta q_1 \\ \vdots \\ \Delta q_i \\ \vdots \\ \Delta q_N \end{Bmatrix} = \begin{Bmatrix} \Delta F_1 \\ \vdots \\ \Delta F_i \\ \vdots \\ \Delta F_N \end{Bmatrix} \tag{17}$$

Suppose one wants to prescribe the displacement α at the load nodal point i, say $\Delta q_i = \alpha$. This can be done by setting all of the elements in the ith row k_{ij} $(j = 1 \ldots N,\ j \neq i)$ and the ith column $k_{mi}(m = 1, \ldots N,\ m \neq i)$ of the stiffness matrix equal to zero and by modifying $\Delta F_i = \alpha$. The diagonal term K_{ii} is made unity. Thus, Equation (17) becomes:

$$[K]^* \{\Delta q\} = \{\Delta F\}^* - \alpha\{B\} \tag{18}$$

or

$$\begin{bmatrix} K_{11} & \cdots & 0 & \cdots & K_{1N} \\ \vdots & & \vdots & & \vdots \\ 0 & \cdots & 1 & \cdots & 0 \\ \vdots & & \vdots & & \vdots \\ K_{N1} & \cdots & 0 & \cdots & K_{NN} \end{bmatrix} \begin{Bmatrix} \Delta q_1 \\ \vdots \\ \Delta q_i \\ \vdots \\ \Delta q_N \end{Bmatrix} = \begin{Bmatrix} \Delta F_1 \\ \vdots \\ \alpha \\ \vdots \\ \Delta F_N \end{Bmatrix} - \alpha \begin{Bmatrix} K_{1i} \\ \vdots \\ 0 \\ \vdots \\ K_{Ni} \end{Bmatrix}$$

As discussed in the previous section the global stiffness matrix has been ingeniously stored in the rectangular banded form, and therefore a corresponding modification must be made. This scheme is displayed in Figure 16. The corresponding column {B} of Equation (18) is shown by the shaded region if the diagonal term K_{ii} is made zero.

APPENDIX D

ILLUSTRATIONS*

*For publication purposes, the title of each figure is made in an appropriate way instead of typing.

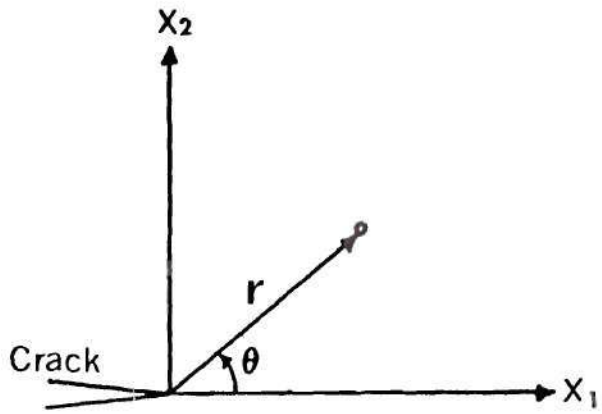

FIG.1 Polar Coordinates at the Crack-Tip

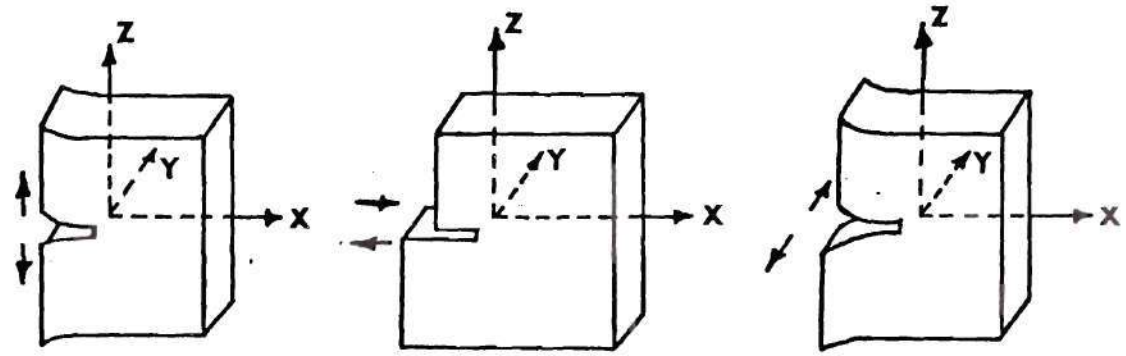

Mode I or Opening Mode

Mode II or Sliding Mode

Mode III or Tearing Mode

FIG. 2 Three Basic Modes of Crack Tip Deformation

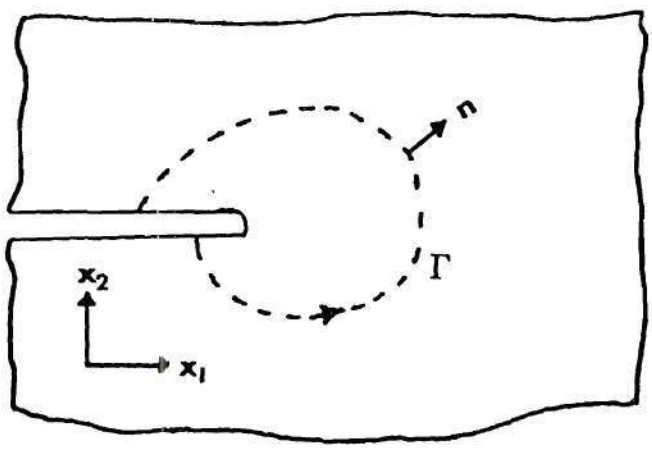

FIG.3 J-Integral

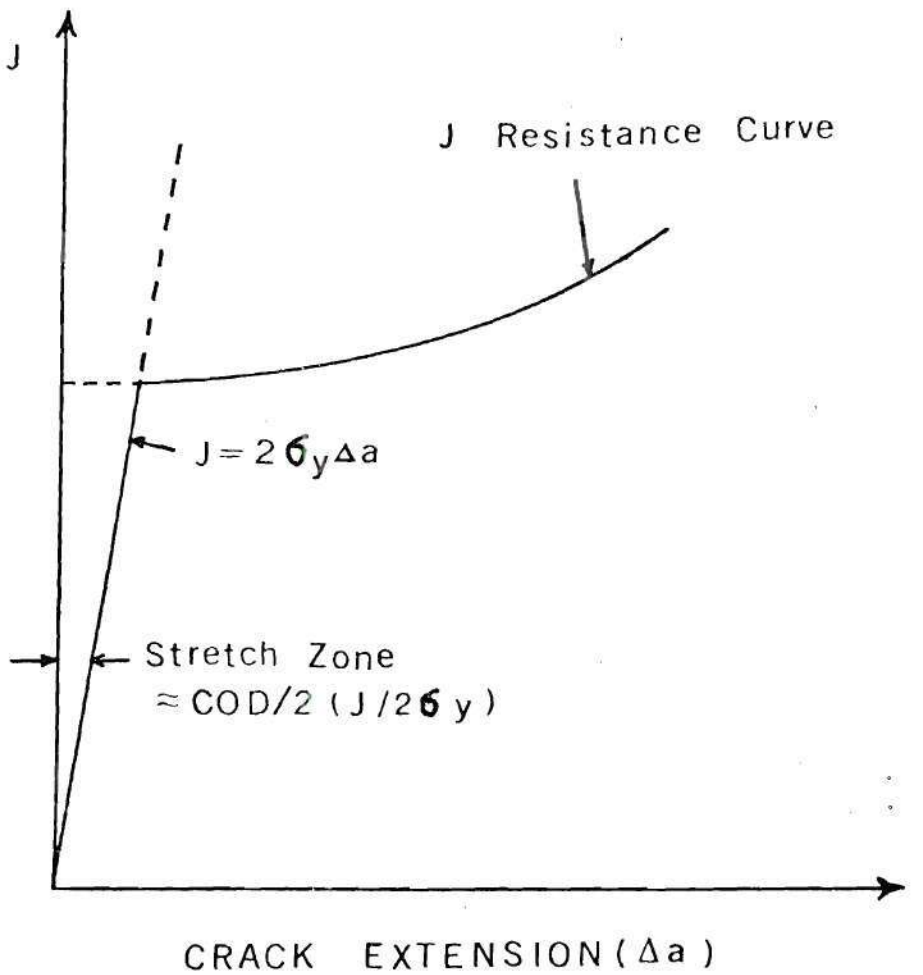

FIG.4 Schematic of J Resistance Curve

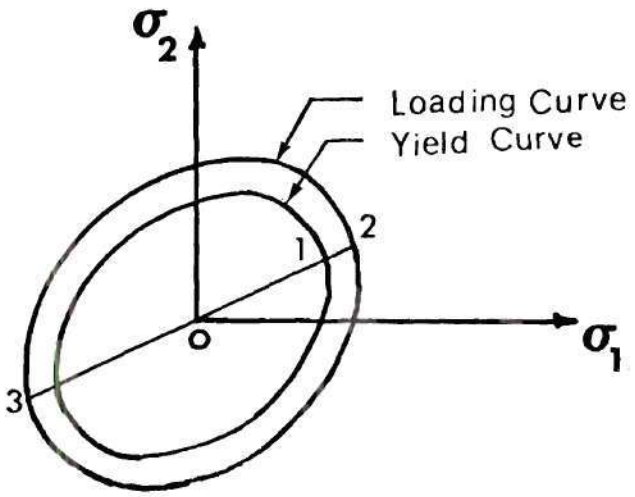

ISOTROPIC HARDENING

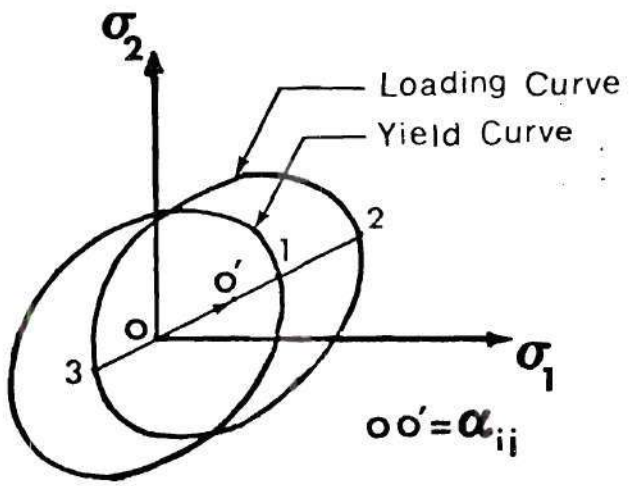

KINEMATIC HARDENING

FIG.5 Isotropic and Kinematic Hardening

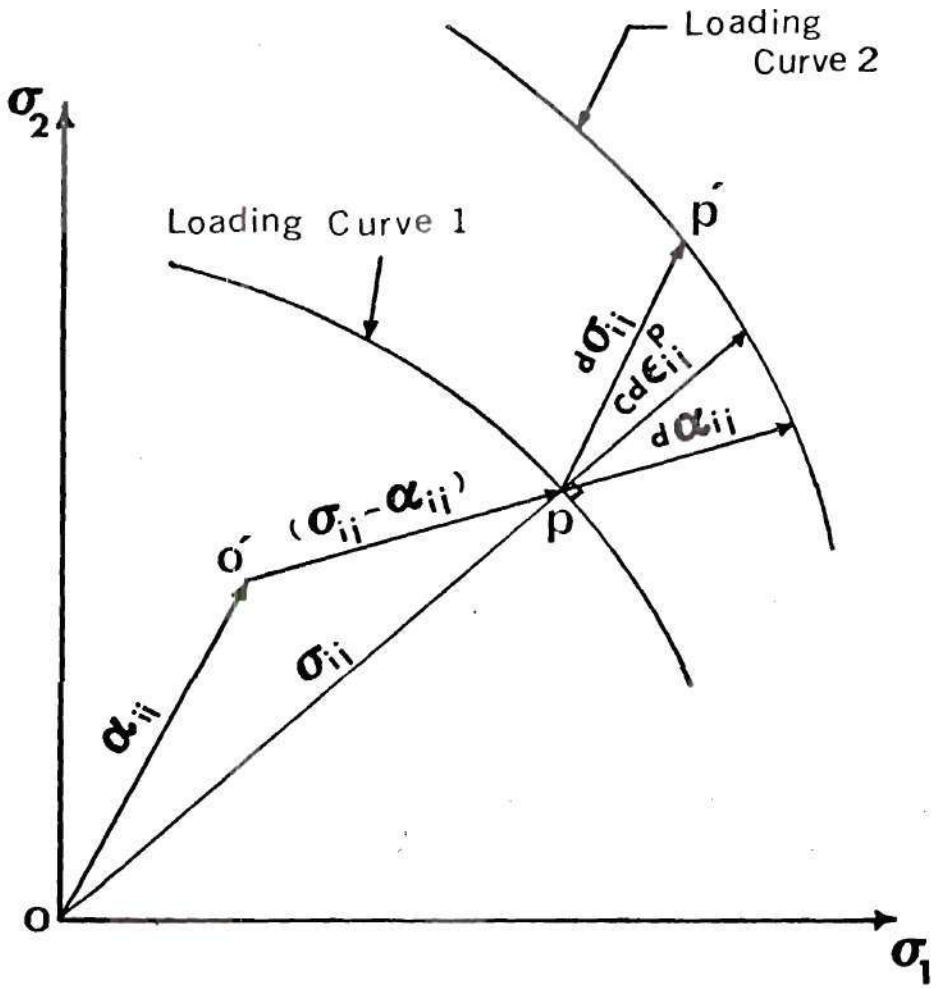

FIG.6 Hardening Rule Using Ziegler's Modification

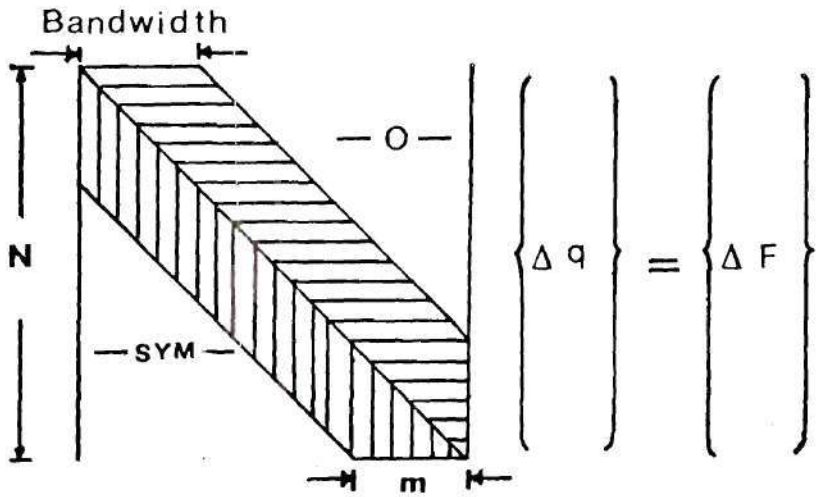

FIG. 7 Original Global Stiffness Matrix

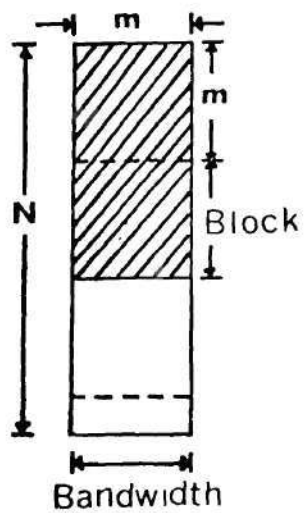

FIG. 8 Storage of Global Stiffness Matrix

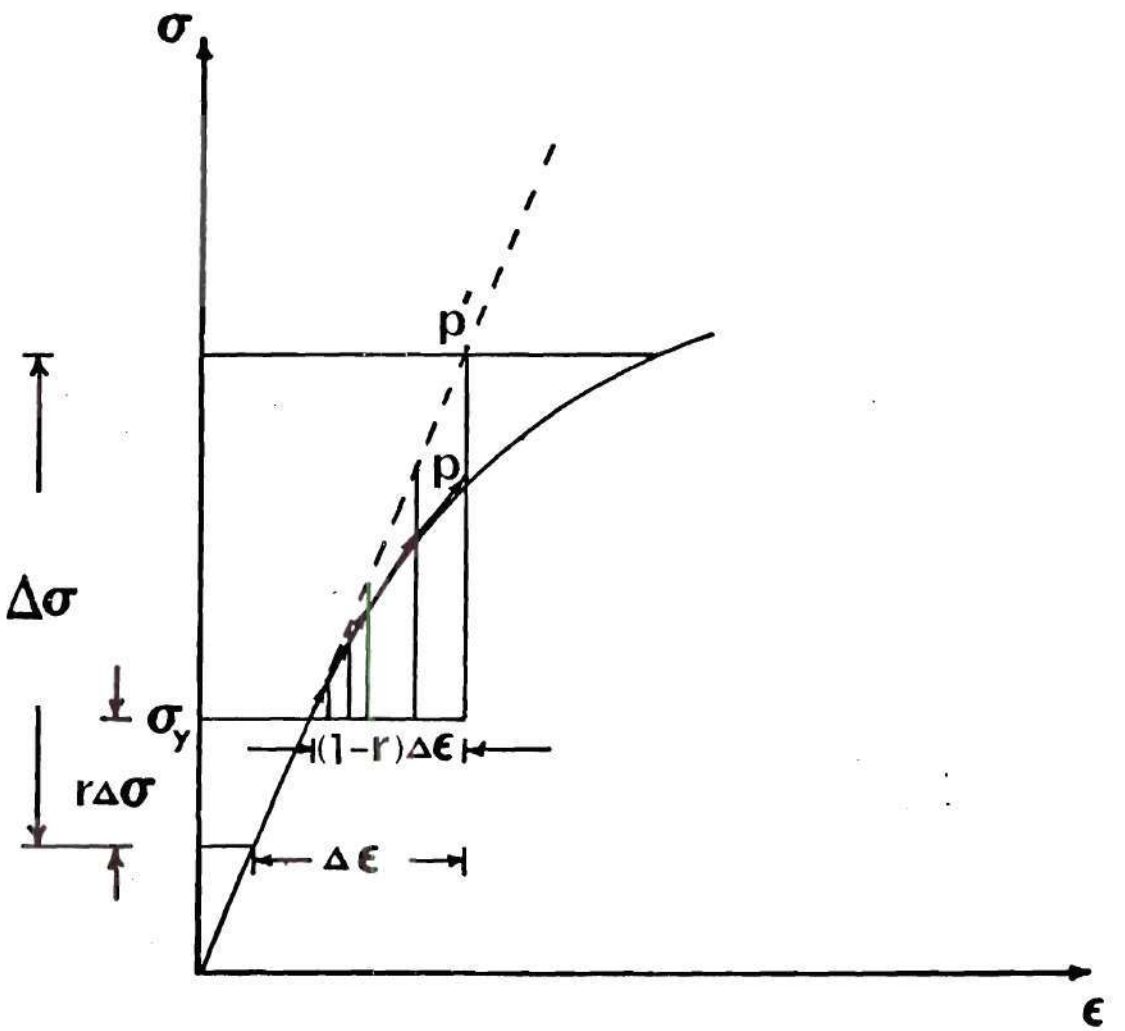

FIG.9 Knee Correction

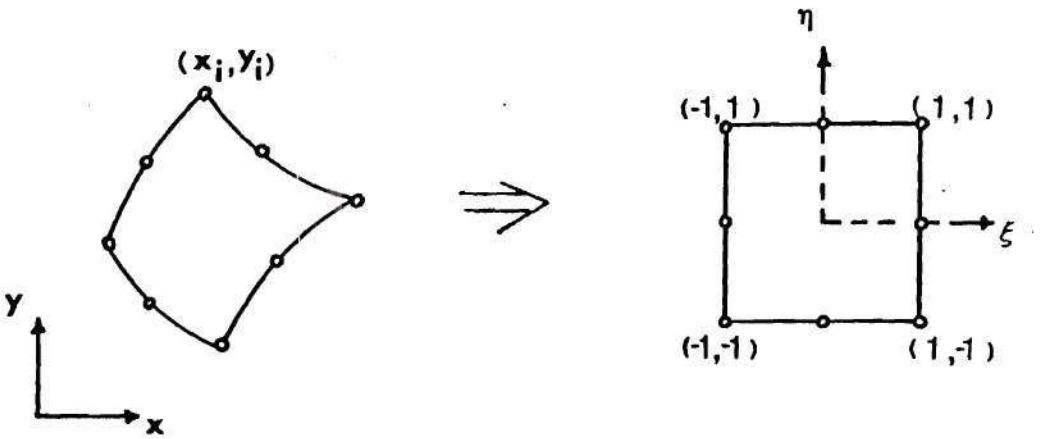

FIG.10 Isoparametric Transformation

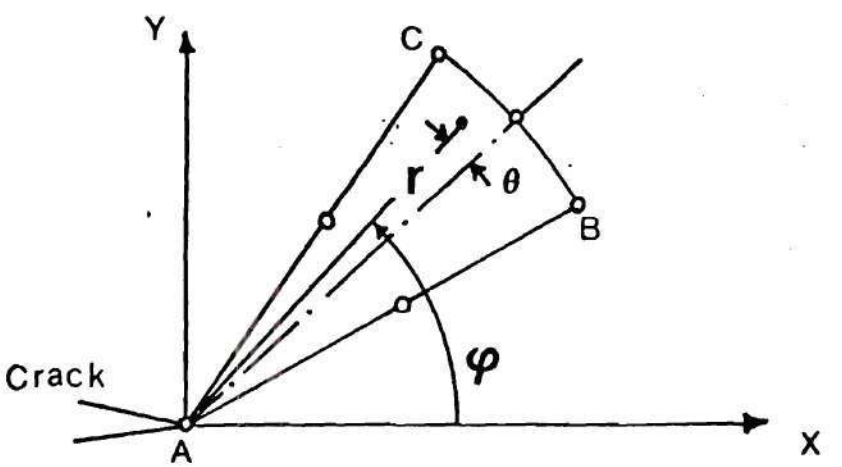

FIG.11 Nomenclature For a Singular Element

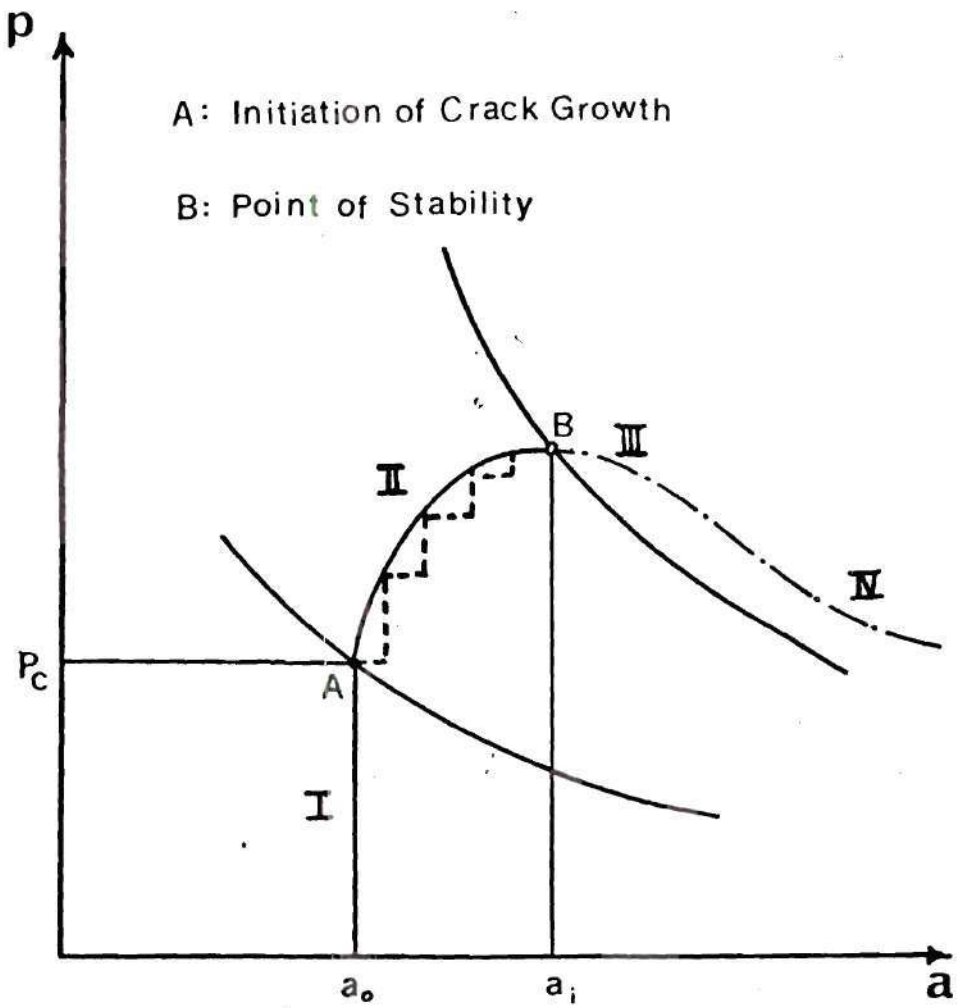

FIG.12 Stability of Crack Growth

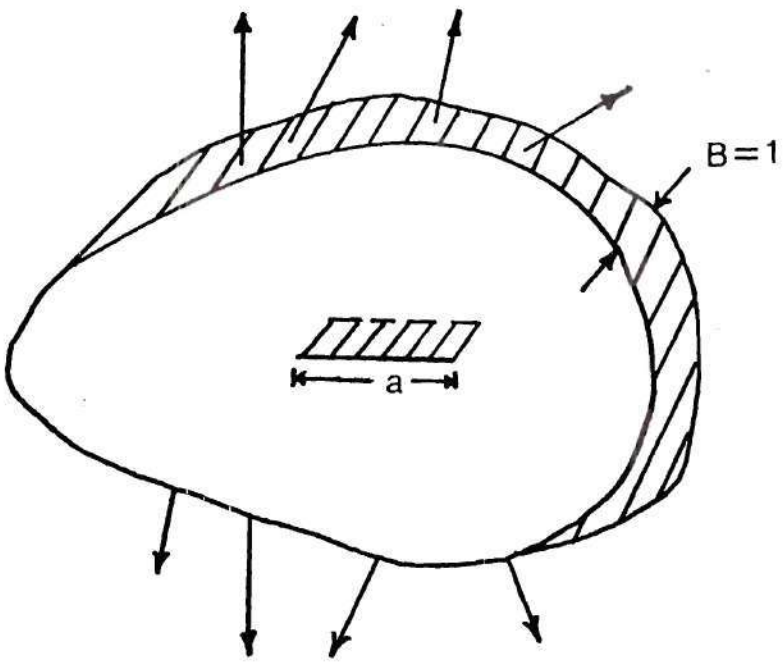

FIG.13 General Representation of a Cracked-Body

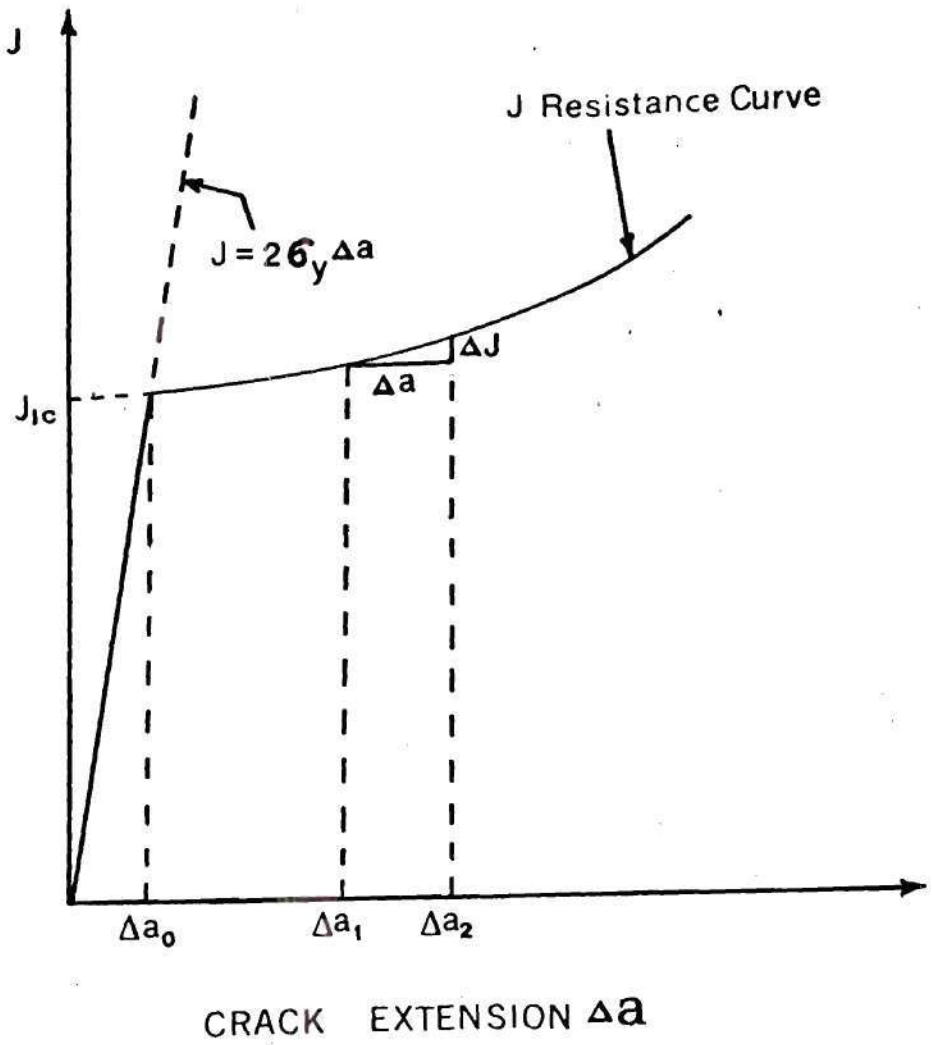

FIG.14 Study of Crack Growth Process

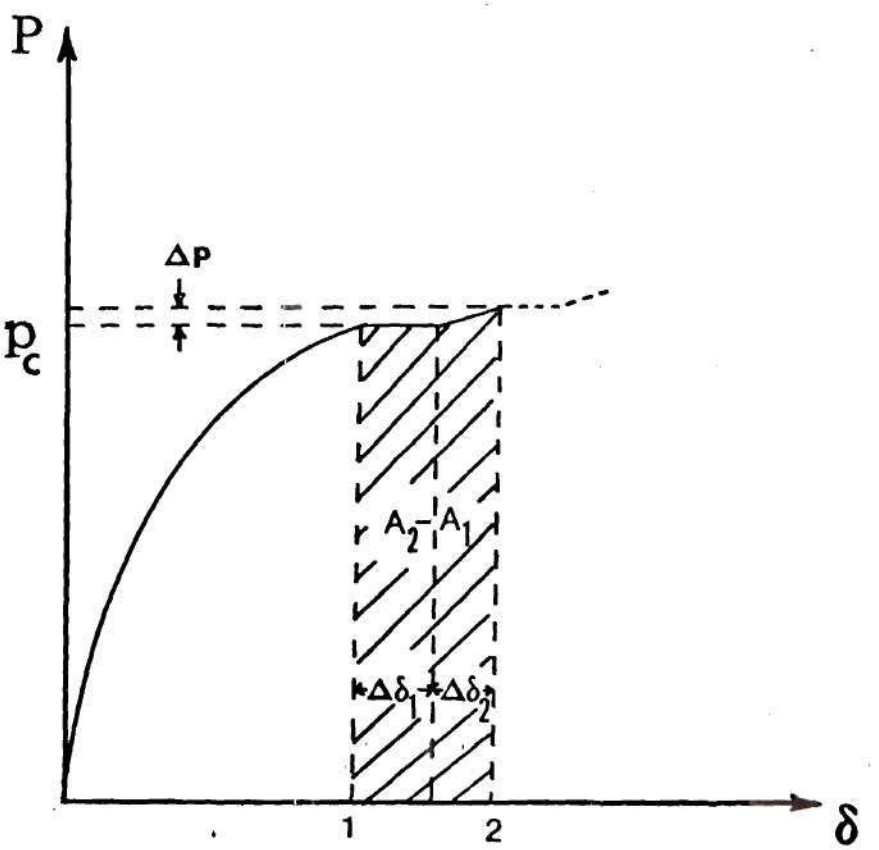

FIG.15 Load--Displacement Relation for Crack Extension

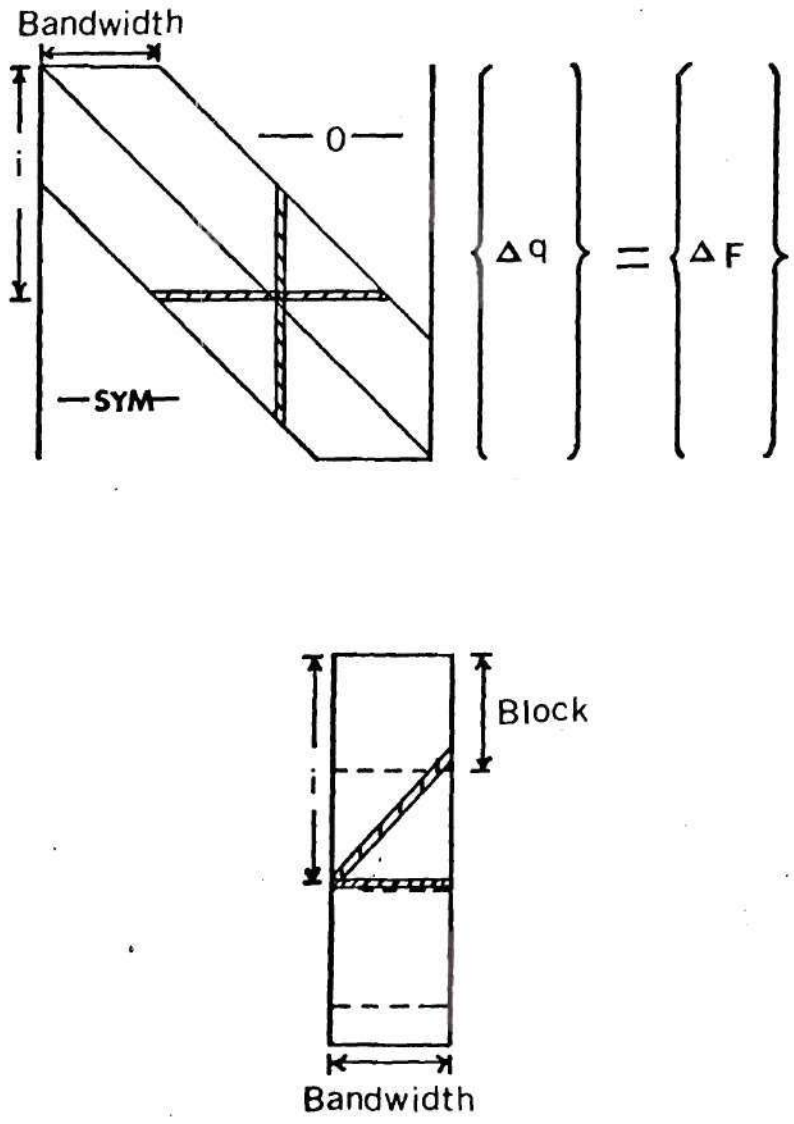

FIG.16 Displacement-Control Loading Modification

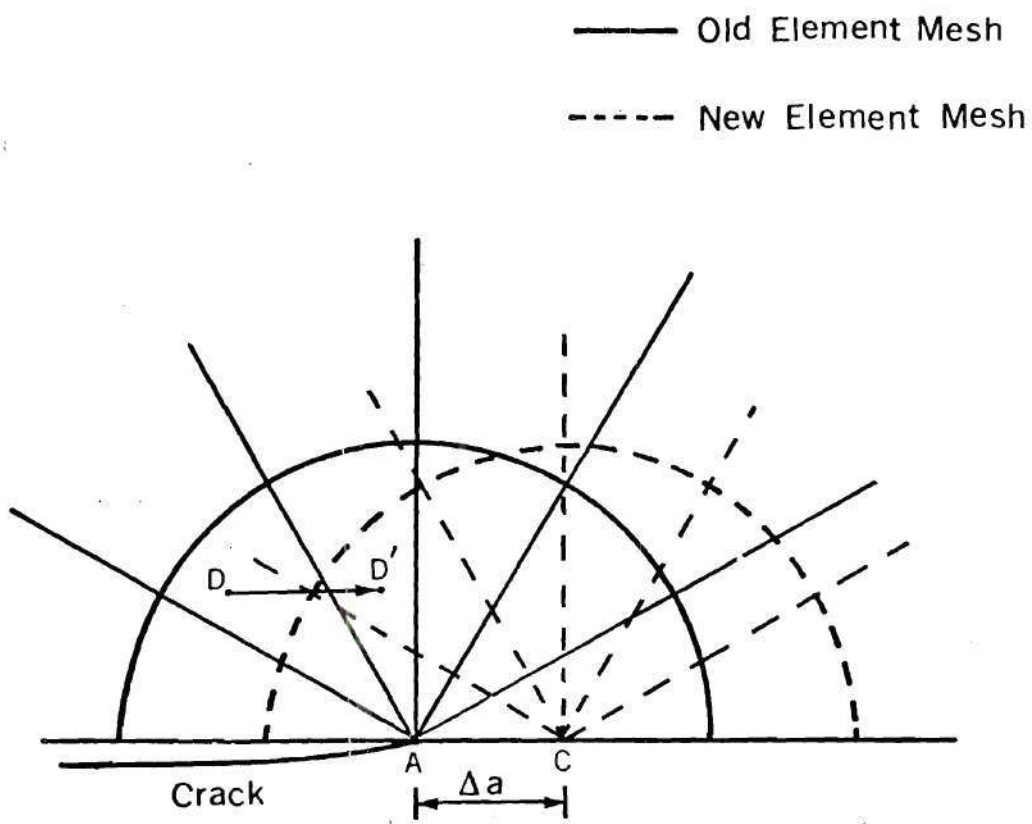

FIG.17 Element Translation for Crack Growth

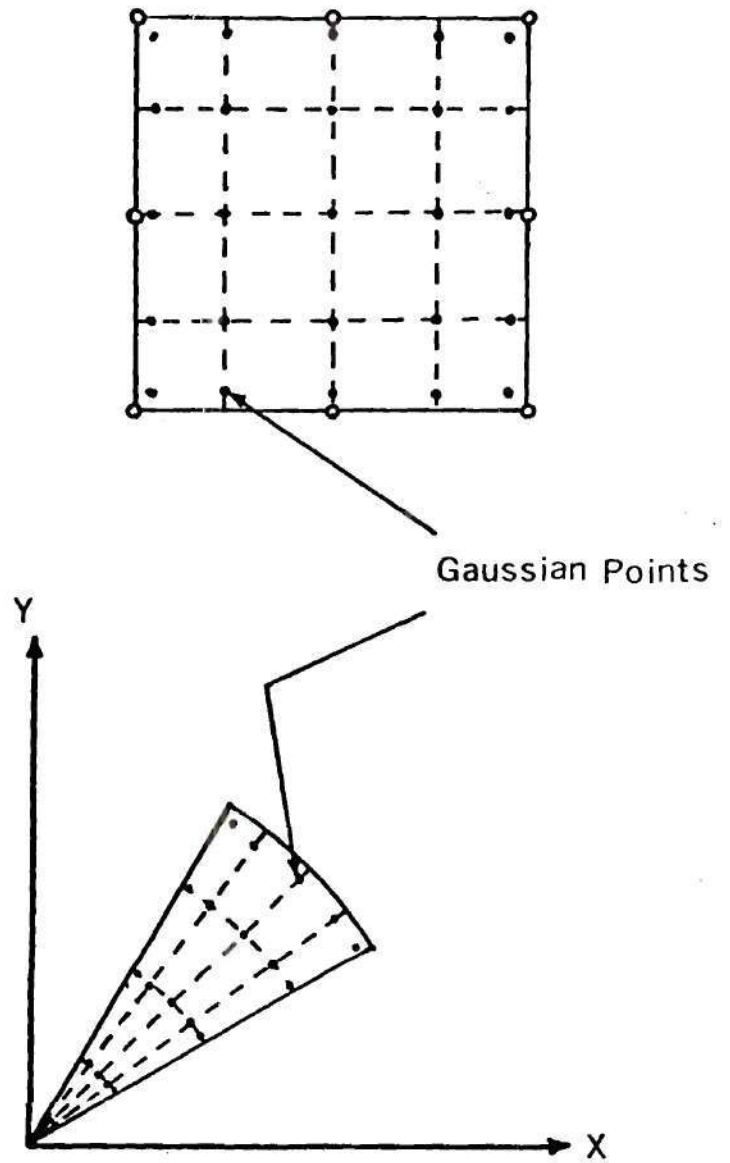

FIG.18 Each Element Contains 16 Fitting Regions

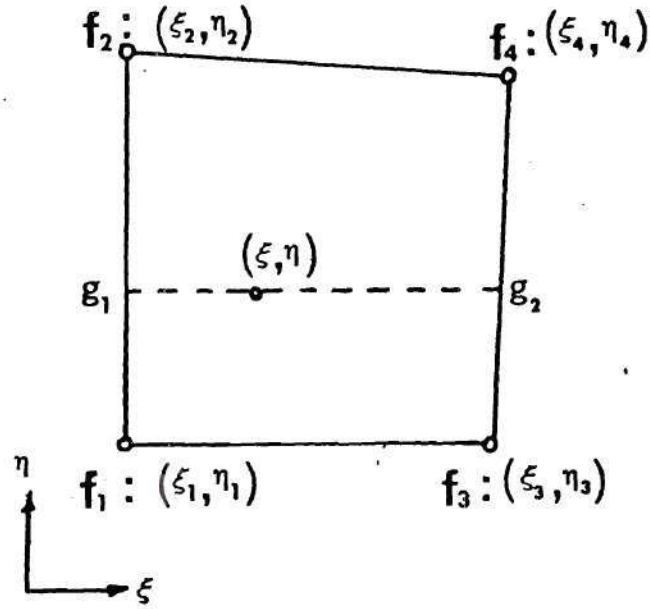

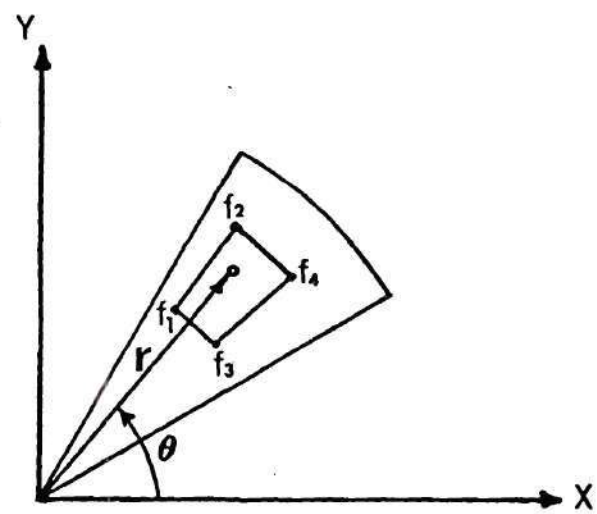

FIG.19 Determine Fitting Function

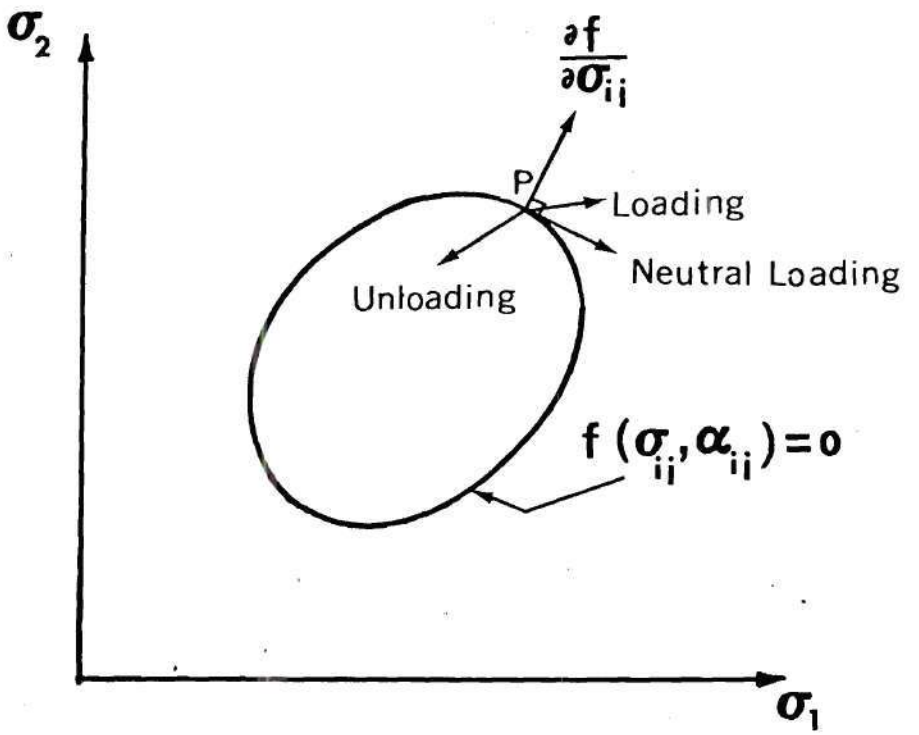

FIG.20 Loading, Neutral Loading and Unloading

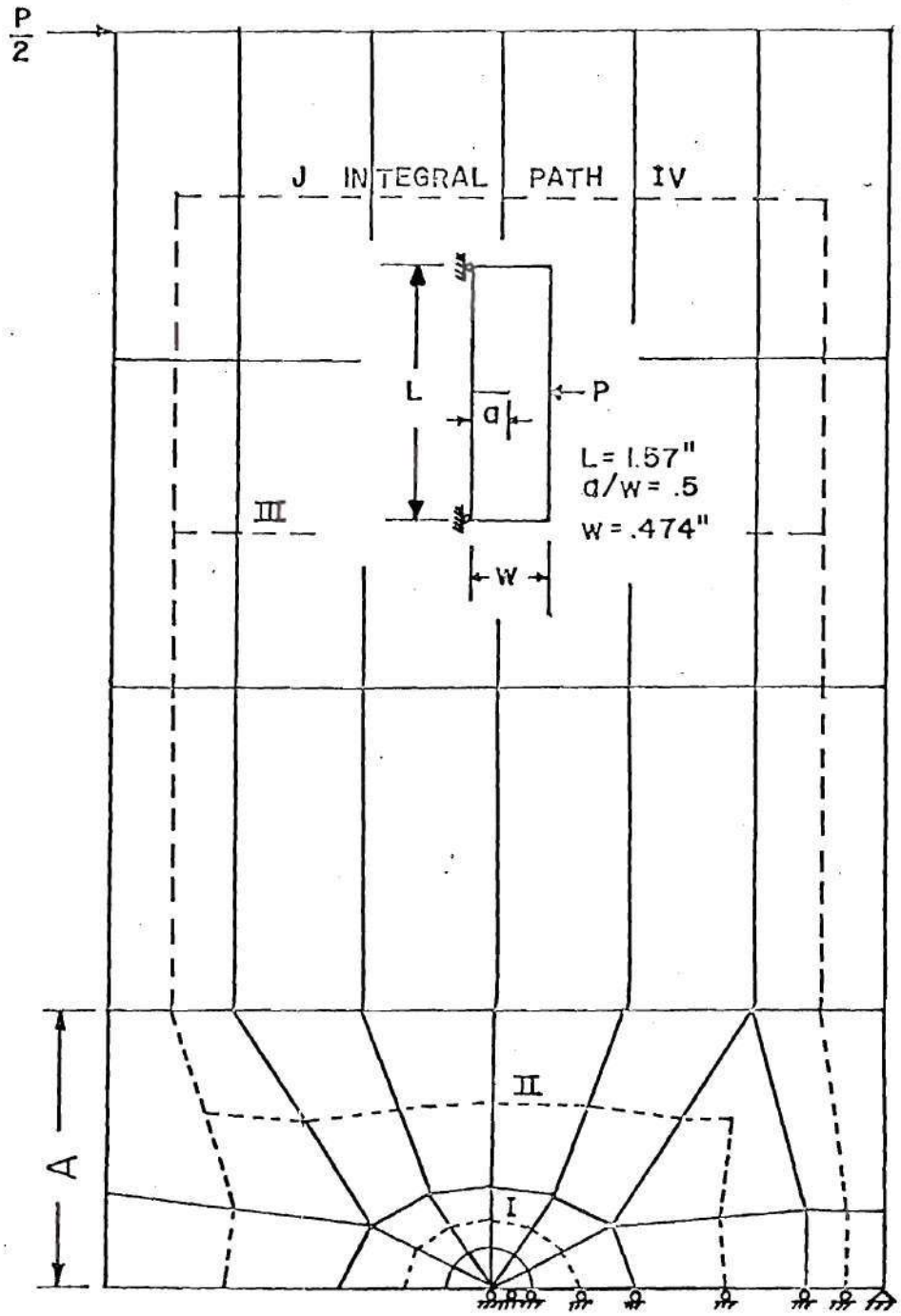

FIG. 21: Finite-Element Model of 3-Point Bend Bar (shown in insert) and J-Integral Paths

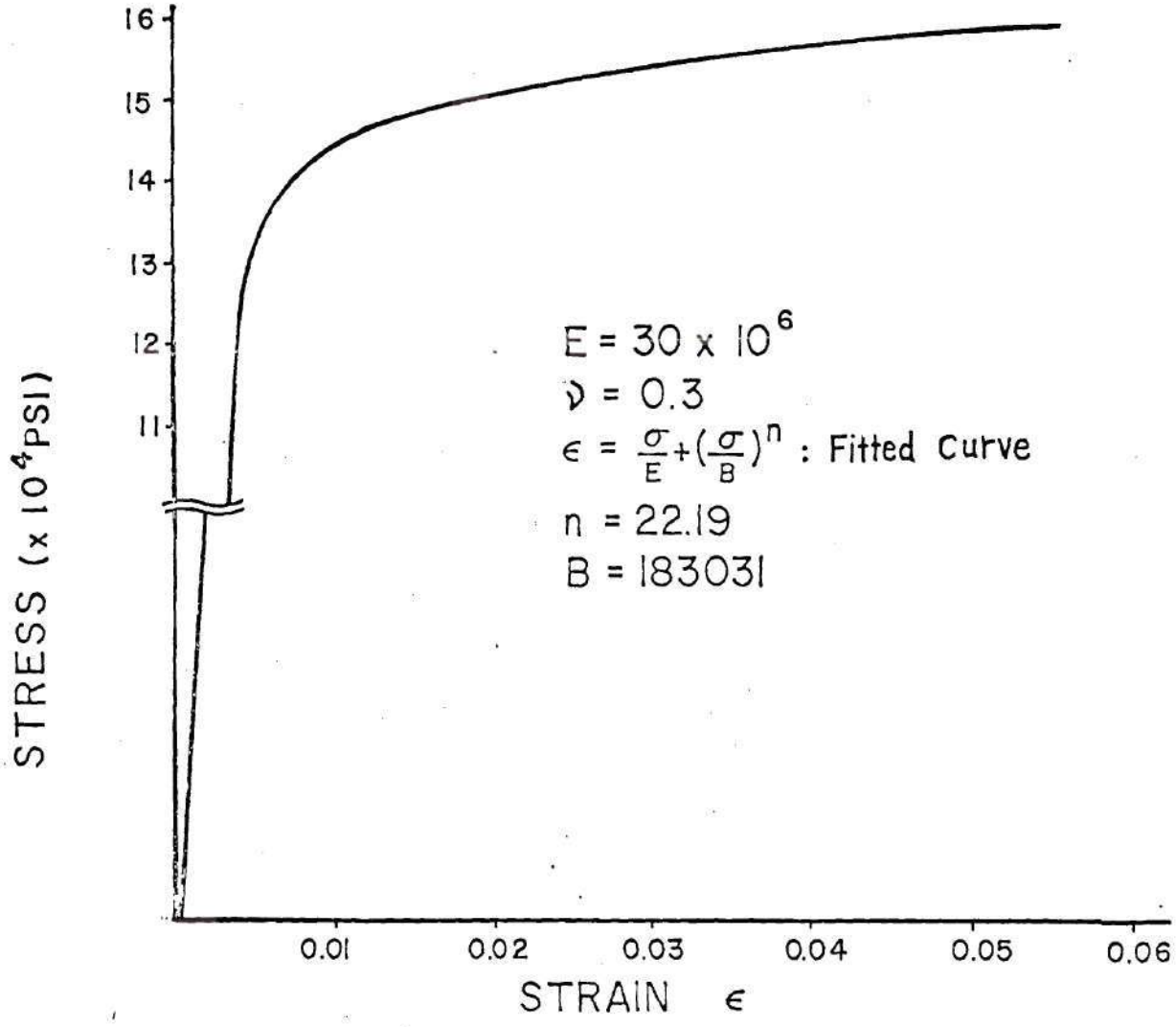

FIG. 22: Uniaxial Stress-Strain Curve for Ni-Cr-Mo-V Steel

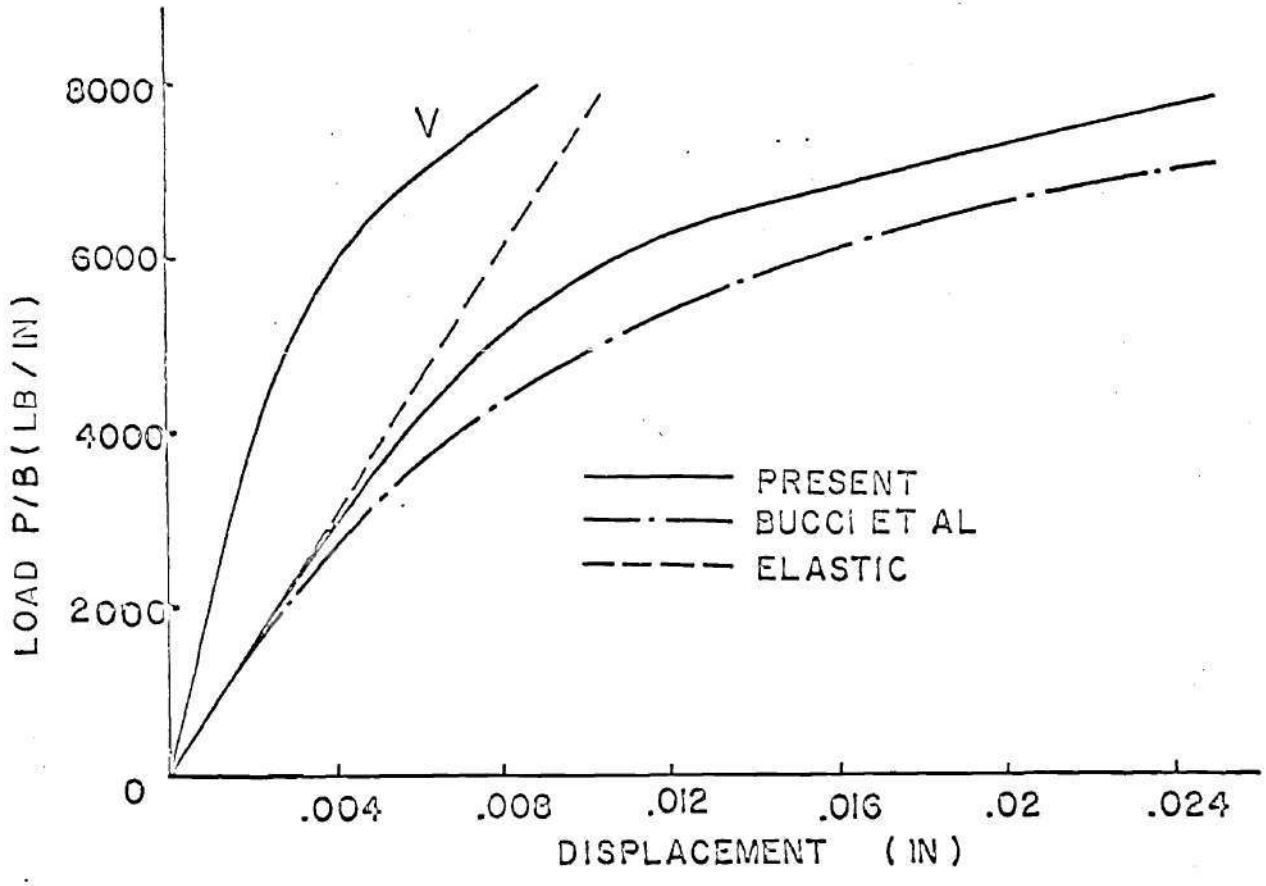

FIG.23: LOAD VS. LOAD-POINT DISPLACEMENT FOR 3-POINT BEND BAR.

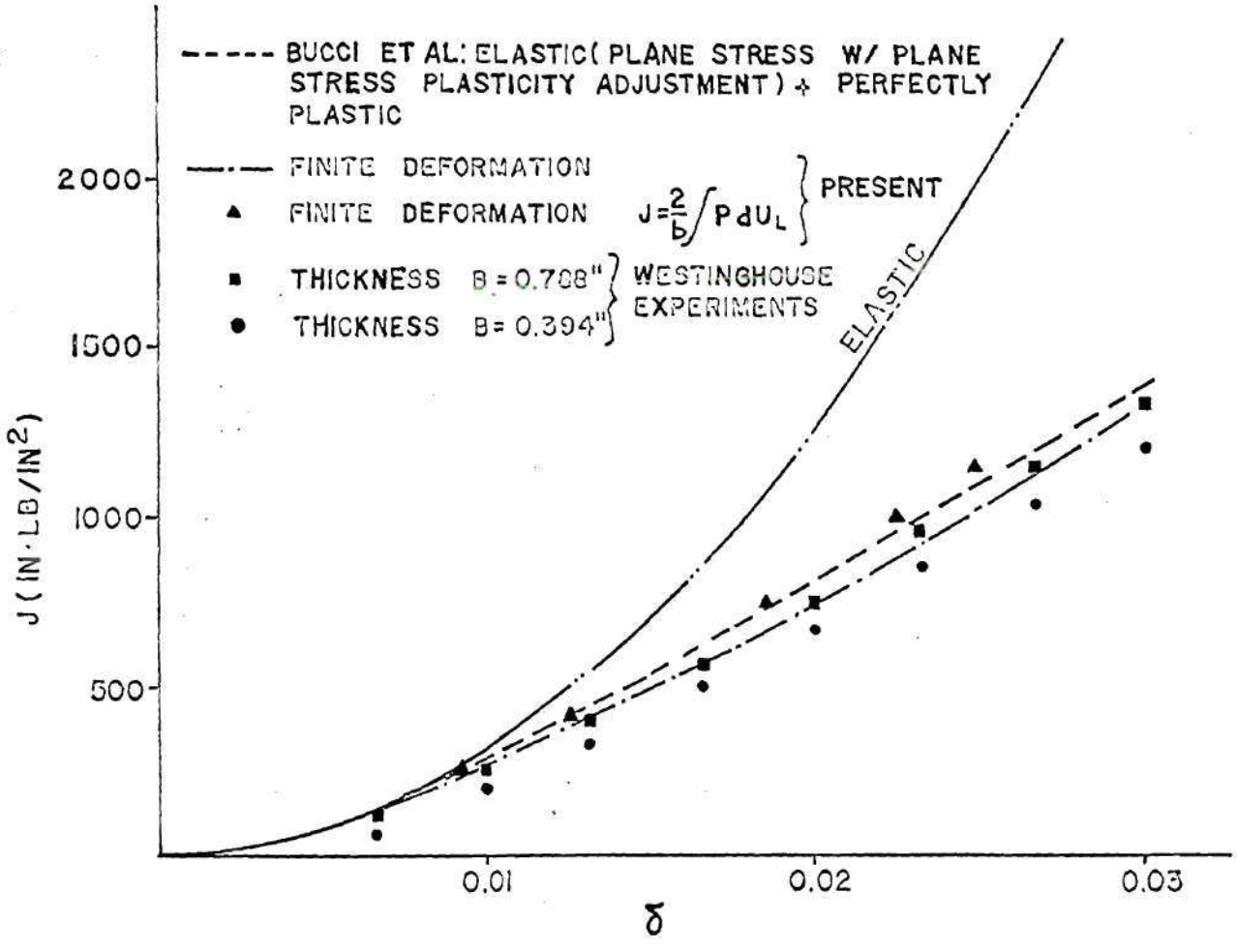

FIG .24 J - Integral vs δ Curve for 3 - Point Bend Bar.

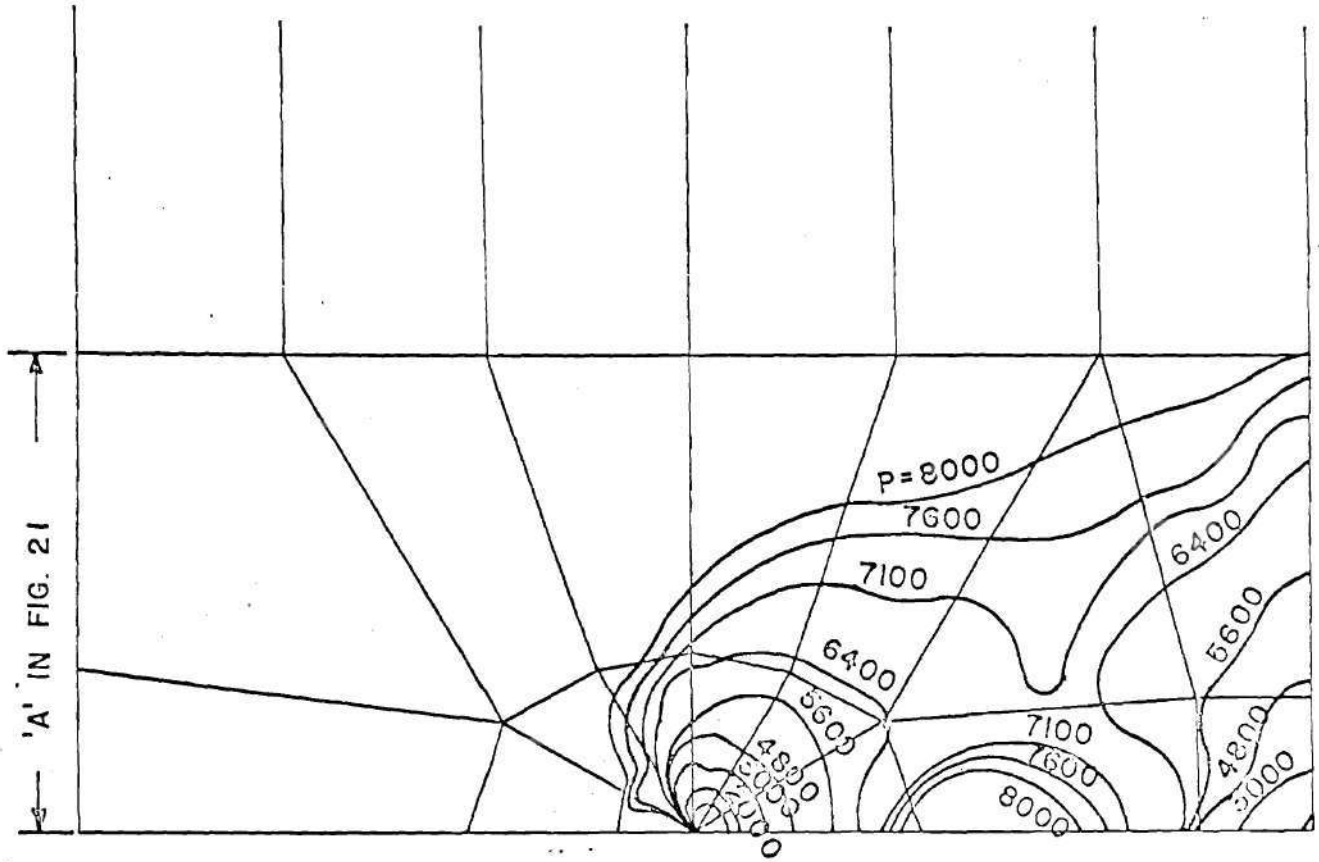

FIG.25 Yield-Zones at Various Load Levels for 3-Point Bend Bar

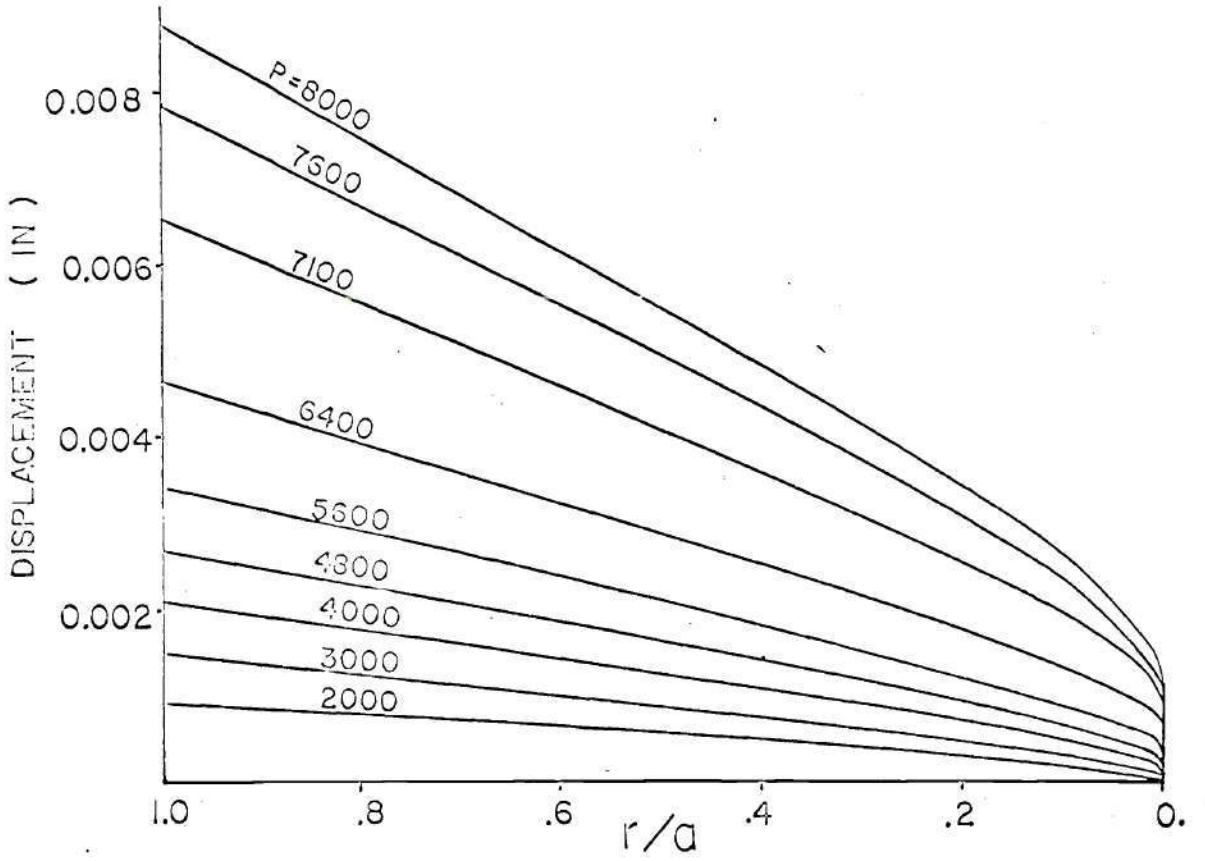

FIG .26 CRACK-SURFACE DEFORMATION PROFILES AT VARIOUS LOAD LEVELS FOR 3-POINT BEND BAR.

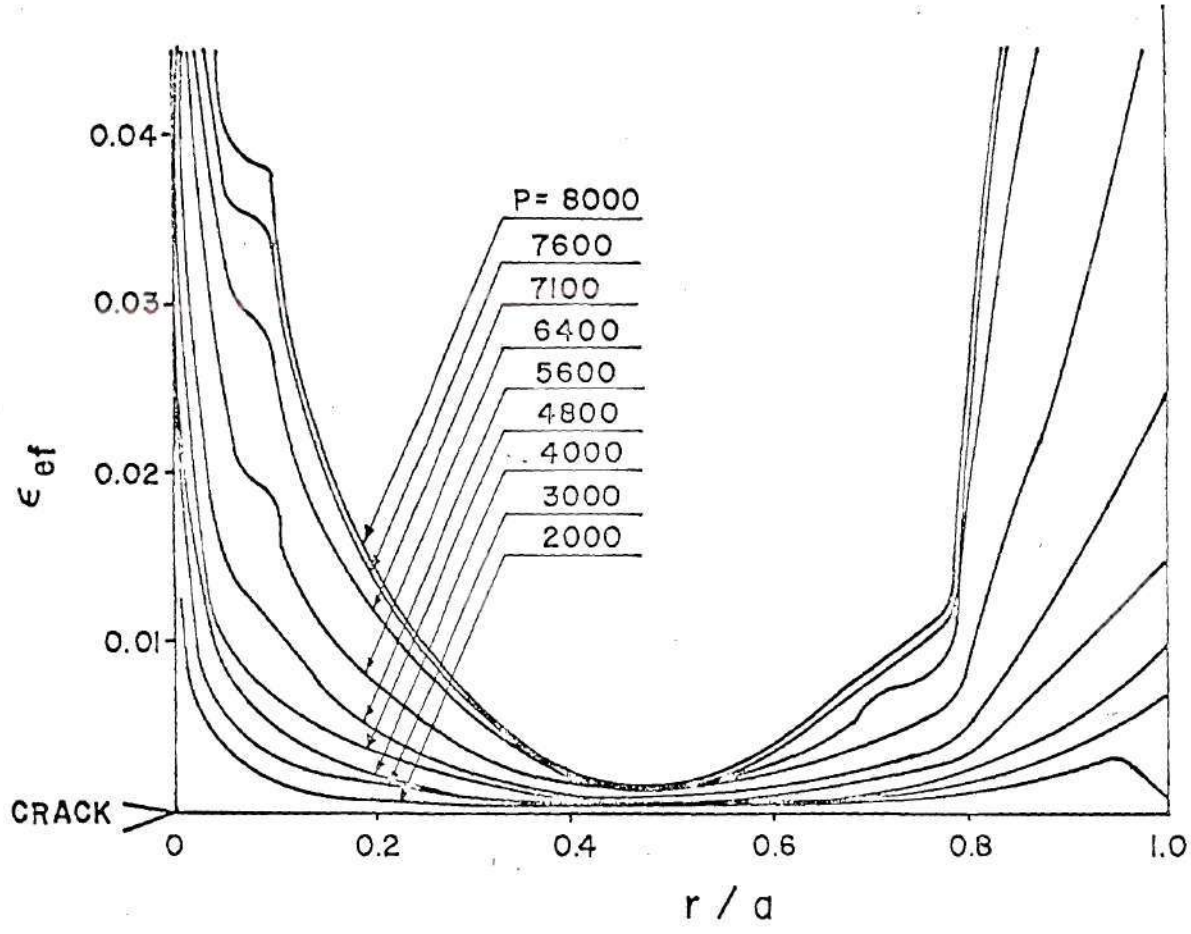

FIG. 27 Effective Strain Distribution in the Uncracked Ligament

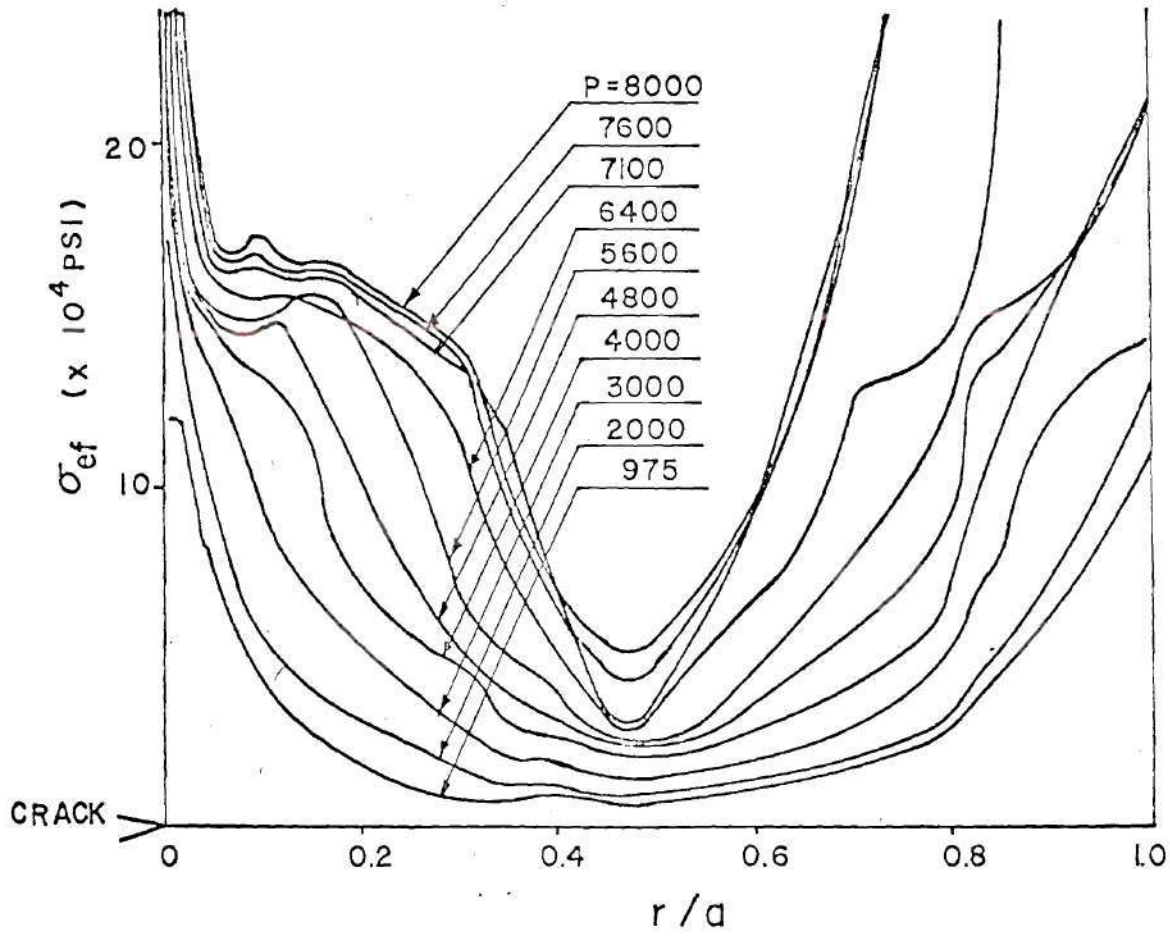

FIG. 28 Effective Stress Distribution in the Uncracked Ligament

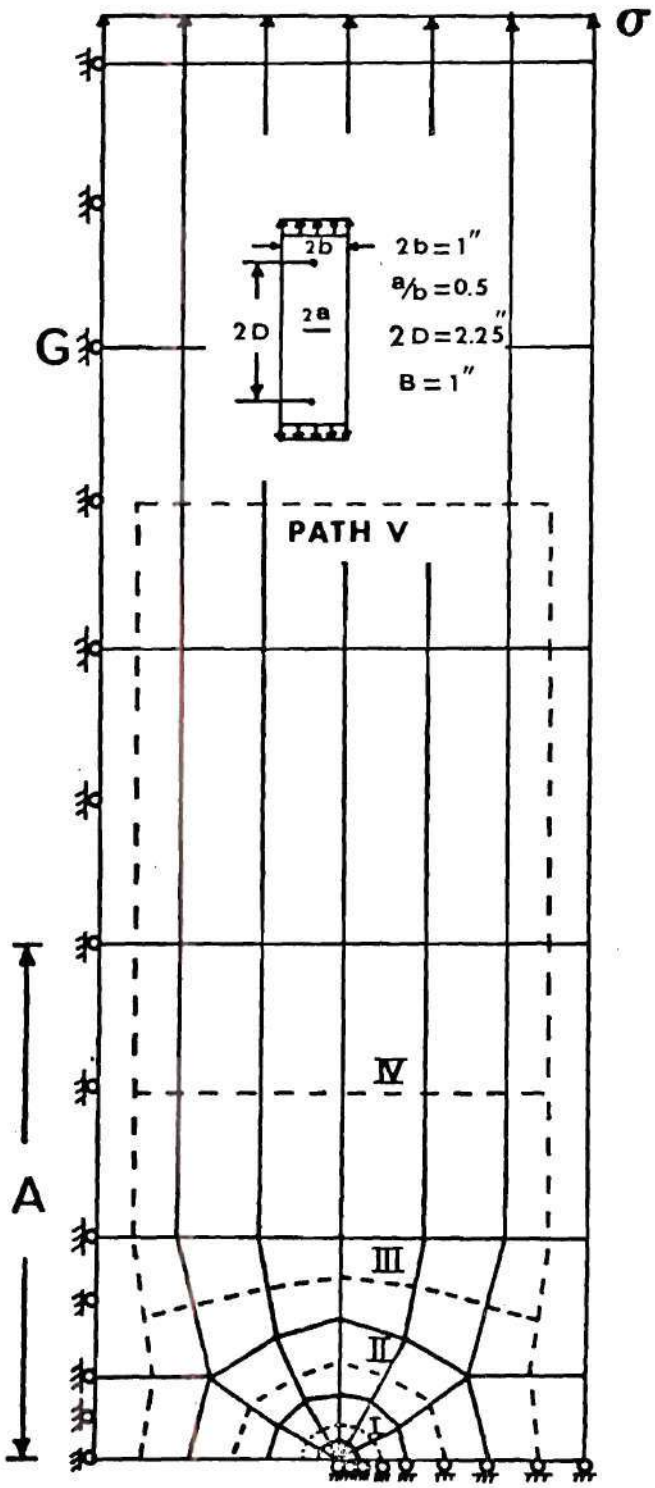

FIG. 29 Finite Element Model for the Center-Cracked Specimen

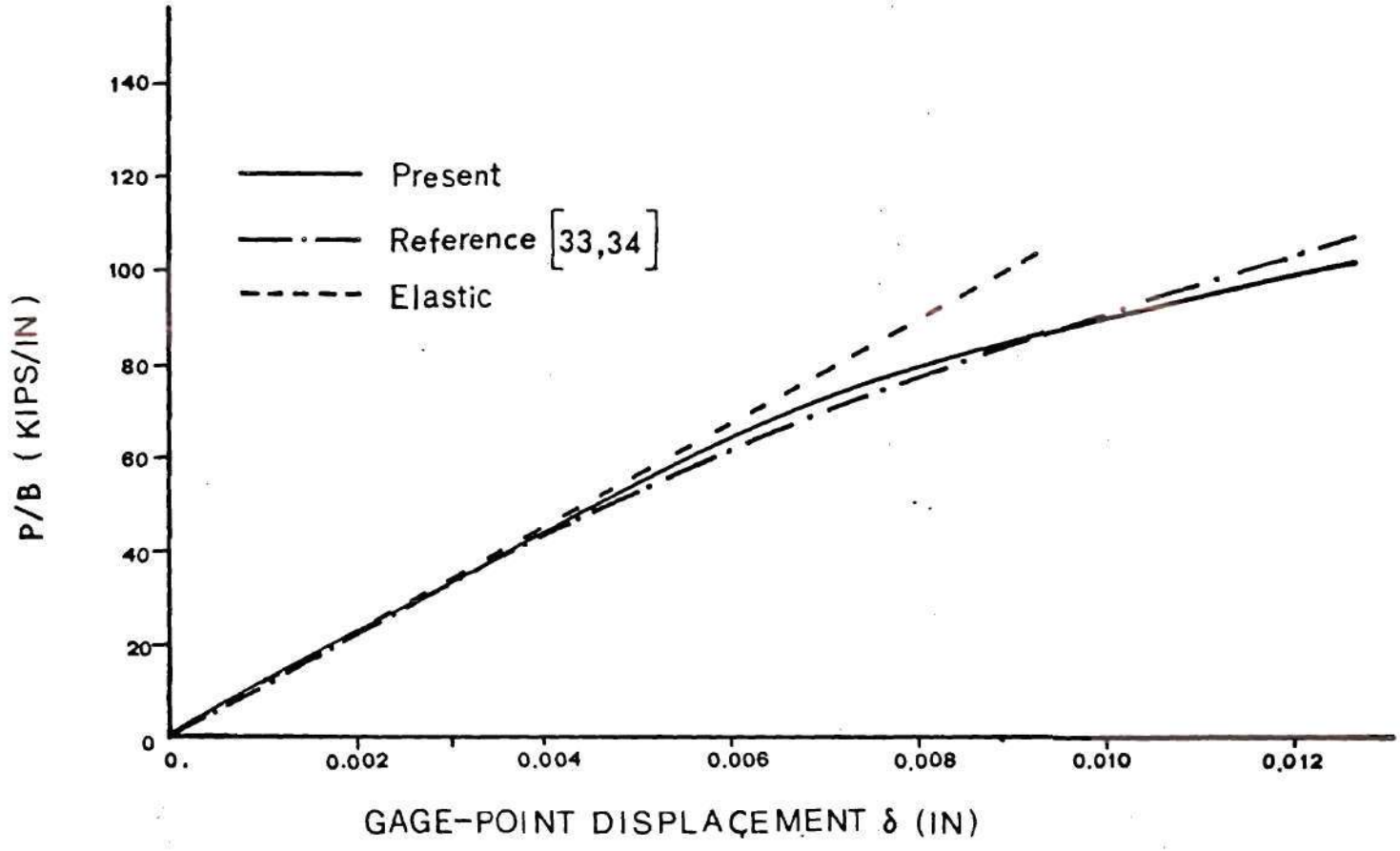

FIG.30 Load vs. Gage-Point Displacement for Center-Cracked Specimen

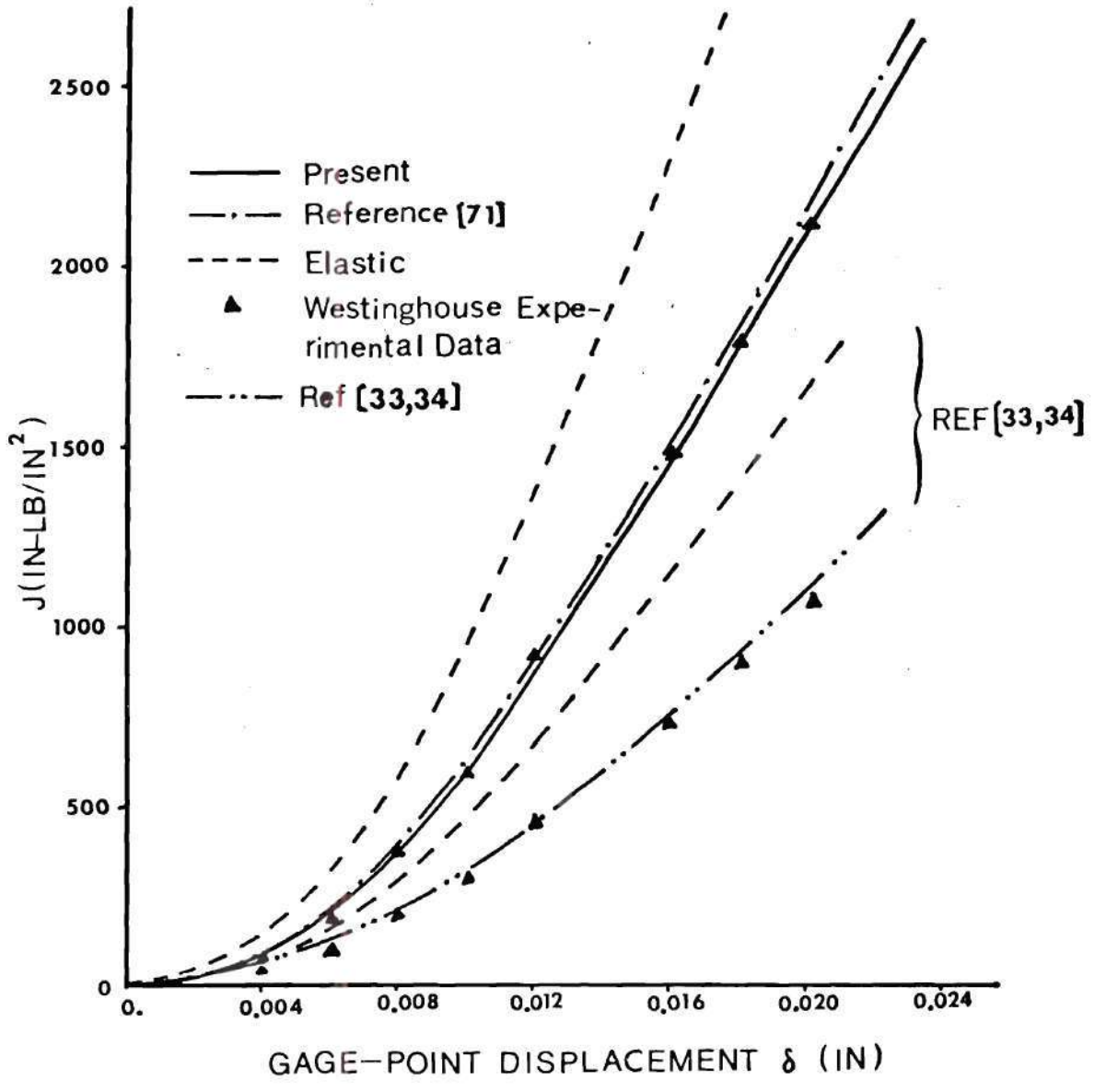

FIG.31 J-Integral vs. Gage-Point Displacement for Center-Cracked Specimen

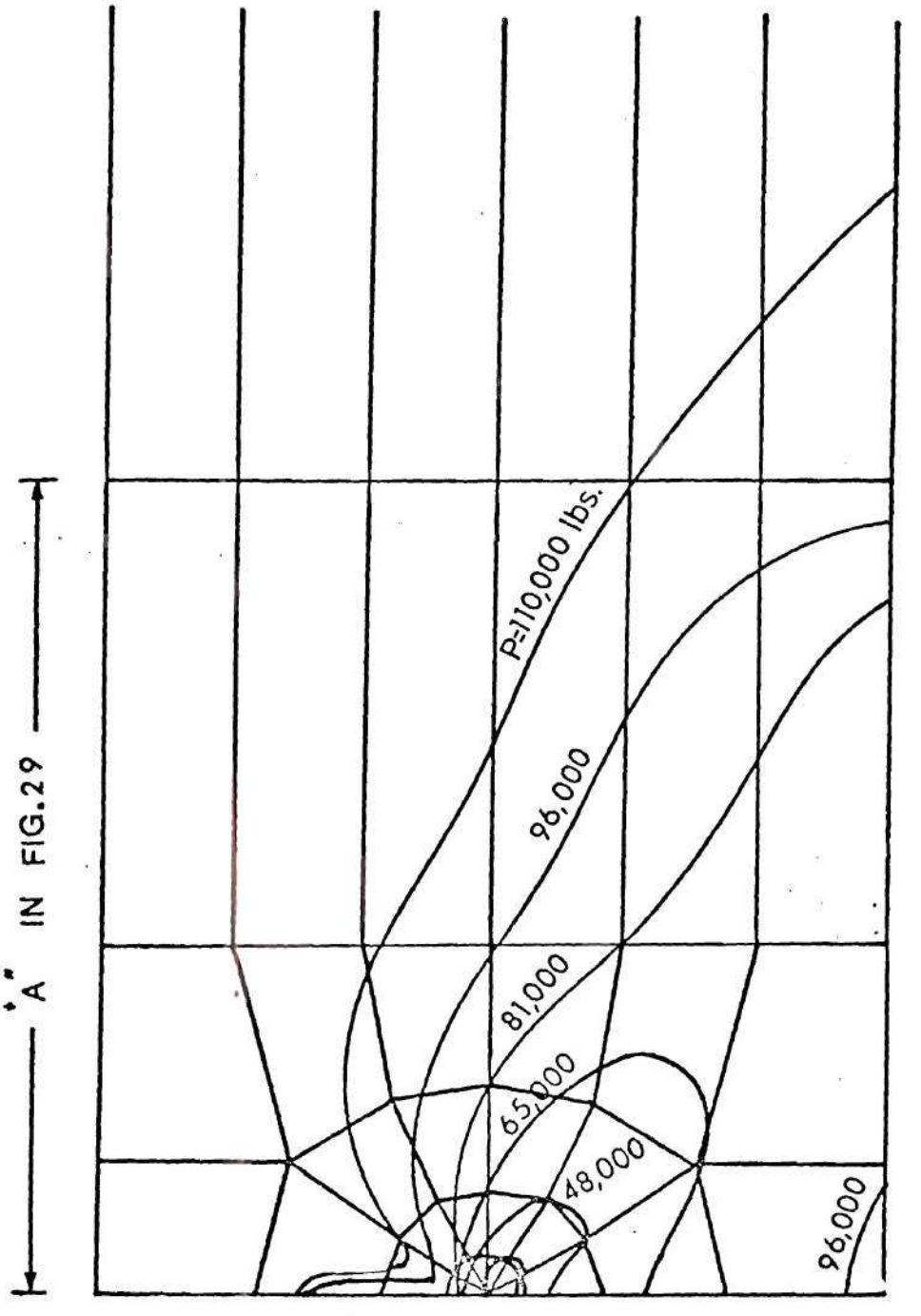

FIG.32 Yield Zones at Various Load Levels for Center-Cracked Specimen

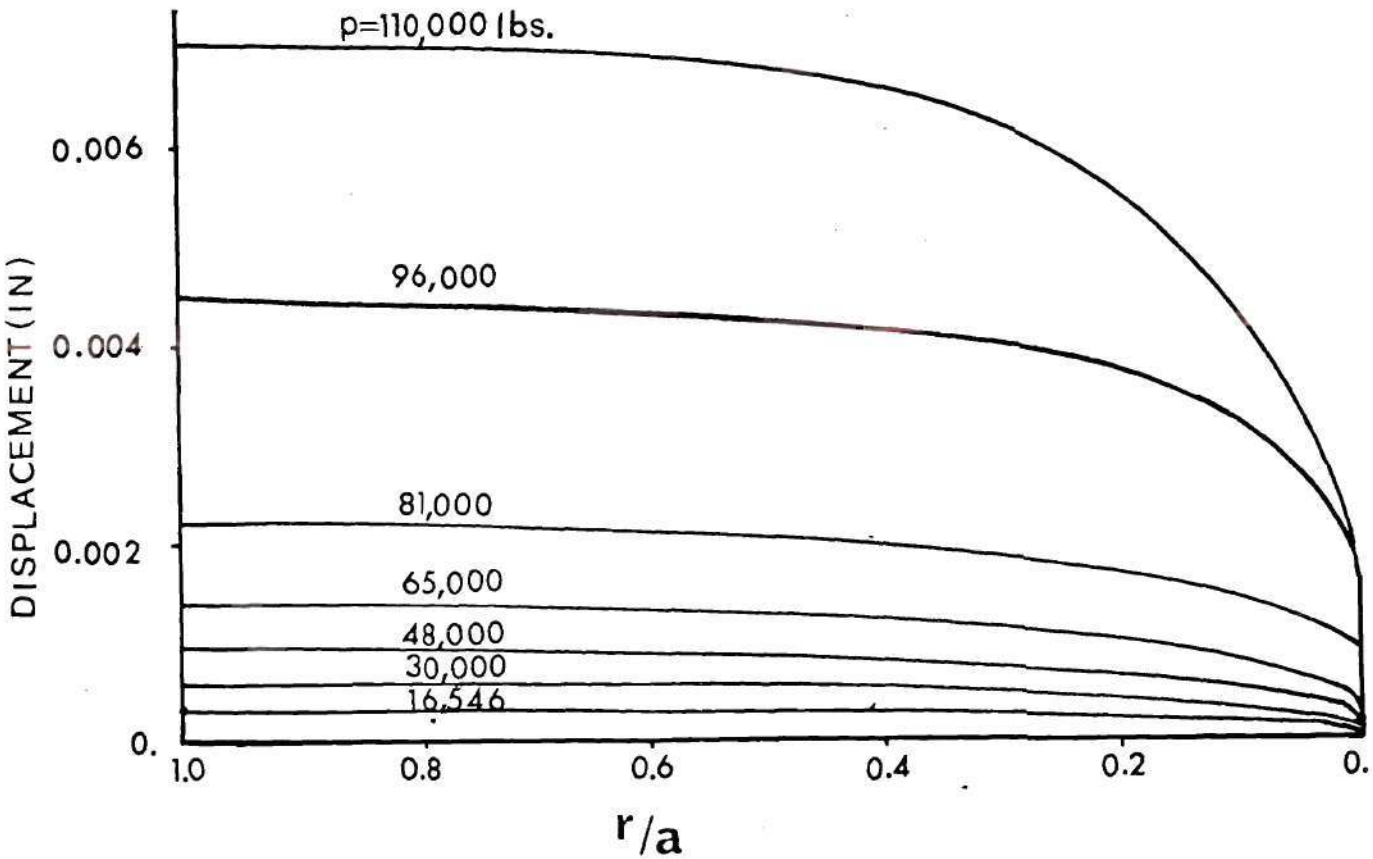

FIG.33 Crack-Surface Deformation Profiles at Various Load Levels for Center-Cracked Specimen

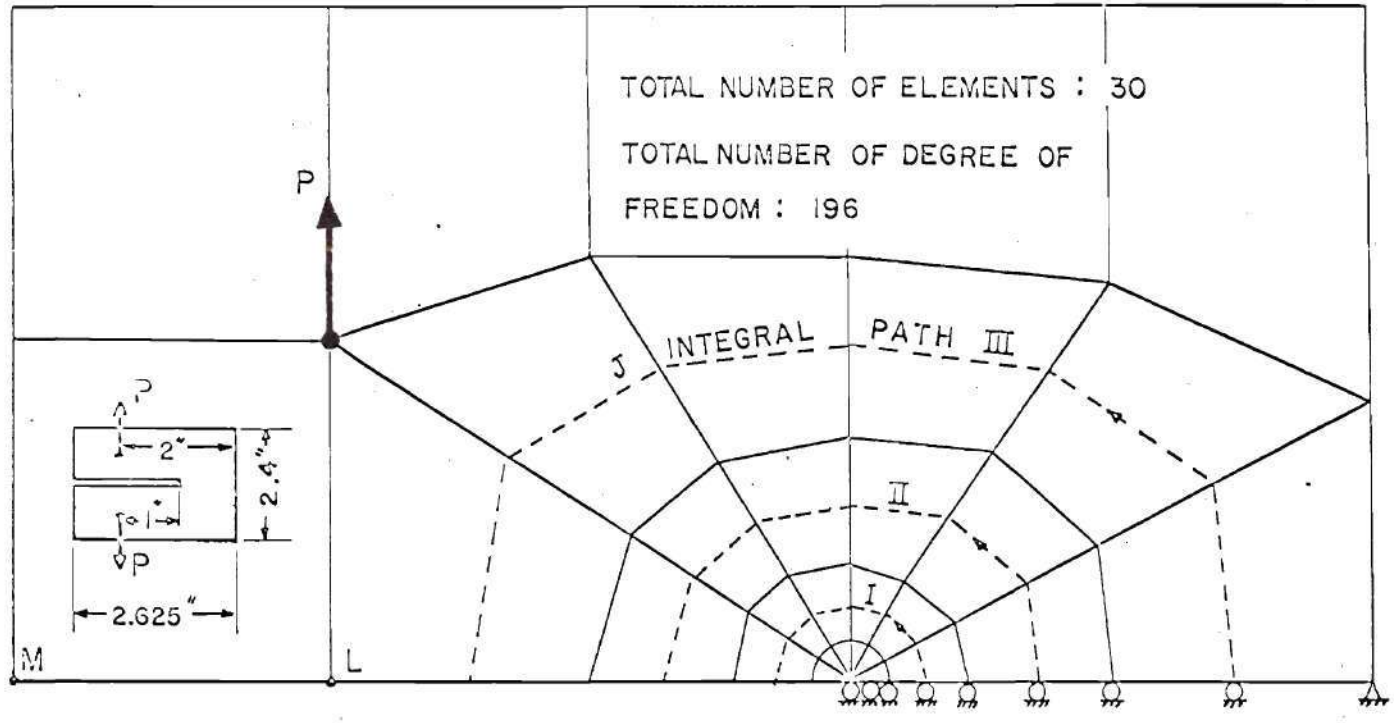

FIG.34 FINITE ELEMENT MODEL FOR THE COMPACT TENSION SPECIMEN.

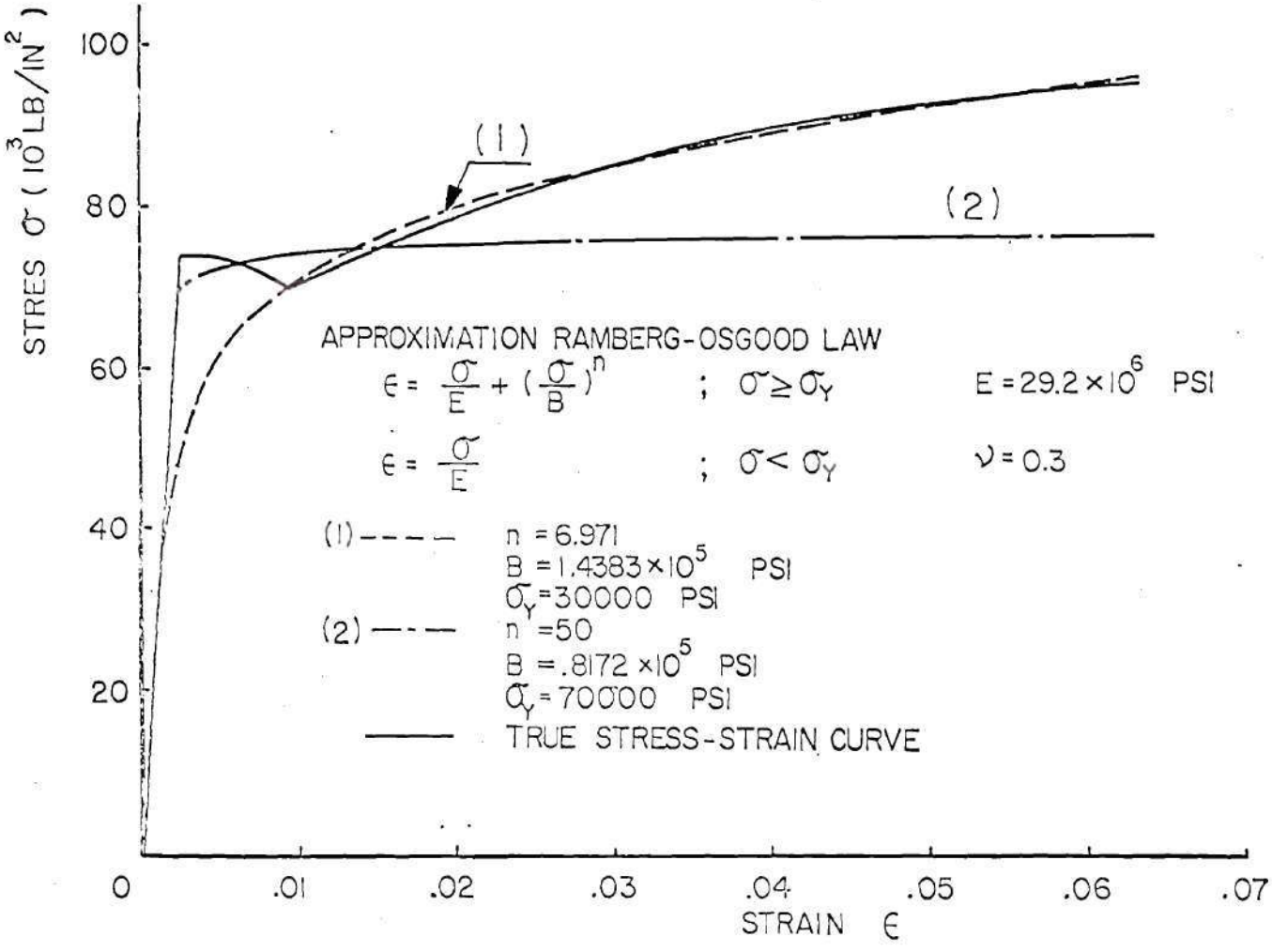

FIG. 35 UNIAXIAL STRESS-STRAIN CURVE FOR A533B STEEL.

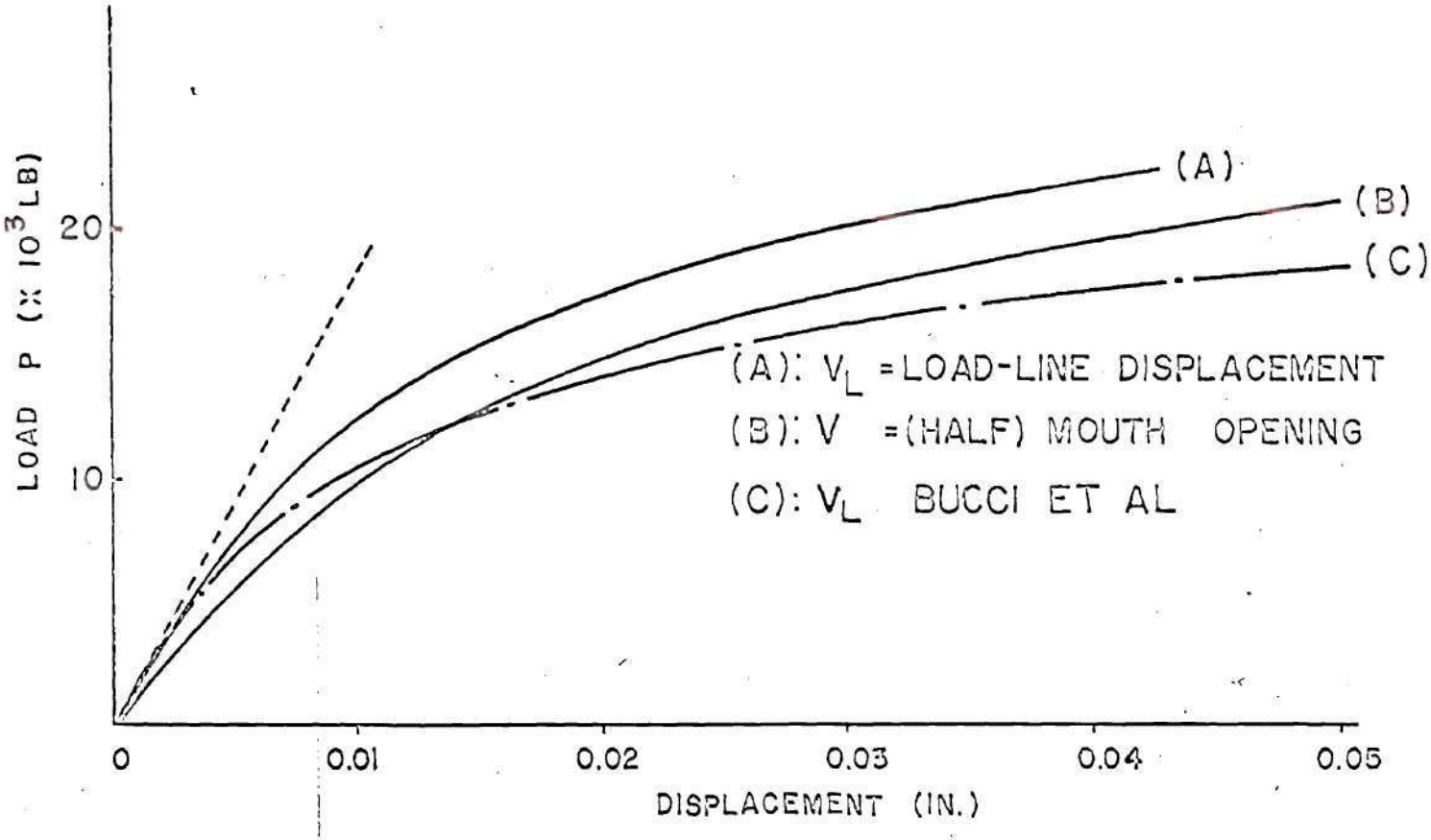

FIG. 36 Load vs Load - Line & Mouth - Opening Displacements for a CT Specimen.

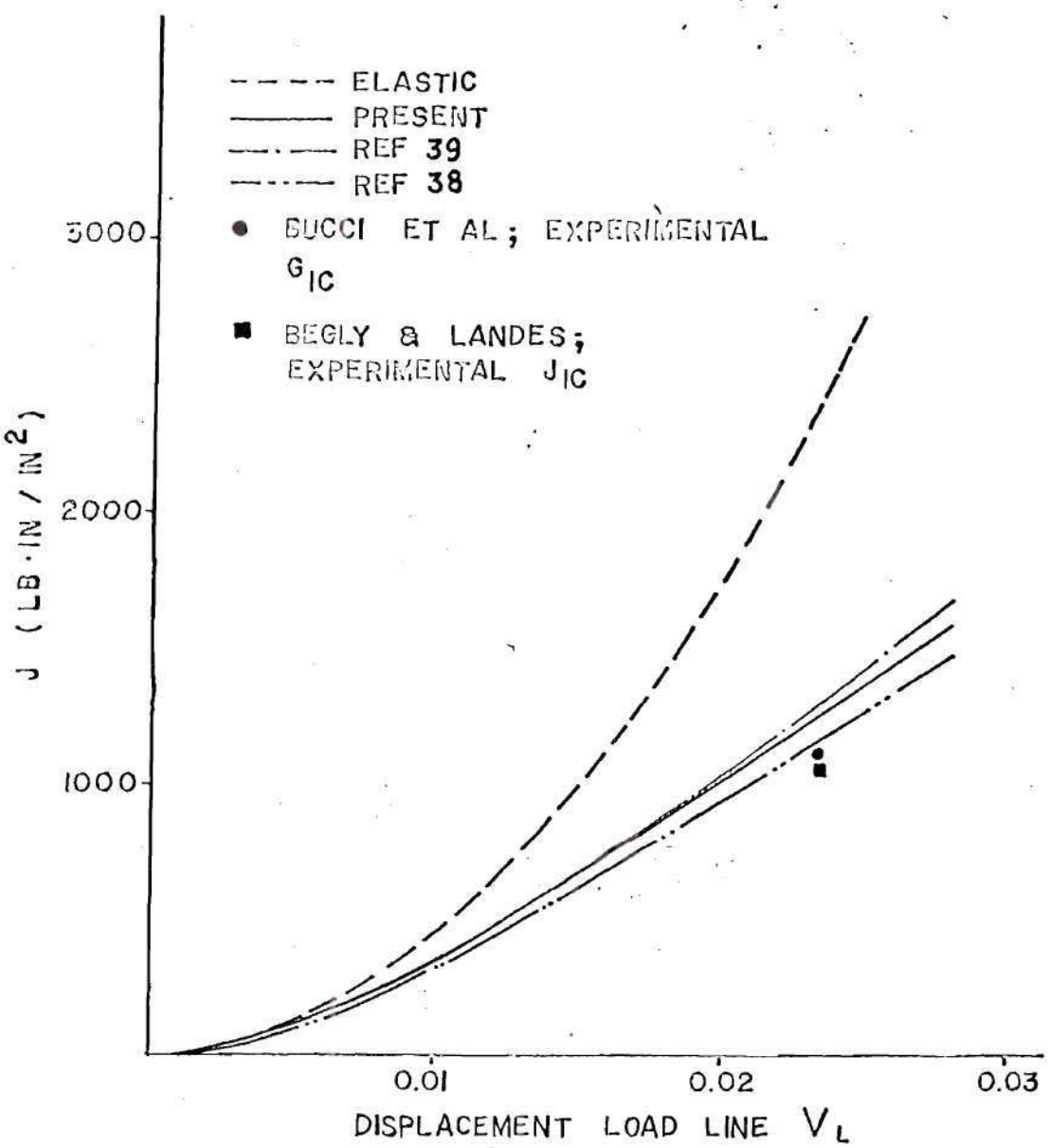

FIG.37 J vs V_L Curves for Compact Tension Specimen

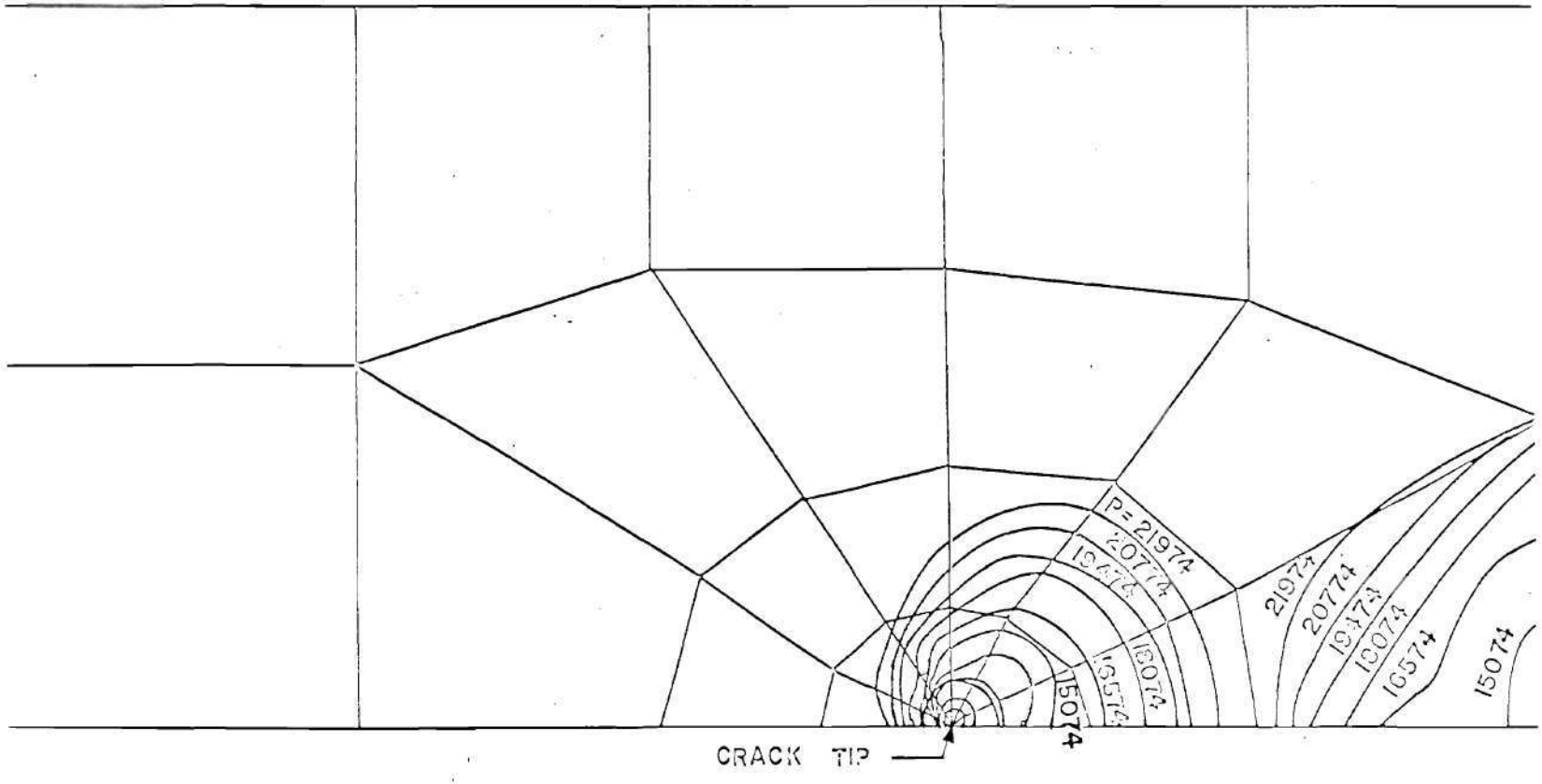

FIG. 38 Yield Zones at Various Load Levels for a C T Specimen

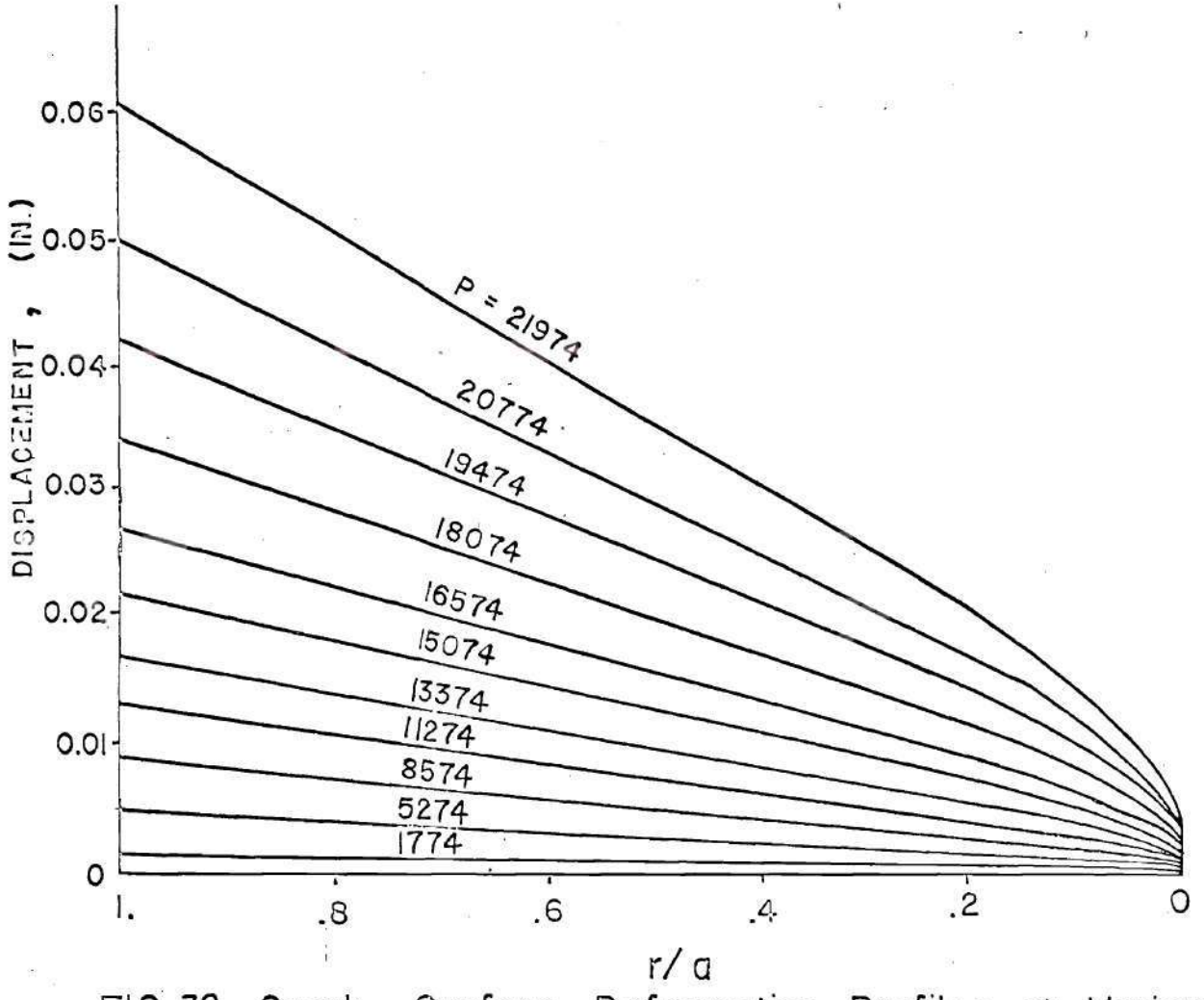

FIG. 39 Crack- Surface Deformation Profiles at Various Load Levels for a C T Specimen.

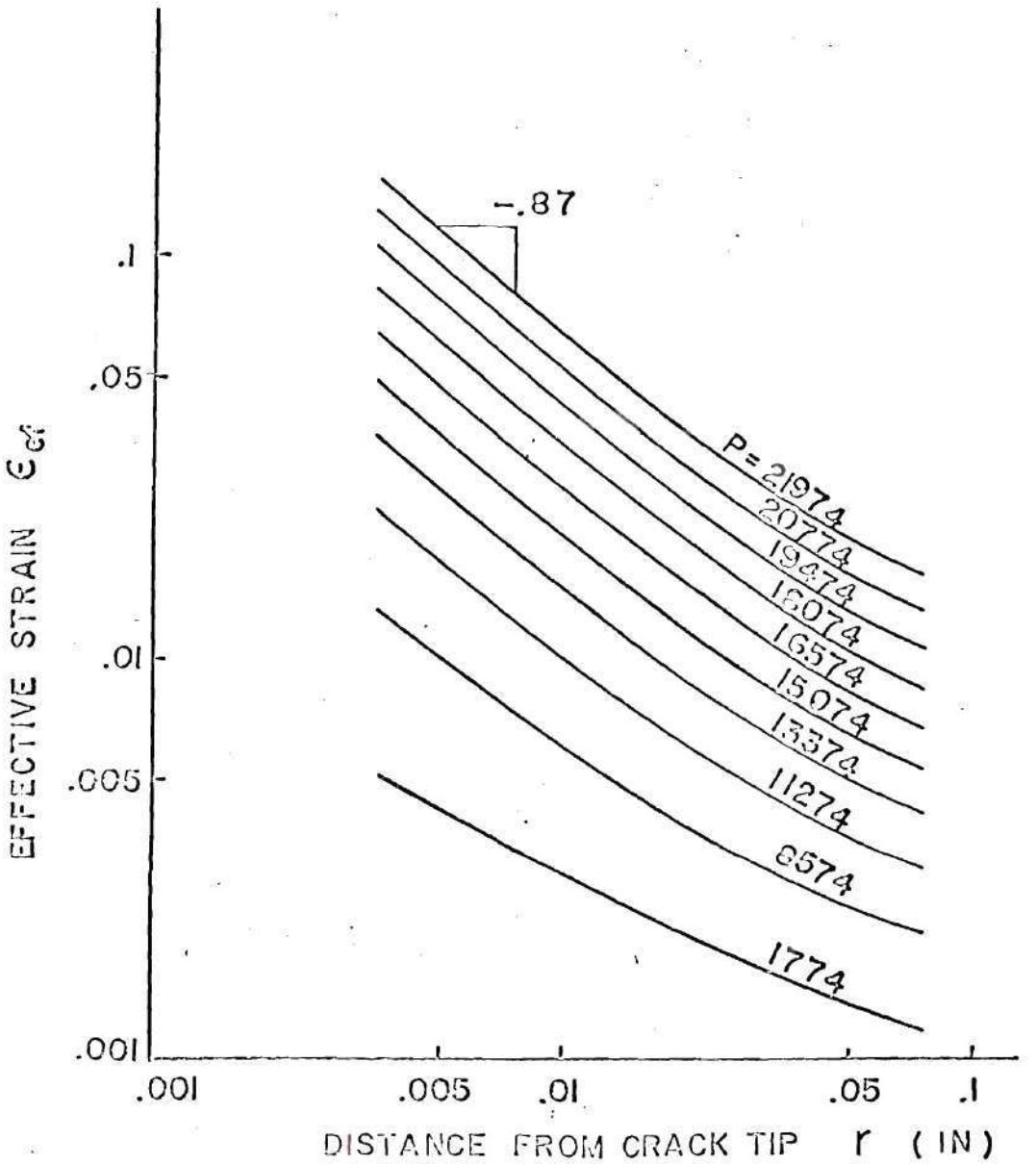

FIG.40 BEHAVIOR OF STRAIN SINGULARITY NEAR THE CRACK TIP FOR A CT SPECIMEN.

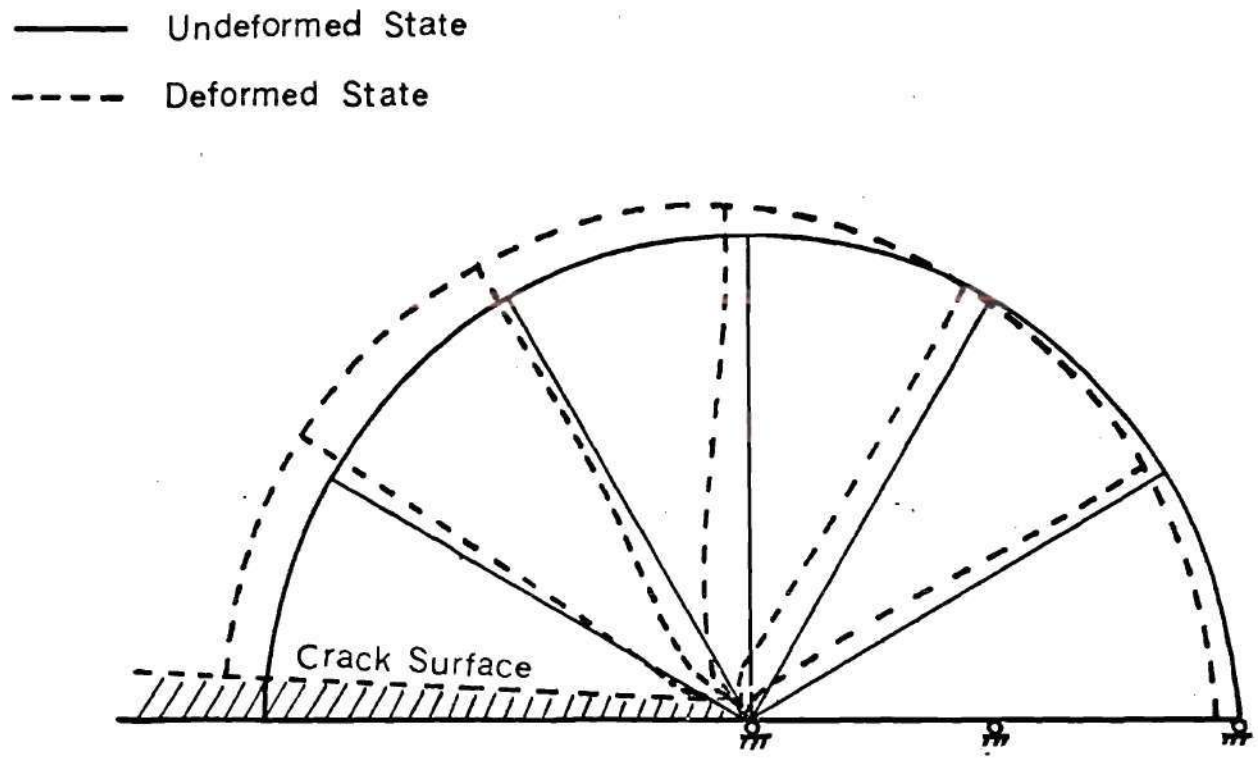

FIG.41 Deformation of the "Singular" Crack-Tip Elements for a CT Specimen

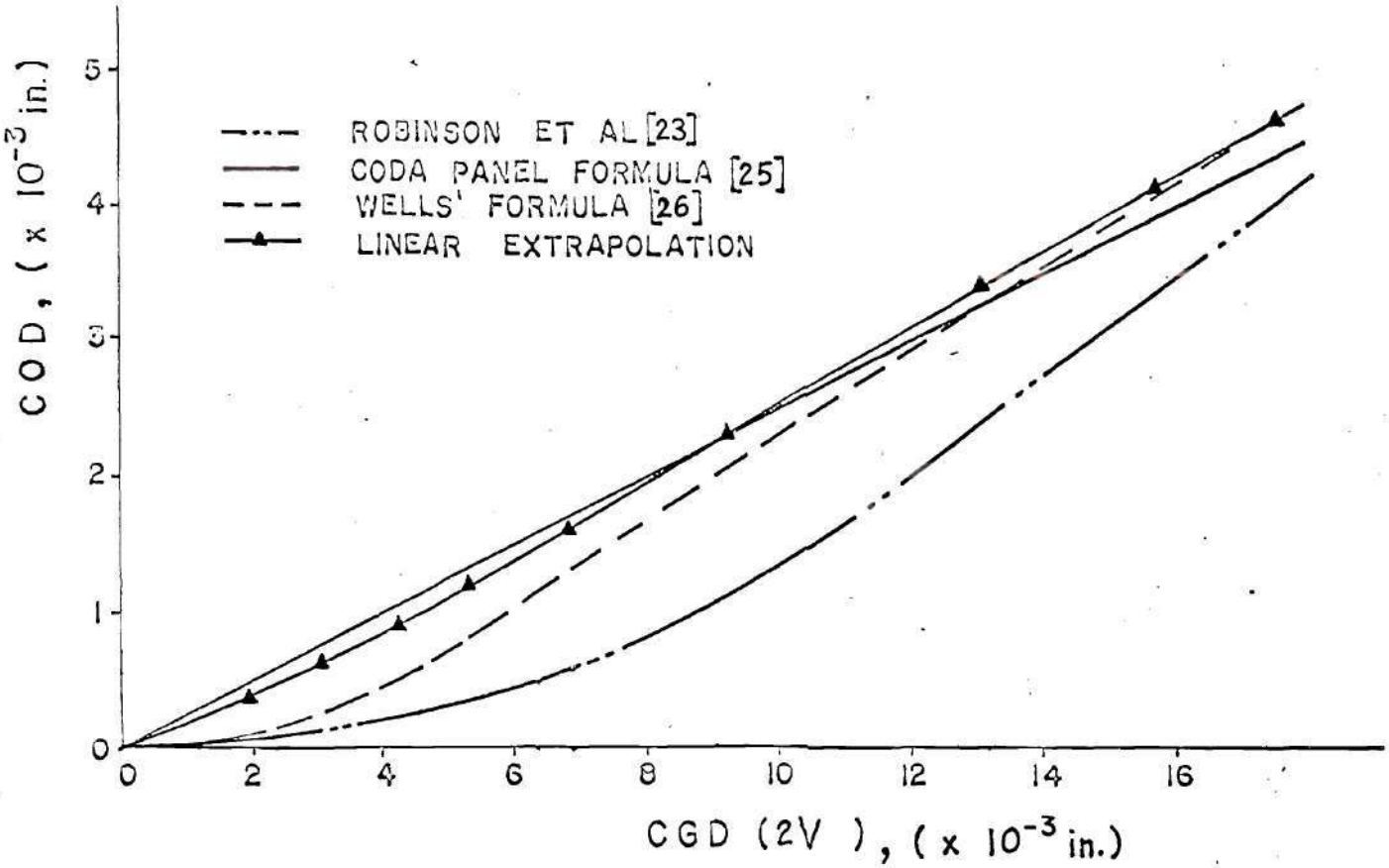

FIG. 42 COD vs CGD Relation for a 3-Point Bend Bar.

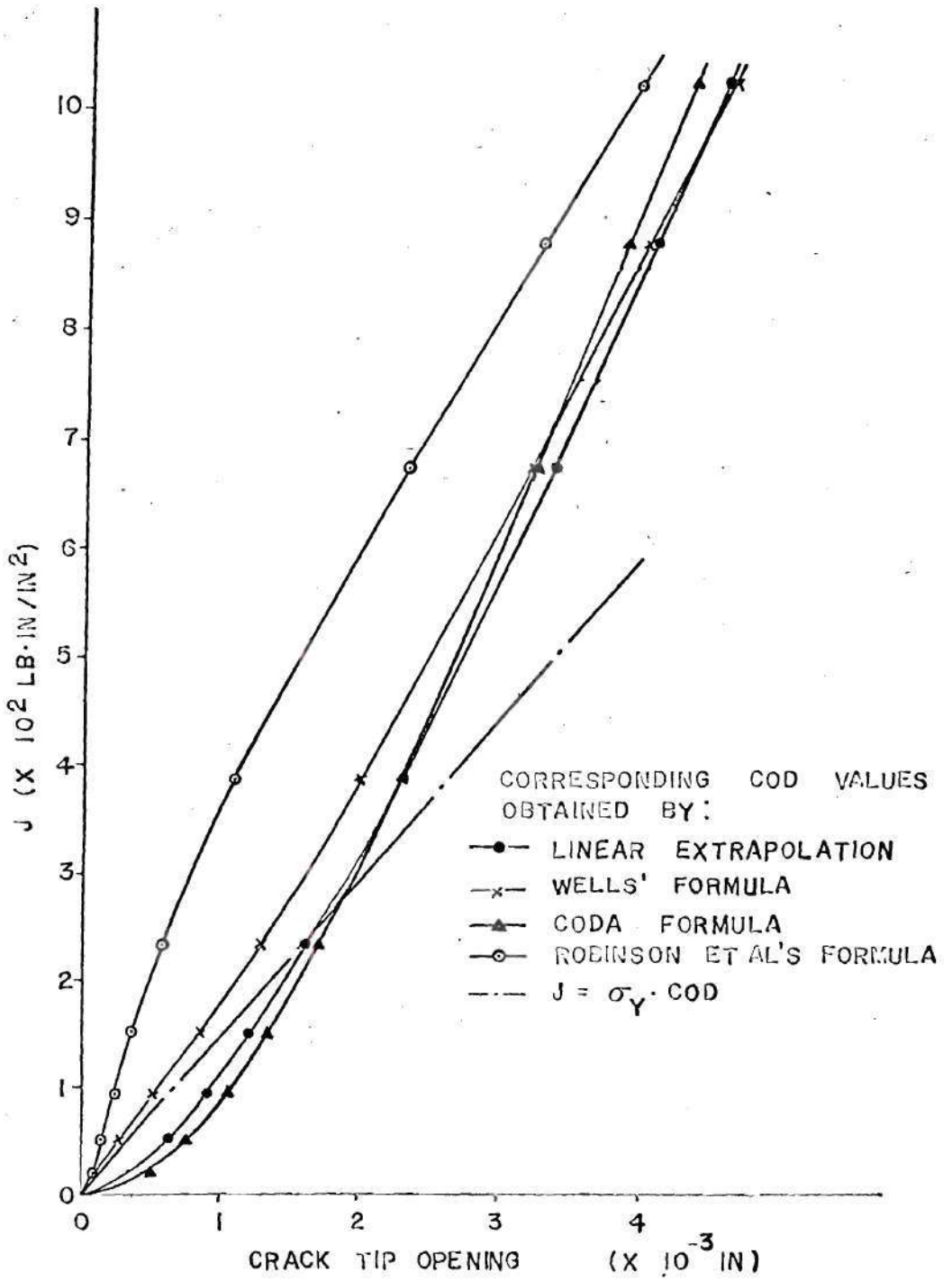

FIG.43 J vs COD Relation for a 3-Point Bend Bar.

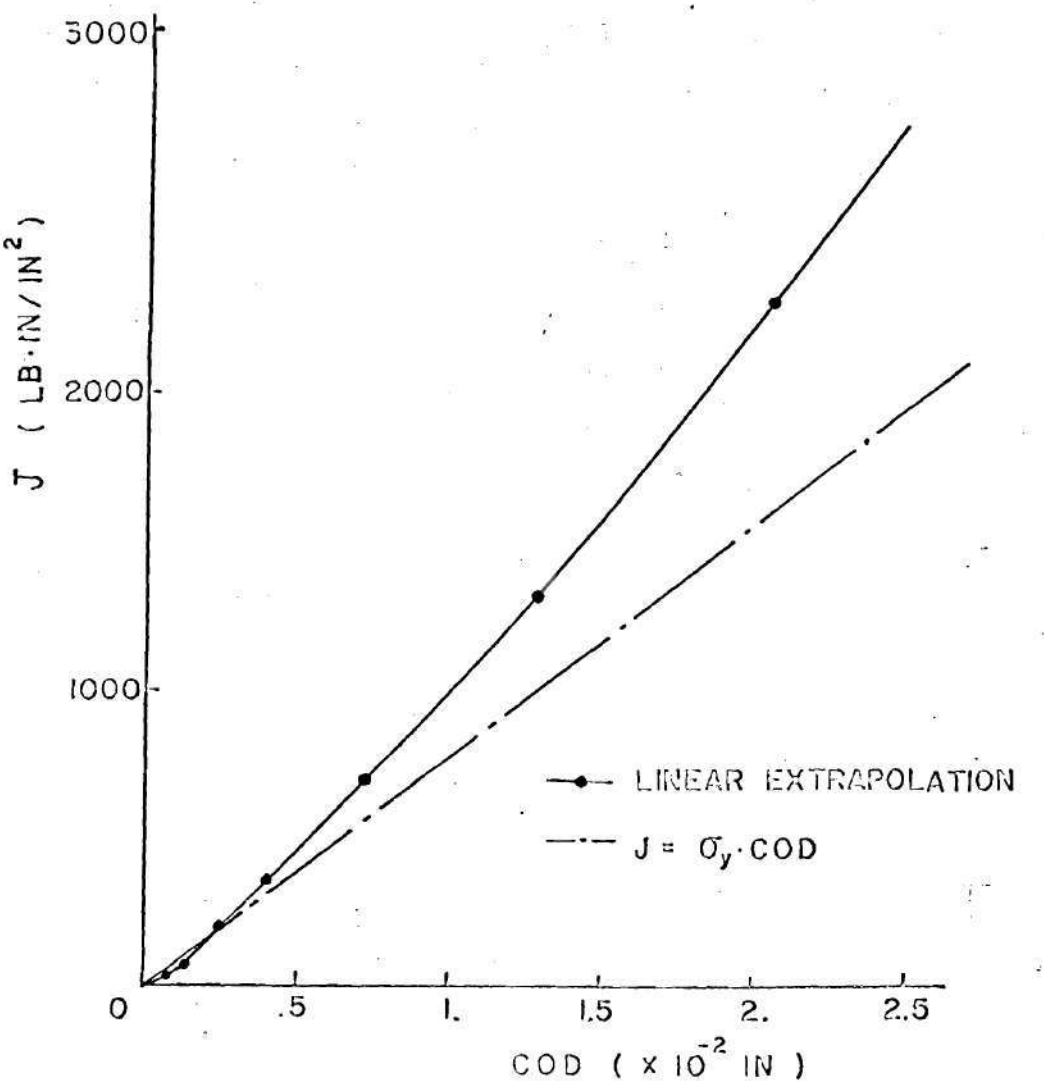

FIG.44 J VS. COD RELATION FOR A CT SPECIMEN.

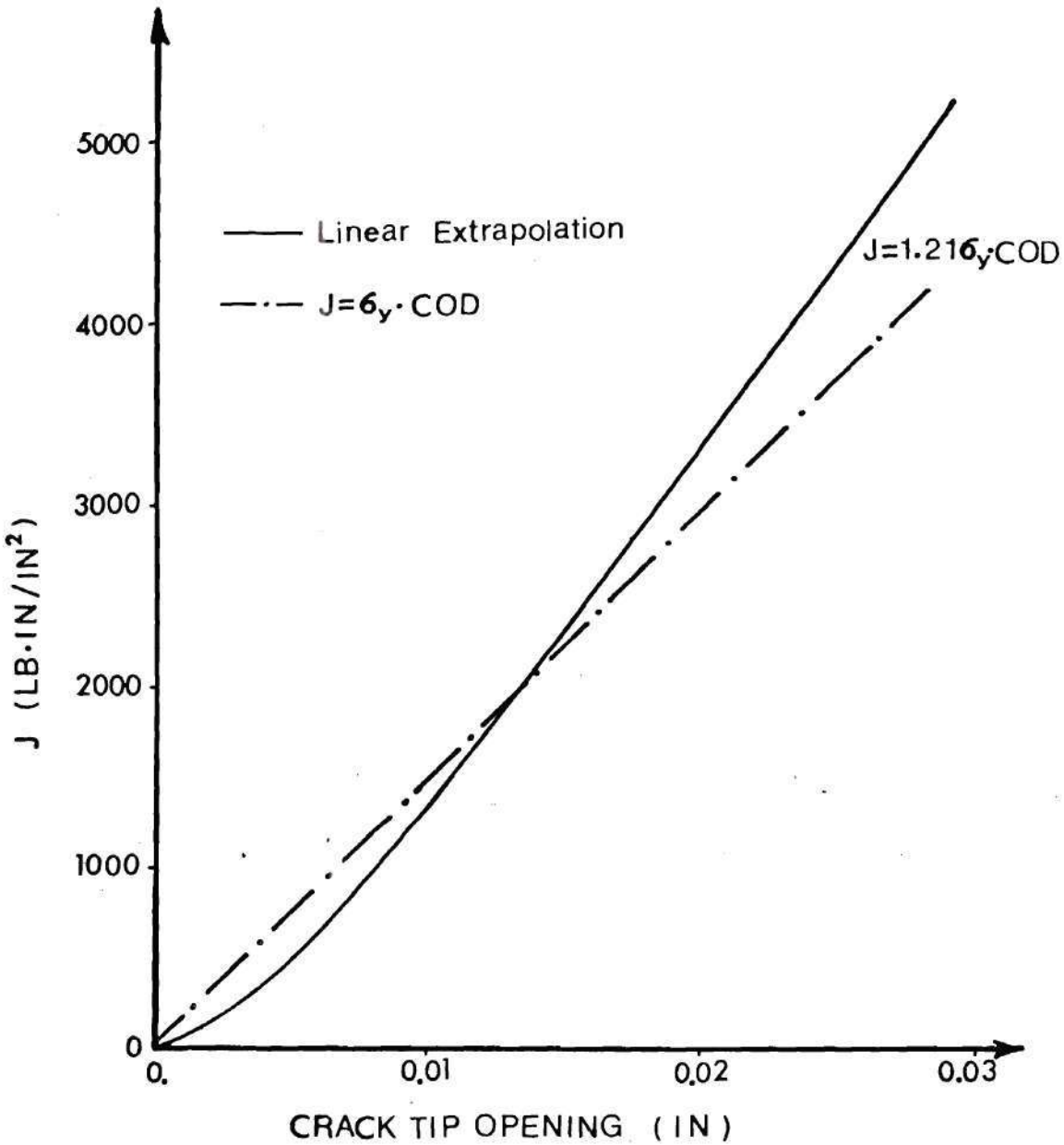

FIG.45 J vs. COD Relation for the Center-Cracked Specimen

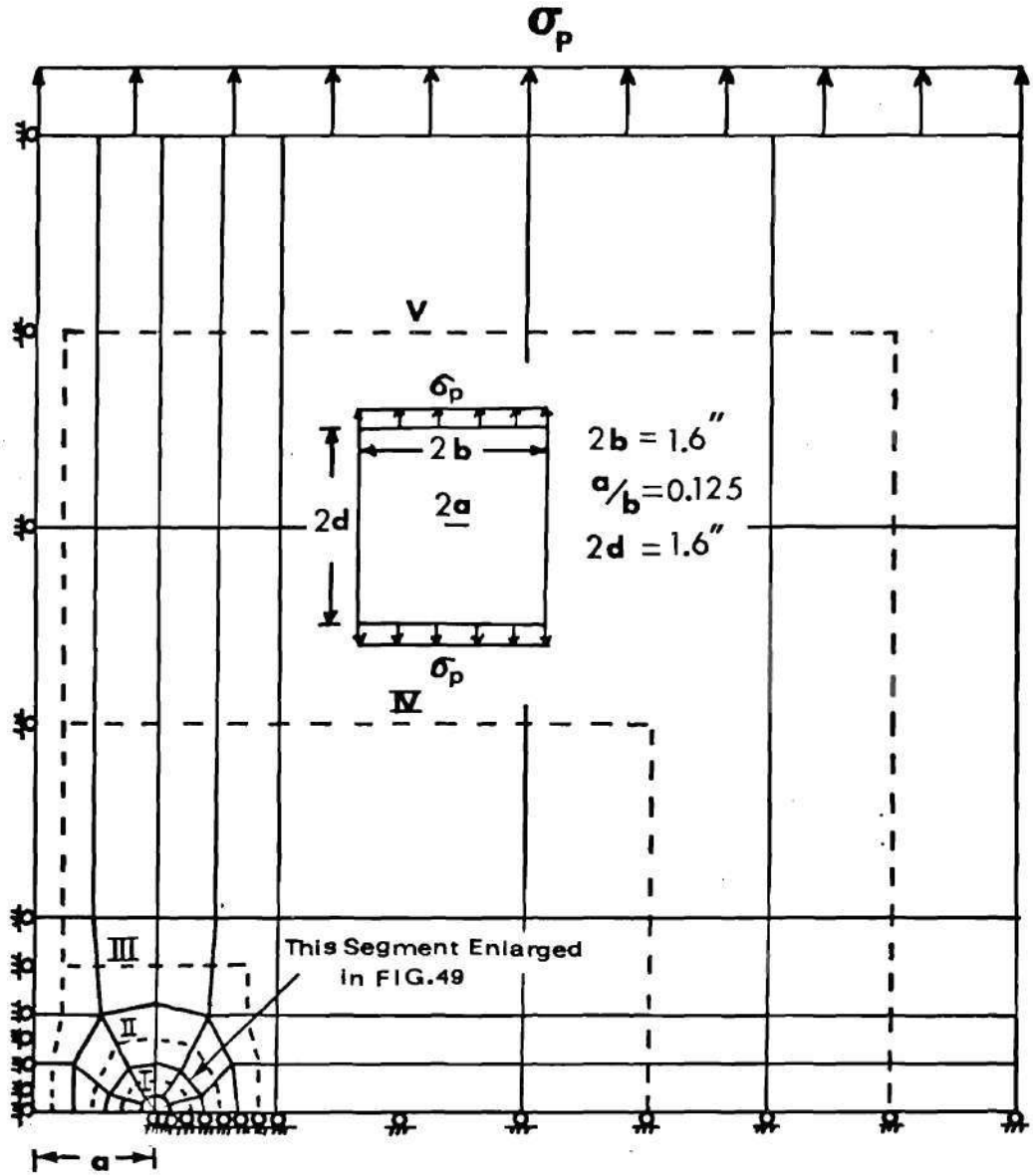

FIG.46 Finite-Element Model for Center -Cracked Specimen as Studied in Kfouri et al [74,75]

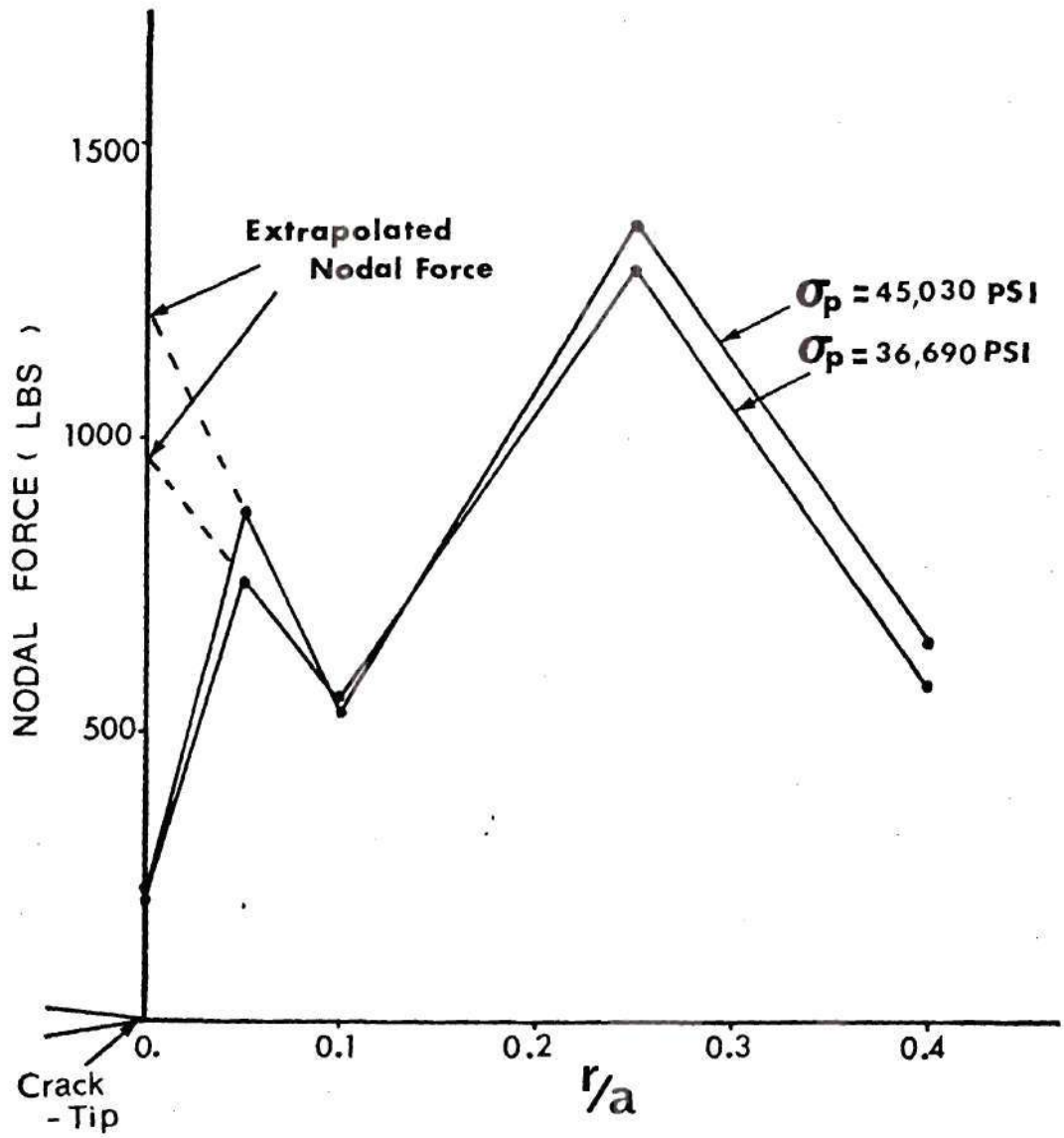

FIG.47 Nodal Force Distribution in the Uncracked Ligament for Center-Cracked Specimen as Studied in Kfouri et al [74,75]

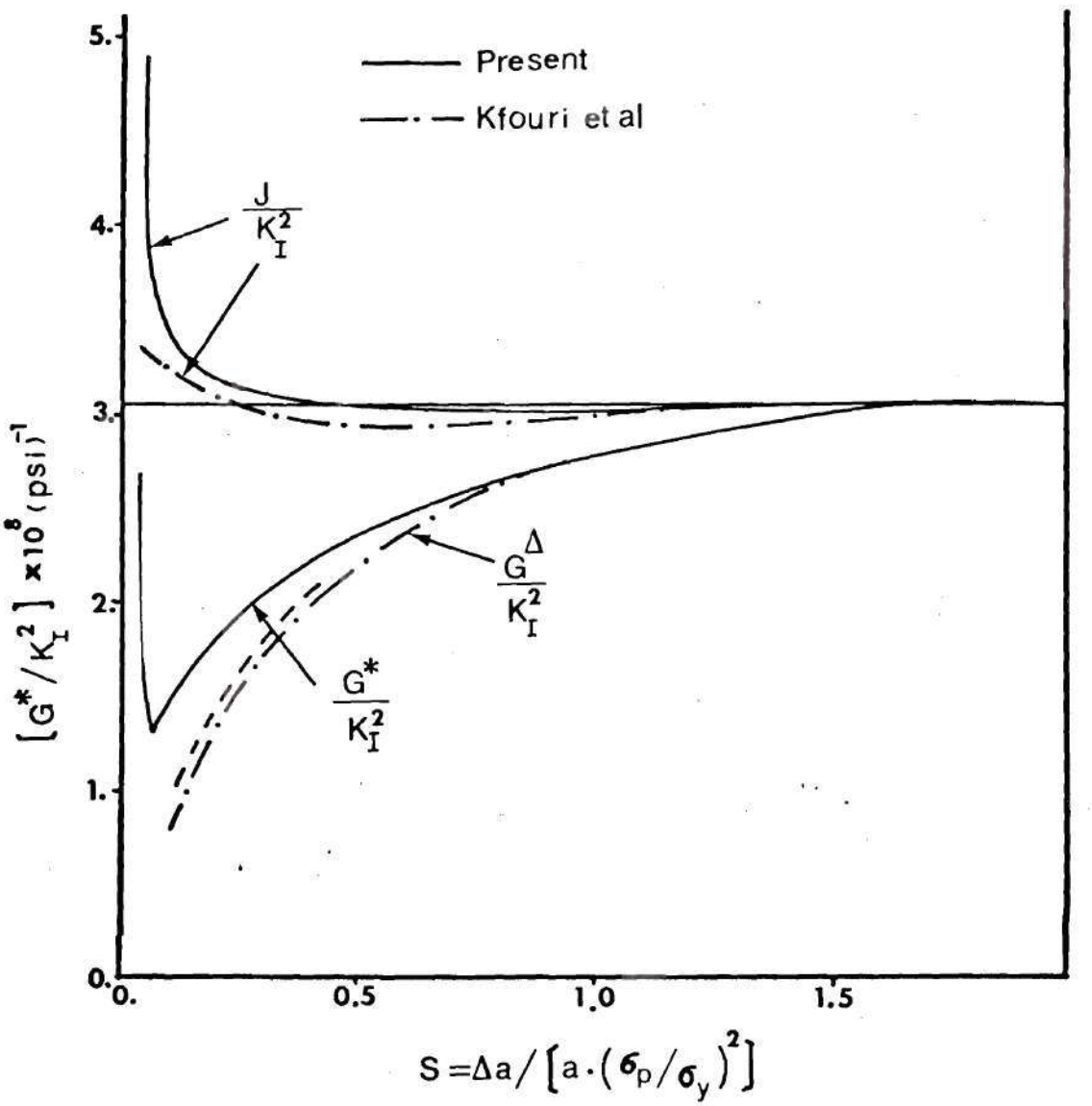

FIG.48 Variation of G^*, G^Δ and J with Decreasing Values of S for Kfouri et al's Specimen

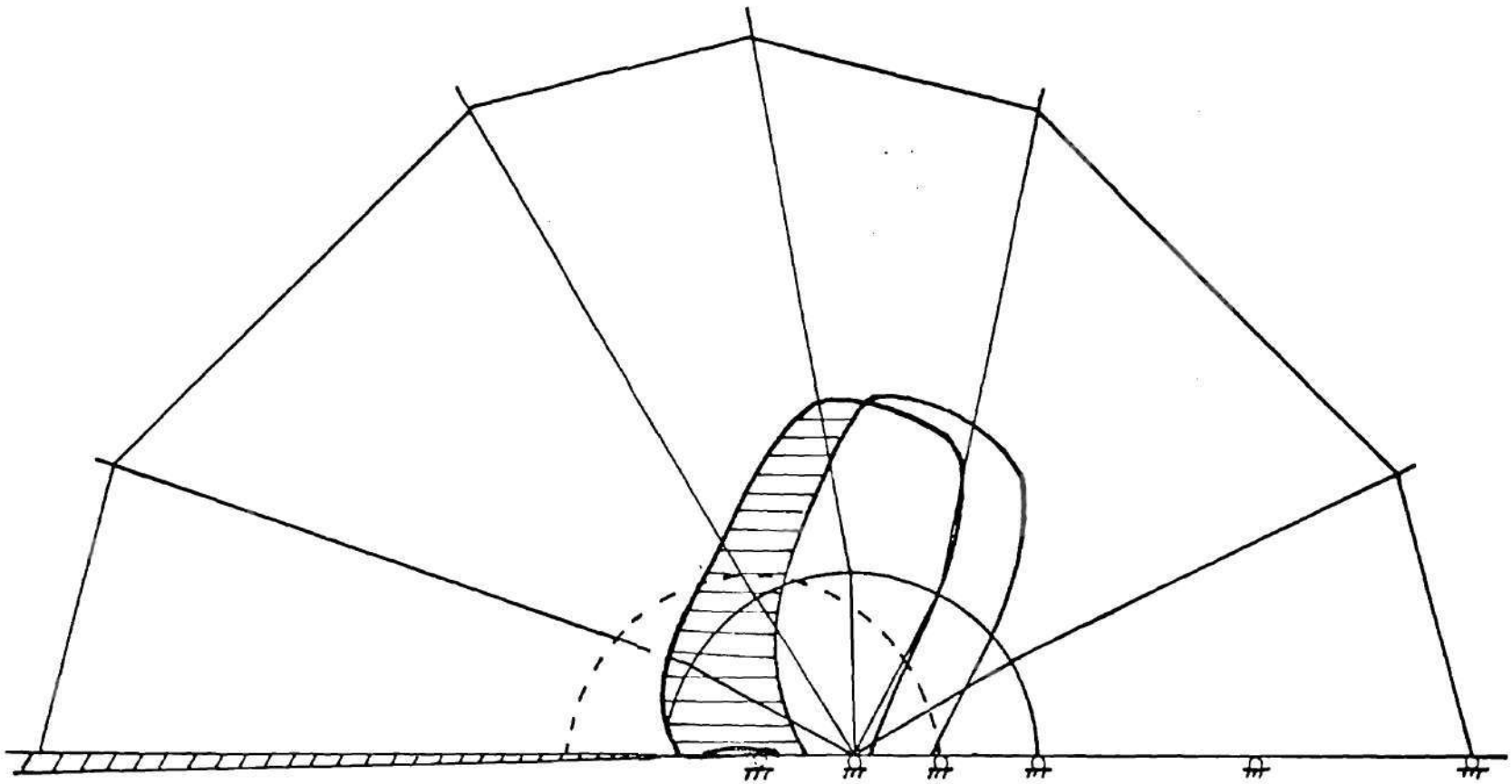

FIG.49 Development of the Crack-Tip Plastic Zone During Crack Extension Under Constant Load Condition

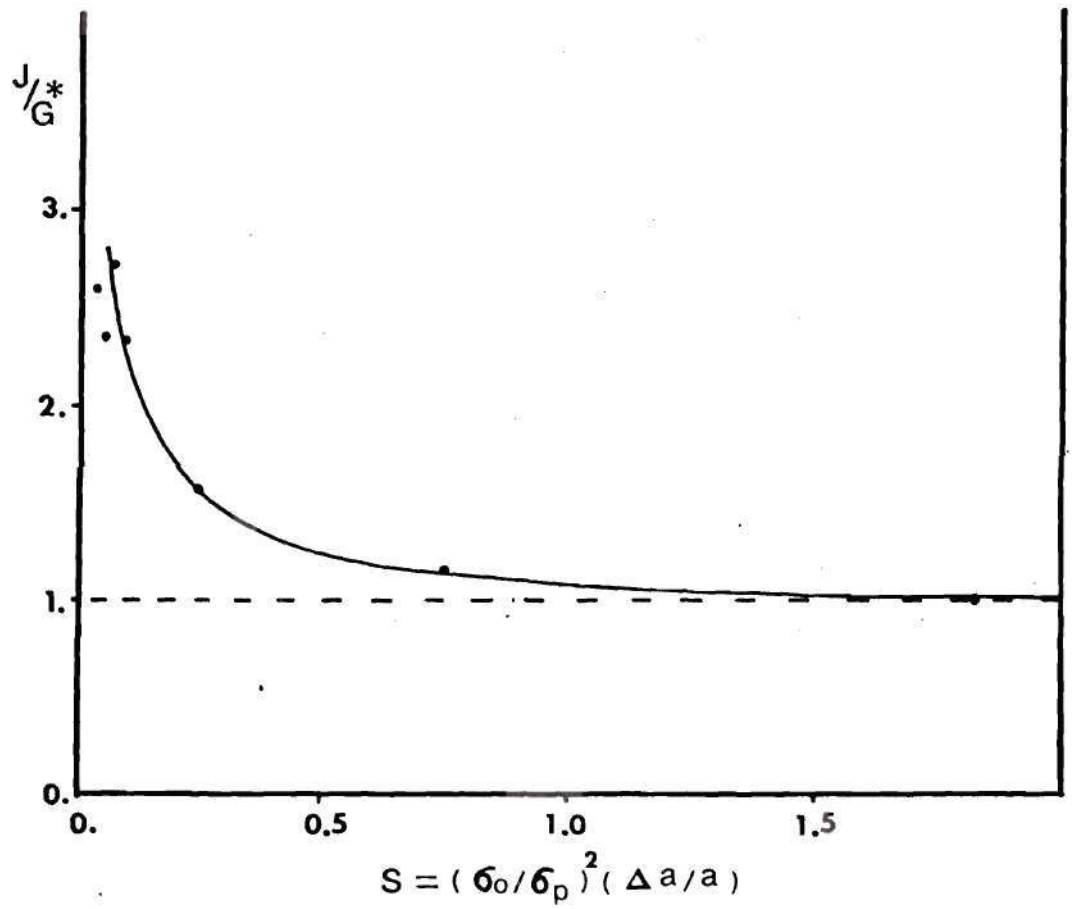

FIG. 50 Variation of J/G^* with Decreasing Values of S for Center-Cracked Specimen as Studied in Kfouri at el [74, 75]

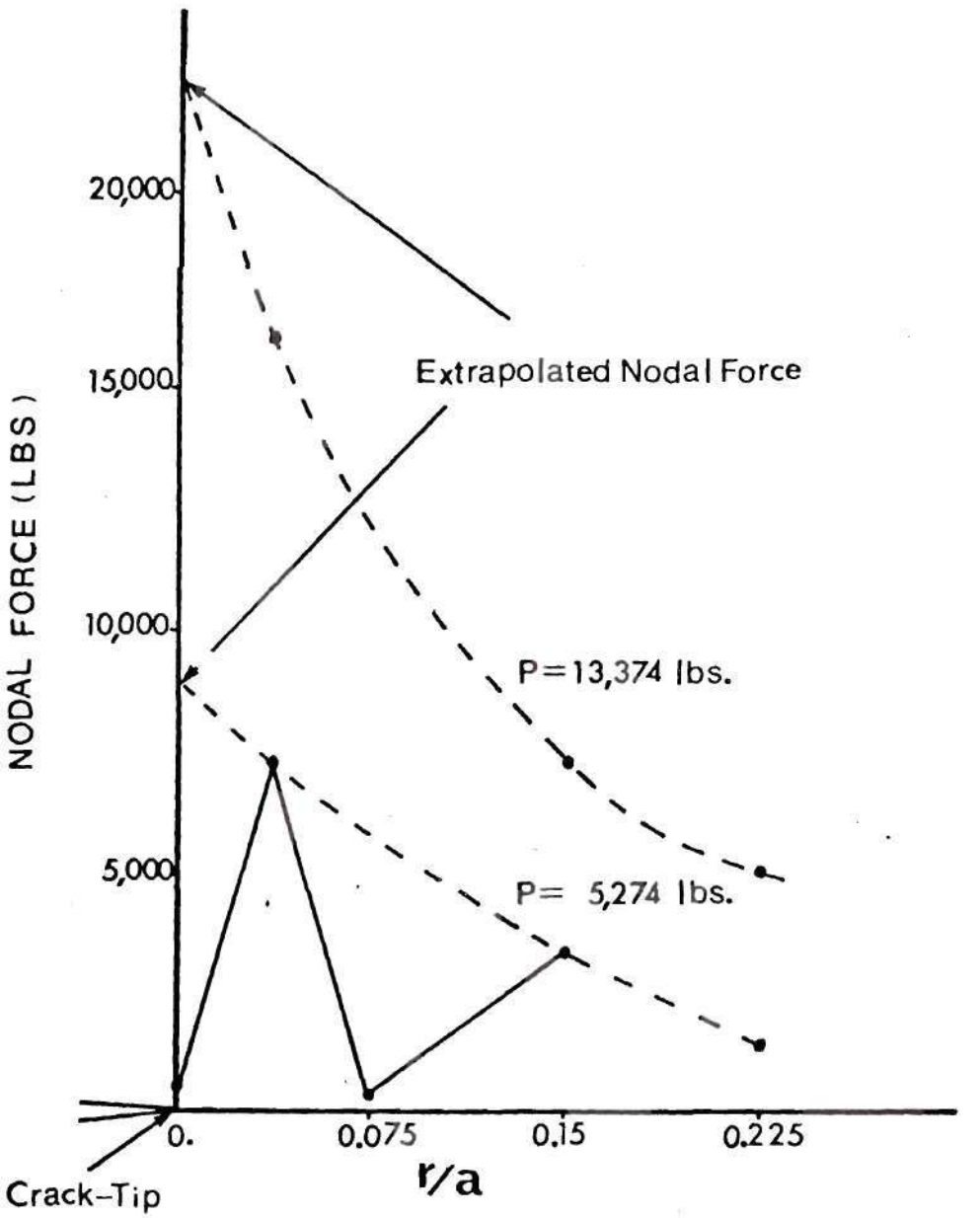

FIG. 51 Nodal Force Distribution in the Uncracked Ligament for A533B Compact Tension Specimen

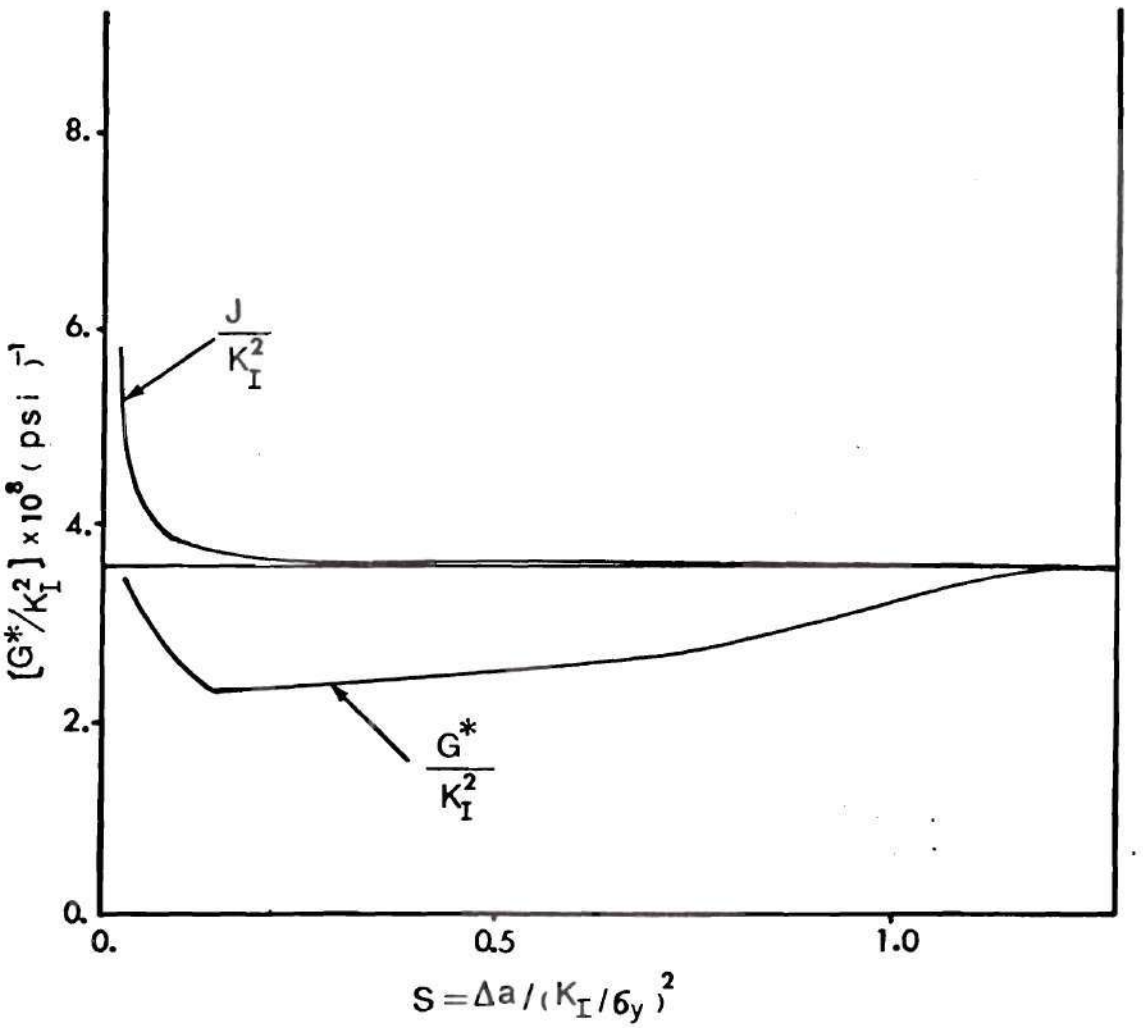

FIG. 52 Variation of G^* and J with Decreasing Values of S for A533B Compact Tension Specimen

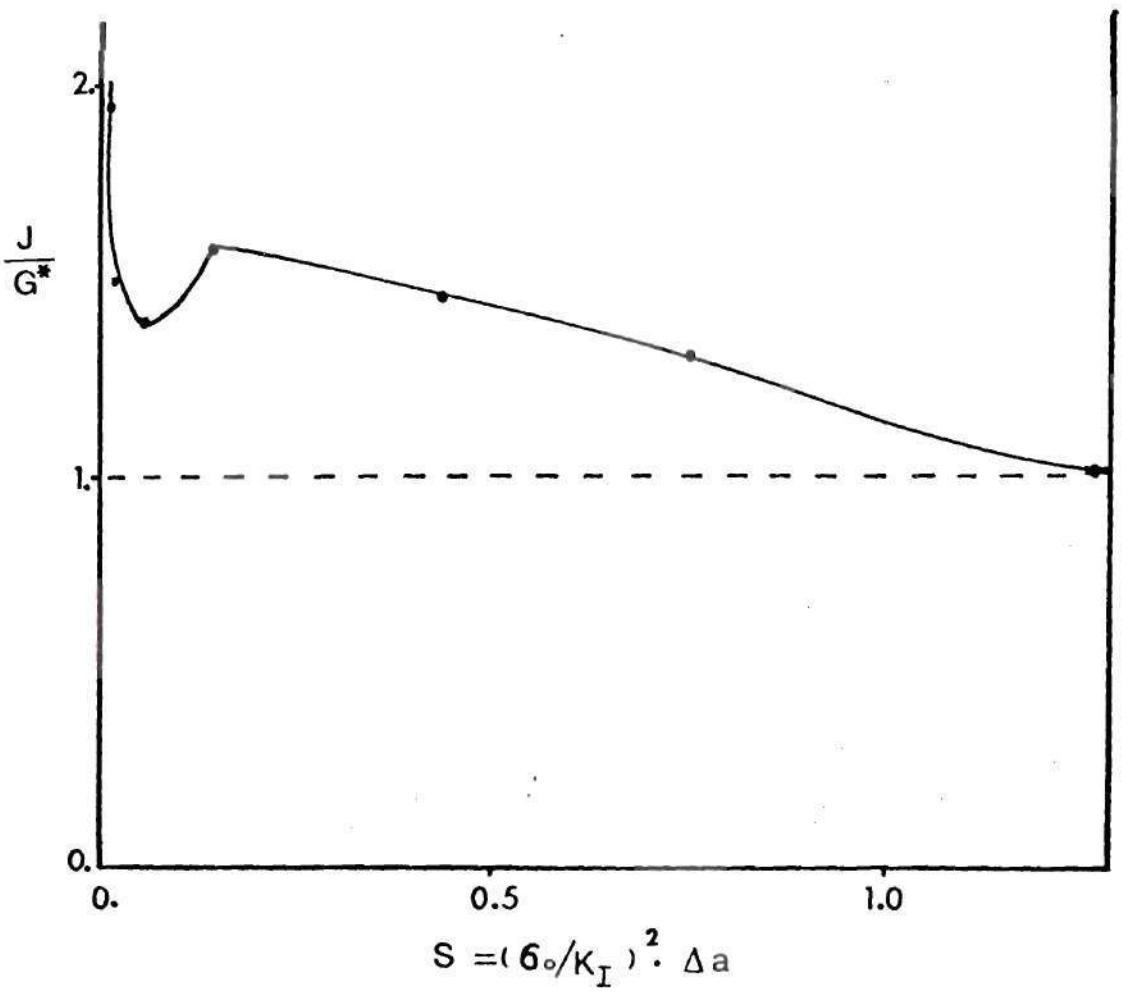

FIG. 53 Variation of J/G^* with Decreasing Values of S for A533B Compact Tension Specimen

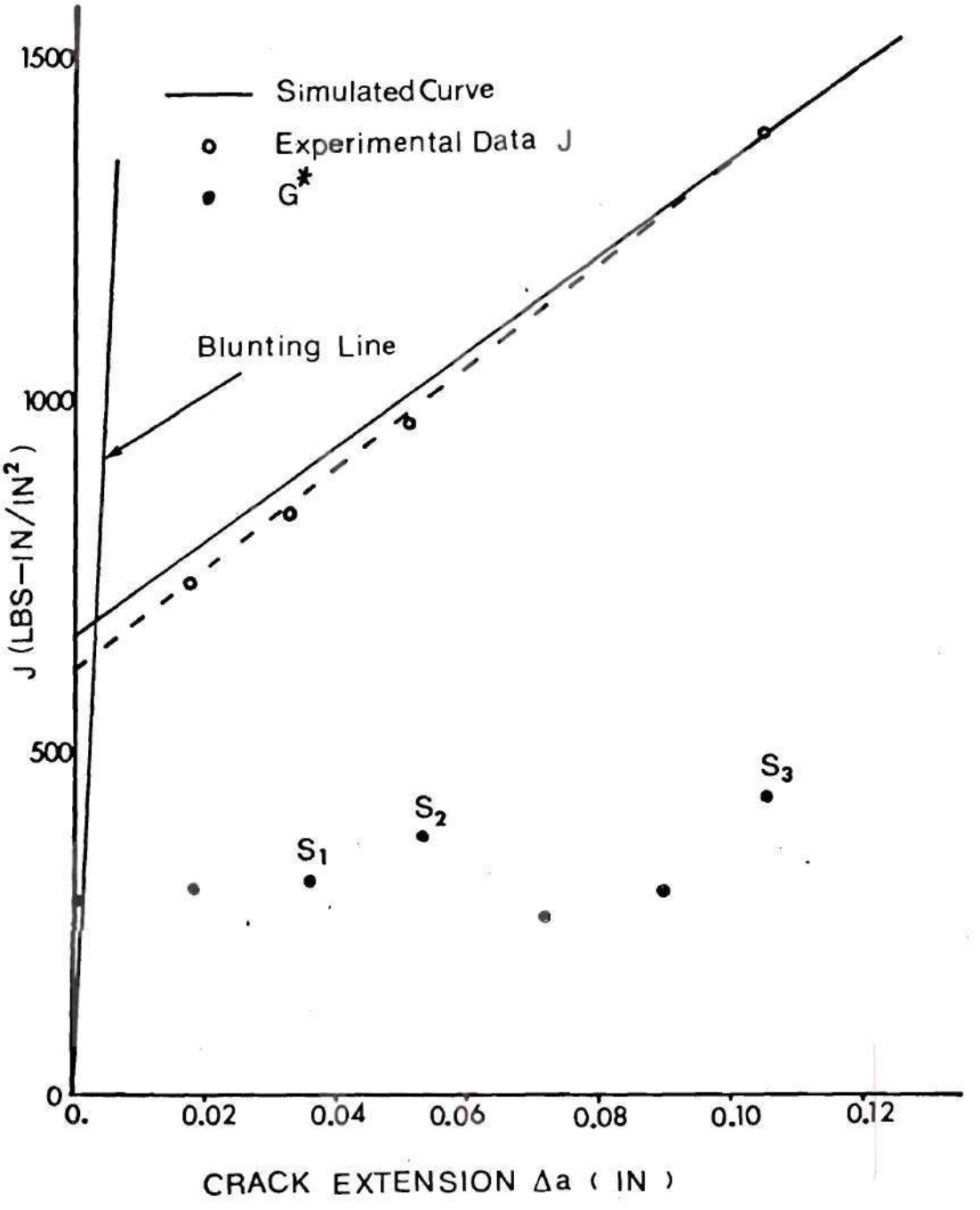

FIG. 54 Variation of G^* for Crack Extention

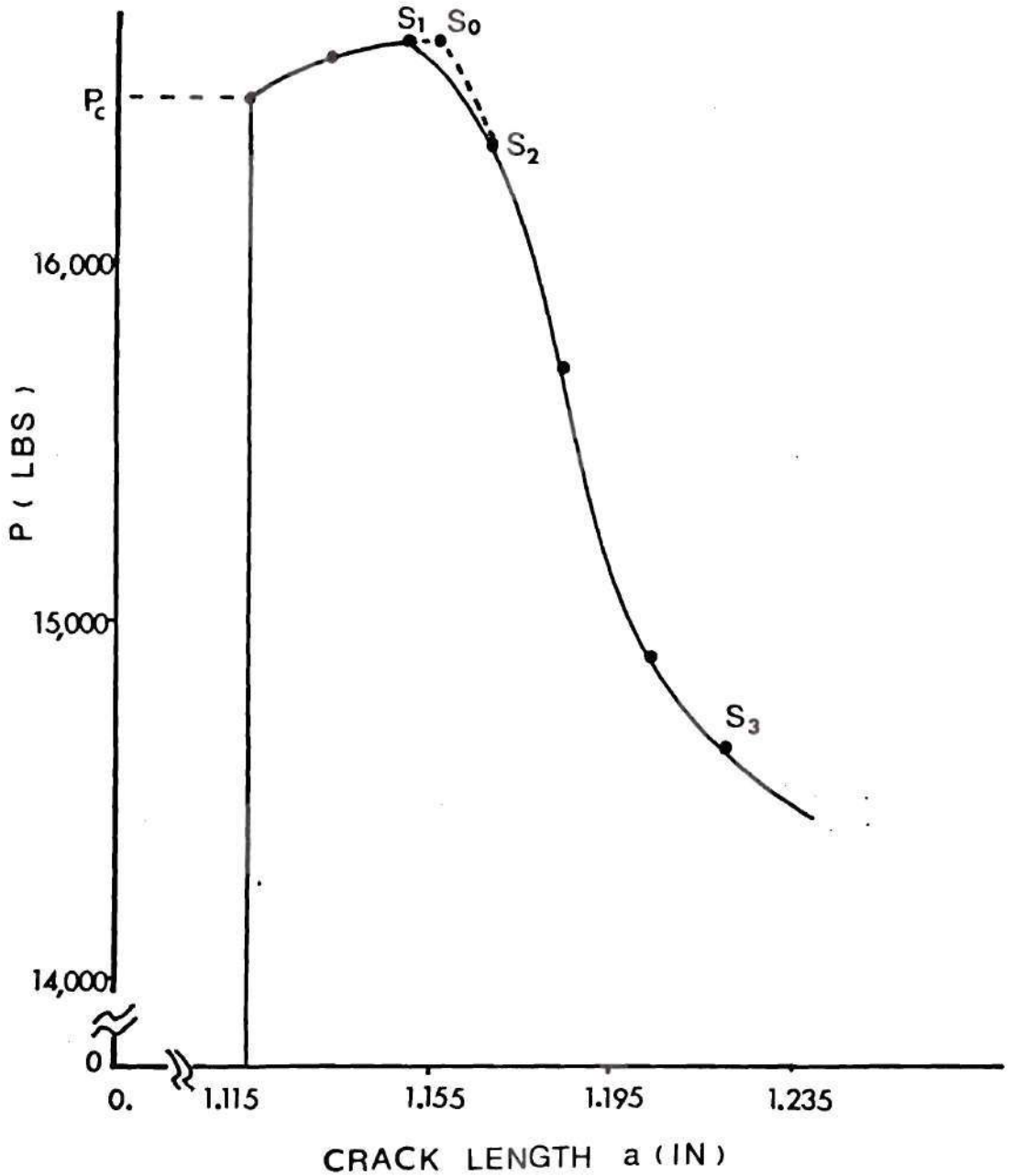

FIG. 55 Load vs. Crack Length Relationship for Crack Extension

BIBLIOGRAPHY

1. Williams, M., "On the Stress Distribution at the Base of a Stationary Crack," Journal of Applied Mechanics, Vol. 24, No. 1, 1957, p. 109.

2. Rice, J. R. and Rosengren, C. F., "Plane Strain Deformation Near a Crack Tip in a Power-Law Hardening Material," Journal of Mechanics and Physics of Solids, Vol. 16, No. 1, 1968, p. 1-12.

3. Hutchinson, J. W., "Singular Behavior at the End of a Tensile Crack in a Hardening Material," Journal of Mechanics and Physics of Solids, Vol. 16, 1968, pp. 13-31.

4. Hutchinson, J. W., "Plastic Stress and Strain Fields at a Crack Tip," Journal of Mechanics and Physics of Solids, Vol. 16, No. 5, 1968, pp. 337-347.

5. Rice, J. R., "Mathematical Analysis in the Mechanics of Fracture," Fracture: An Advanced Treatise, 2, edited by H. Liebowitz, Academic Press, New York, 1968.

6. Zienkiewicz, O. C., "The Finite Element Method in Engineering Science," McGraw-Hill, London, 1971.

7. Martin, H. C. and Carey, G. F., "Introduction to Finite Element Analysis: Theory and Application," McGraw-Hill, 1973.

8. Watwood, V. B., Jr., "The Finite Element Method for Prediction of Crack Behavior," Nuclear Engineering and Design, Vol. II, 1969, pp. 323-332.

9. Chan, S. K., Tuba, I. S. and Wilson, W. K., "On the Finite Element Method in Linear Fracture Mechanics," Engineering Fracture Mechanics, Vol. 2, 1970, pp. 1-17.

10. Anderson, G. P., Ruggles, V. L. and Stikor, G. S., "Use of Finite Element Computer Programs in Fracture Mechanics," International Journal of Fracture Mechanics, Vol. 7, 1971, pp. 63-76.

11. Byskov, E., "The Calculation of Stress Intensity Factors Using the Finite Element Method with Cracked Elements," International Journal of Fracture Mechanics, Vol. 6, No. 2, 1970, pp. 159-167.

12. Tracey, D. M., "Finite Elements for Determination of Crack Tip Elastic Stress Intensity Factors," Engineering Fracture Mechanics,

Vol. 3, No. 3, 1971, pp. 255-266.

13. Tong, P. and Pian, T. H. H., "The Convergence of Finite Element Methods in Solving Linear Elastic Problems," International Journal of Solids and Structures, Vol. 3, pp. 865-879.

14. Atluri, S., Kobayashi, A. S. and Nakagaki, M., "An Assumed Displacement Hybrid Finite Element Model for Linear Fracture Mechanics," International Journal of Fracture Mechanics, Vol. 11, No. 2, 1975, pp. 251-271.

15. Atluri, S. N., Kobayashi, A. S. and Nakagaki, M., "Fracture Mechanics Application of an Assumed Displacement Hybrid Finite Element Procedure," AIAA Journal, Vol. 13, No. 6, 1975, pp. 734-740.

16. Atluri, S. N., Kobayashi, A. S. and Cheng, J. S., "Brain Tissue Fragility-A Finite Strain Analysis by a Hybrid Finite-Element Method," Journal of Applied Mechanics, Paper No. 75-APMW-46, 1975.

17. Desai, C. S. and Abel, J. F., "Theory of the Finite Element Method," New York, Van Nostrand Reinhold Co., pp. 215-243.

18. Hofmeister, L., Greenbaum, G., and Evensen, D., "Large Strain Elasto-Plastic Finite Element Analysis," AIAA Journal, Vol. 9, No. 7, 1971, pp. 1248-1254.

19. Prager, W., "The Theory of Plasticity: A Survey of Recent Achievements," Proc. Inst. Mech. Engrs., 169, 41, 1955.

20. Ziegler, Hans, "A Modification of Prager's Hardening Rule," Quarterly of Applied Mechanics, Vol. 17, 1959, p. 55.

21. Rice, J. R., "A Path Independent Integral and the Approximate Analysis of Strain Concentration by Notches and Cracks," Journal of Applied Mechanics, Vol. 35, Trans. ASME, Vol. 90, Series E, June 1968, pp. 379-386.

22. Eshelby, J. D., "The Continuum Theory of Lattice Defects," Solid State Physics, Vol. III, eds. Seitz, F., and Turnbull, D., Academic Press, 1956.

23. Robinson, J. N. and Tetelman, A. S., "Measure of K_{IC} on Small Specimens Using Critical Crack Tip Opening Displacement," ASTM STP 559, 1973, pp. 139-158.

24. Srawley, J. E., Swedlow, J. L., and Roberts, E., "Discussions of 'On the Sharpness of Cracks Compared with Wells' COD' by A. A. Wells and F. M. Burdekin and by L. P. Pook," International Journal of Fracture Mechanics, Vol. 7, 1971, pp. 242-246.

25. CODA. Fracture Toughness Testing of Metallic Materials, Part II, Crack Opening Displacement (COD) Testing, December 1970, p. 54.

26. Wells, A. A., "The Mechanics of the Fracture Transition in Yielding Materials," CODA paper p. 46, also published in Cancam, 1971.

27. Broek, D., "Some Considerations on Slow Crack Growth," International Journal of Fracture Mechanics, Vol. 4, 1968, pp. 19-34.

28. Link, F., and Muntz, D., Material Prüf, Vol. 13, 1971, p. 407.

29. Bergkvist, and Anderson, H., "Plastic Deformation at a Stably Growing Crack-tip," International Journal of Fracture Mechanics, Vol. 8, 1972, pp. 139-156.

30. Logsdon, W. A., "Elastic Plastic (J_{IC}) Fracture Toughness Values: Their Experimental Determination and Comparison with Conventional Linear Elastic (K_{IC}) Fracture Toughness Values for Five Materials," Mechanics of Crack Growth, STP 590, American Society for Testing and Materials, Philadelphia 1976, pp. 43-60.

31. Washizu, K., "Variational Principles in Elasticity and Plasticity," Vol. 2, Pergamon Press, Oxford 1975.

32. Begley, J. A. and Landes, J. D., "The J-integral as a Fracture Criterion," ASTM STP 514, American Society for Testing and Materials, 1972, pp. 1-20.

33. Begley, J. A. and Landes, J. D., "The Effect of Specimen Geometry on J_{IC}," ASTM STP 514, 1972, pp. 21-39.

34. Bucci, B. J., Paris, P. C., Landes, J. D. and Rice, J. R., "J-Integral Estimation Procedures," ASTM STP 514, 1972, pp. 40-69.

35. Griffith, A. A., "The Phenomena of Rupture and Flow in Solids," Phil. Trans. Roy. Soc. of London, A221, 1921, pp. 163-197.

36. Budiansky, B. and Rice, J. R., "Conversation Laws and Energy-Release Rates," Journal of Applied Mechanics, Vol. 40E, No. 1, March 1973, pp. 201-203.

37. Landes, J. D. and Begley, J. A., "Test Results from J-Integral Studies: An Attempt to Establish a J_{IC} Testing Procedure," Fracture Analysis, ASTM STP 560, 1973, pp. 170-186.

38. Rice, J. R., Parris, P. C., and Merkle, J. G., "Some Further Results of J-Integral Analysis and Estimates," Progress in Flaw Growth and Fracture Toughness Testing, ASTM STP 536, American

Society of Testing and Materials, 1973, pp. 231-245.

39. Merkle, J. G. and Corten, H. T., "A J-Integral Analysis for the Compact Specimen, Considering Axial Force as Well as Bending Effects," Journal of Pressure Vessel Technology, Nov. 1974, pp. 286-292.

40. Goldman, N. L. and Hutchinson, J. W., "Fully Plastic Crack Problems: The Center-Cracked Strip Under Plane Strain," Dept. S-7, Division of Engineering and Applied Physics, Harvard University, February 1974.

41. Knowles, J. K. and Sternberg, E., "On a Class of Conservation Laws in Linearized and Finite Elastostatics," Archive for Rational Mechanics and Analysis, Vol. 44, No. 3, 1972, pp. 187-211.

42. Wells, A. A., "Unstable Crack Propagation in Metals-Cleavage and Fast Fracture," Proc. Crack Propagation Symposium, Granfield, 1961, pp. 210-230.

43. Wells, A. A., "Application of Fracture Mechanics at and Beyond General Yielding," British Welding Research Assoc. Rpt. M13, 1963.

44. Broek, D., "Elementary Engineering Fracture Mechanics," Noordhoff International Publishing, Leyden, 1974.

45. Rice, J. R. and Johnson, M. A., "The Role of Large Crack-Tip Geometry Changes in Plane Strain Fracture," Inelastic Behavior of Solids, McGraw-Hill, New York (M.F. Kanninen, Ed.), 1970, pp. 641-672.

46. Burdekin, F. M. and Stone, D. E. W., "The Crack Opening Displacement Approach to Fracture Mechanics in Yielding," Journal of Strain Analysis, Vol. 1, No. 2, 1966, pp. 145-153.

47. Bilby, B. A., Cottrell, A. H. and Swinden, K. H., "The Spread of Plastic Yield from a Notch," Proceedings of the Royal Society (London), Series A, Vol. 272, 1963, pp. 304-314.

48. Hayes, D. J. and Turner, C. E., "An Application of Finite Element Techniques to Post Yield Analysis of a Practical Fracture Test Specimen," International Journal of Fracture Mechanics, Vol. 10, No. 1, March 1974, pp. 17-33.

49. Levy, N., Marcal, P. V., Ostergren, W. J. and Rice, J. R., "Small Scale Yielding Near a Crack in Plane Strain: A Finite Element Analysis," International Journal of Fracture Mechanics, Vol. 7, No. 2, 1971, pp. 143-156.

50. Yamada, Y., Yoshimura, N. and Sakurai, T., "Plastic Stress-Strain Matrix and its Application for the Solution of Elastic-Plastic Problems by the Finite Element Method," International Journal Mechanics Sciences, Pergamon Press, 1968, Vol. 10.

51. Miyamoto, H. and Shiratori, M., "Elastic-Plastic Response of Kinematically Hardening Cracked Sheet Under Cyclic Loading," Proceedings of the 21st Japan National Congress for Applied Mechanics, 1971.

52. Hill, R., "The Mathematical Theory of Plasticity," Oxford Engineering Science Series, 1950.

53. Drucker, D. C., "A More Fundamental Approach to Plastic Stress-Strain Solutions," Proceedings 1st U.S. National Congress Applied Mechanics, 1951, pp. 487-491.

54. Hodge, P. G., Jr., "The Theory of Piecewise Linear Isotropic Plasticity," IUTAM Colloquium Madrid, 1955.

55. Isakson, G., Armen, H., Jr., and Pifko, A., "Discrete-Element Methods for the Plastic Analysis of Structures," NASA CR-803, October 1967.

56. Armen, H., Jr., Pifko, A., and Levine, H., "Finite Element Analysis of Structures in the Plastic Range," NASA CR-1649, February 1971.

57. Armen, H., Levine, H., Pifko, A., and Levy, A., "Nonlinear Analysis of Structures," NASA CR-2351, March 1974.

58. Hildebrand, F. B., "Advanced Calculus for Applications," Prentice-Hall, Inc., New York, New York.

59. Pian, T. H. H. and Tong, P., "Basis of Finite Element Methods for Solid Continua," International Journal for Numerical Methods in Engineering, Vol. 1, 1969, pp. 3-28.

60. Atluri, S. N., "On Hybrid Finite-Element Models in Solid Mechanics," AICA International Symposium on Computer Methods for Partial Differential Equations, June 1975, Lehigh University.

61. Gallagher, R. H., Padlog, J. and Bijlaard, P. P., "Stress Analysis of Heated Complex Shapes," Journal American Rocket Society, Vol. 32, No. 5, May 1962, pp. 700-707.

62. Marcal, P., "A Comparative Study of Numerical Methods of Elastic-Plastic Analysis," AIAA Journal, Vol. 6, No. 1, Jan. 1968, pp. 157-158.

63. Zienkiewicz, O. C., Valliappan, S. and King, I. P.,

"Elasto-Plastic Solutions of Engineering Problems 'initial stress, Finite Element Approach," International Journal for Numerical Methods in Engineering, Vol. 1, 1969, pp. 75-100.

64. Nayak, G. C., Zienkiewicz, O. C., "Elasto-Plastic Stress Analysis. A Generalization for Various Constitutive Relations Including Strain Softening," International Journal for Numerical Methods in Engineering, Vol. 5, 1972, pp. 113-135.

65. Ergatoudis, I., Irons, B. M. and Zienkiewicz, O. C., "Curved, Isoparametric, 'Quadrilateral' Elements for Finite Element Analysis," International Journal of Solids Structure, Vol. 4, 1968, pp. 31-42.

66. Haggerty, G. B., "Elementary Numerical Analysis with Programming," Allyn and Bacon, Inc., pp. 341-348.

67. Mendelson, A., "Plasticity: Theory and Application," The MacMillan Company, New York, 1968, pp. 92-93.

68. Fung, Y. C., "Foundations of Solid Mechanics," Prentice-Hall, Englewood Cliffs, N.J., 1969.

69. Atluri, S. N., and Nakagaki, M., "J-Integral Estimates for Strain Hardening Materials in Ductile Fracture Problems," Proceedings of AIAA/ASME/SAE 17th Structures, Structural Dynamics and Material Conference, Valley Forge, Pennsylvania, May 1976.

70. Riccardella, P. C. and Swedlow, J. L., "A Combined Analytical-Experimental Fracture Study," Fracture Analysis, ASTM STP 560, 1973, pp. 134-154.

71. Begley, J. A., and Landes, J. D., "Serendipity and the J-Integral," International Journal of Fracture Mechanics, Dec. 1976, pp. 764-766.

72. McClintock, F. A., "Plasticity Aspects of Fracture," in Fracture: An Advanced Treatise (ed. H. Leibowitz), Vol. 3, Academic Press, 1971, pp. 47-225.

73. Chitaley, A. D. and McClintock, F. A., "Elastic-Plastic Mechanics of Steady Crack Growth under Anti-Plane Shear," Journal of the Mechanics and Physics of Solids, Vol. 19, 1971, pp. 147-163.

74. Kfouri, A. P. and Miller, K. J., "Stress, Displacement, Line Integral and Closure Energy Determinations of Crack Tip Stress Intensity Factors," International Journal of Pressure Vessels and Piping, 1974, Vol. 2, pp. 179-191.

75. Kfouri, A. P. and Miller, K. J., "Crack Separation Energy Rates in Elastic-Plastic Fracture Mechanics," Proceedings of the Institution of Mechanical Engineers, London, Vol. 190, 1976, pp. 571-584.

76. Rice, J. R., "An Examination of the Fracture Mechanics Energy Balance from the Point of View of Continuum Mechanics," in Proceedings of the 1st International Congress on Fracture (Sendai, 1965), (ed. T. Yokobori et al.). Japanese Society for Strength and Fracture, Tokyo, Vol. 1, 1966, pp. 309-340.

77. Rice, J. R., "Elastic-Plastic Fracture Mechanics," presented at ASME Winter Annual Meeting, New York, Dec. 1976, The Mechanics of Fracture, AMD, Vol. 19, pp. 23-54.

78. Anderson, H., "A Finite-Element Representation of Stable Crack-Growth," Journal of the Mechanics and Physics of Solids, Vol. 21, 1973, pp. 337-356.

79. Anderson, H., "Finite Element Treatment of a Uniformly Moving Elastic-Plastic Crack Tip," Journal of the Mechanics and Physics of Solids, Vol. 22, 1974, pp. 285-308.

80. Palmer, A. C. and Rice, J. R., "The Growth of Slip Surfaces in the Progressive Failure of Overconsolidated Clay," Proceedings of the Royal Society, London, Vol. A332, 1973, pp. 527-548.

81. Irwin, G. R., "Analysis of Stresses and Strains Near the End of a Crack Traversing a Plate," Journal of Applied Mechanics, Vol. 24, 1957, pp. 361-364.

82. Elber, W., "The Significance of Fatigue Crack Closure," ASTM STP-486, 1971.

83. Elber, W., "Fatigue Crack Closure under Cyclic Tension," Engineering Fracture Mechanics, Vol. 2, No. 1, 1970.

VITA

Wen-Hwa Chen was born on August 15, 1948, in Taiwan, China. He received his Bachelor's Degree in Engineering Science from National Cheng-Kung University, Tainan, Taiwan, in June 1971. During the period from August 1971, to July 1973, he participated in the Reserve Officer Training Program of the Chinese Air Force. In September 1973, he was awarded the "President's Fellowship" for graduate study in the School of Engineering Science and Mechanics at Georgia Institute of Technology.

In 1972, he was married to the former Miss Hsiao-Chen Chang of Tainan, Taiwan. They have a son, Tine.